

4th Malaysia-Japan Tribology Symposium 2016 (MJTS 2016)



25th & 26th August 2016
Malaysia-Japan International Institute of Technology
Universiti Teknologi Malaysia
Kuala Lumpur, Malaysia

Organized by Tribology and Precision Machining i-Kohza (TriPreM)
In collaboration with Japanese Society of Tribologists (JAST) and Malaysian Tribology Society (MYTRIBOS)

Supported by Universiti Teknologi Malaysia (UTM)
And

NSK Microprecision Sdn Bhd
DEWE Solutions Sdn Bhd
Taat Bestari Sdn Bhd
MSI Technologies (M) Sdn Bhd



DEWE Solutions



MJTS 2016 Proceedings Book

Organizing Committee

MJTS 2016 Chairperson
Prof. Dr. Kanao Fukuda

MJTS 2016 Co-chairperson
Prof. Dr. Yoshinori Sawae

MJTS 2016 Secretary
Dr. Jun Ishimatsu

MJTS 2016 Committee Members
Zaid Ali Subhi
Muhammad Faidhi b Mohd Radzi
Ahmad Aizuddin b Abd Aziz
Muhammad Faiz b Wahab
Noor Dalilah bt Abd Manaf

MJTS 2016 Proceedings Book

MJTS 2016 Keynote speakers



Prof. Dr. Salmiah Kasolang, Faculty of Mechanical Engineering, Universiti Teknologi MARA, Malaysia.

Different Facets of Tribology

Tribology literally is a study of ‘rubbing’, a form of motion that is very common in machine interactions. Generally, Tribology looks into three key concerns in engineering applications namely friction, wear, and lubrication. By nature, Tribology is green because of its fundamental concern on reducing friction to prolong the life service of engineering components and efficiency of engineering system. Similarly, by nature, Tribology is a multidisciplinary study that goes beyond boundaries of research areas. This has contributed to different facets of research work associated with tribology as evident by the voluminous publications presented to academic community. This signifies the horizon of opportunity and applications awaiting tribology enthusiasts and advocates to explore and investigate for the advancements of related knowledge and technology in Tribology.



Prof. Dr. Shinya Sasaki, Tokyo University of Science, Japan.

Sustainable Tribology

The global warming problem has reached a point at which action cannot be delayed. It is necessary not only to expect novel technological development but also to create realistic solutions by renovating conventional technologies. Tribology has supported various technological developments over the years and has also responded promptly to societal demands for decreasing substances from engineering products that would be hazardous to the environment. As societies aim to become sustainable, tribology needs to be involved and contribute to the solution more than ever before. Sustainable tribology is an effective engineering technology that can contribute to solve the global environmental issues.

MJTS 2016 Proceedings Book

MJTS 2016 Invited speakers



Prof. Dr. Hitoshi Washizu, University of Hyogo, Japan.

Simulation Studies of Micro/Nano Tribology

Molecular based simulations for tribology is first applied for Micro/Nano devices, such as hard disk drive in 1990s. As a member of automotive industry, we started our research to extend the applicability of the nano-scale knowledge to macroscopic phenomena. In this presentation, we show our atom based studies for the origin of solid friction, low friction mechanism of lamellar materials, molecular origin of elastohydrodynamic lubrication and boundary lubrication, always taking into account of the relation between nano and macro. Some applications for the powertrain of automobiles are also shown.



Prof. Dr. Jaharah bt A. Ghani, Universiti Kebangsaan Malaysia, Malaysia.

Cutting Tool wear condition Monitoring (TCM) and Dynamic Assisted Tooling for Turning process

Due to rapid and fast growing in technology especially in manufacturing industry, the demand from the customers have urged on the production quality and efficiency. Latest and up-to-date production technology and method are required to ensure the manufacturing industries are competitive at the market place.

Tool wear monitoring is important in machining industries for controlling the quality of machined parts that helps to improve the productivity. To date, many monitoring system methods are developed by utilizing various signals, and cutting force is one of the signals in machining process that has been widely used for tool wear monitoring. The application of the I-kazTM and I-kaz 2D methods to interpret the cutting force signal for detection the tool wear progression in turning process is presented. The focus is on the assessment of these methods via relationship between coefficient values of I-kazTM method and tool wear progression then compared the performance results. The I-kaz coefficient including the I-kaz coefficient of main cutting force ($ZF_{c\infty}$), feed force ($ZF_{f\infty}$), and I-kaz 2D coefficient ($Z2\infty$). Surface texturing in the form of dimples for mechanical components is very important in enhancing tribological properties which are closely associated to wear and friction. In order to minimize friction and wear, there are 4 methods i.e coating on engine component, surface texturing on engine component, lubricant and rolling resistance of tires. The Dynamic Assisted Tooling was developed to enable the fabrication of dimple structures using the turning process.

MJTS 2016 Proceedings Book

Day	Time	Activities	
Day 1 [25 th Aug. 2016 (Thu.)]	09:00-09:30	Registration	
	09:30-09:40	Opening talk Prof. Datin Dr. Rubiyah bt Yusof , Dean of Malaysia-Japan International Institute of Technology	
	09:40-10:00	Introduction to Tribology Dr. Nurin Wahidah binti Mohd Zulkifli, University of Malaya	
	10:00-11:00	Keynote speech 1 (Different Facets of Tribology) Prof. Dr. Salmiah Kasolang, Faculty of Mechanical Engineering, Universiti Teknologi MARA	
	11:00-12:00	Keynote speech 2 (Sustainable Tribology) Prof. Dr. Shinya Sasaki, Department of Mechanical Engineering, Tokyo University of Science	
	12:00-14:00	Photo session and symposium lunch	
	14:00-14:45	Invited speech 1 (Simulation Studies of Micro/Nano Tribology) Prof. Dr. Hitoshi Washizu, Graduate school of simulation studies , University of Hyogo	
	14:45-15:30	Invited speech 2 (Cutting Tool wear condition monitoring (TCM) and Dynamic Assisted Tooling for Turning process) Prof. Dr. Jaharah A. Ghani, Department of Mechanical and Material Engineering, Universiti Kebangsaan Malaysia	
	15:30-16:00	Coffee break	
	General Session 1		
	16:00-16:20	Bio-Medical Tribology (Room A) Session Chair: Assoc. Prof. Dr. Syahrullail bin Samion	Machining Technology (Room B) Session Chair: Dr. Jun Ishimatsu
		A - 1 - 1 Frictional Characteristics of Highly Hydrated Hydrogel Artificial Cartilage Y. Sawae ¹ , R. Baba ² , Y. Hong ² , T. Yamaguchi ¹ , and T. Morita ¹ ¹ Faculty of Engineering, Kyushu University, Japan ¹ Graduate School of Engineering, Kyushu University, Japan.	B - 1 - 1 Surface Roughness of Hyper-Eutectic Al-Si A390 In High Speed Milling K. Othman ¹ , J. A. Ghani ² , C. H. C. Haron ² , and M. S. Kasim ³ ¹ Production Technology Department, German Malaysian Institute, Malaysia. ² Department of Mechanical and Material Engineering, Universiti Kebangsaan Malaysia, Malaysia. ² Department of Process, Universiti Teknikal Malaysia Melaka, Malaysia.
	16:20-16:40	A - 1 - 2 Frictional Properties of Poly Vinyl Alcohol Hydrogel in Pseudo-Synovial Fluid Using A Pendulum-Type Friction Tester C. Sawayama ¹ , T. Iwai ¹ , and Y. Syoukaku ¹ ¹ Graduate School of Natural Science and Technology, Kanazawa University, Japan.	B - 1 - 2 Tribological Action and Cutting Performance of Lubricant Ester in MQL Machining T. Wakabayashi ¹ ¹ Kagawa University, Japan.
	16:40-17:00	A - 1 - 3 Formation Process of Protein Film Adsorbed on Joint Prosthesis Material K. Nakashima ¹ , S. Kudo ¹ , Y. Sawae ¹ , and T. Murakami ² ¹ Kyushu University, Japan. ² Teikyo University, Japan.	B - 1 - 3 The Difference of Dimple Structures Fabricated using Turning and Milling Machines M. N. A. B. Mohd Dali ^{1,2} , J. A.Ghani ² , and C. H. C. Haron ² , and S. Hassan ^{1,2} ¹ Politeknik Ungku Omar, Malaysia. ² Faculty of Engineering and Built Environment, Universiti Kebangsaan Malaysia, Malaysia.

MJTS 2016 Proceedings Book

Day	Time	Activities	
Day 2 [26 th Aug. 2016 (Fri.)]	General Session 2		
		Composite Materials (Room A) Session Chair: Assoc. Prof. Dr. Tomoaki Iwai	Fluid Lubrication (Room B) Session Chair: Prof. Dr. Yoshinori Sawae
	09:00-09:20	A - 2 - 1 Effect of Stir Casting Process Parameters on Tribological Performance of Al6061-SiCp Composite A. A. Adebisi ¹ , M. A. Maleque ¹ , and K. A. Bello ¹ <i>¹Faculty of Engineering, Department of Manufacturing and Material Engineering, International Islamic University Malaysia, Malaysia.</i>	B - 2 - 1 Tribological Performance Evaluation of Palm Trimethylolpropane (TMP) Ester as A Subsitute for Conventional Lubricant Base Oil R. Zahid ^{1,2} , M. B. H. Hassan ¹ , M. Varman ¹ , R. A. Mufti ² , M. A. Kalam ¹ , N. W. B. M. Zulkifli ¹ , and M. Gulzar ¹ <i>¹Center for Energy Sciences, Department of Mechanical Engineering, University of Malaya, Malaysia.</i> <i>²School of Mechanical and Manufacturing Engineering, National University of Sciences and Technology, Pakistan.</i>
		09:20-09:40	A - 2 - 2 The Influence of Friction Force on the Higher-Order Structure of Filled Rubber T. Iwai ¹ , K. Murata ¹ , and Y. Shoukaku ¹ <i>¹College of Science and Engineering, Kanazawa University, Japan.</i>
	09:40-10:00	A - 2 - 3 Bearing Load Capacity of A Palm Kernel Activated Carbon-Epoxy Composite D. N. F. Mahmud ¹ , , M. F. B. Abdollah ² , N. A. B. Masripan ² , F. F. Shuhimi ¹ , H. Amiruddina ² , and N. Tamaldina ² <i>¹Faculty of Mechanical Engineering, Universiti Teknikal Malaysia Melaka, Malaysia.</i> <i>²Centre for Advanced Research on Energy, Universiti Teknikal Malaysia Melaka, Malaysia.</i>	B - 2 - 3 Vibration Characteristic on Ball Bearing Operated With Hexagonal Boron Nitride (HBN) Nanoparticle Mixed with Diesel Engine Oil N. S. R. Apandi ¹ , R. Ismail ¹ , M. F. B. Abdollah ^{1,2} , and R. Ramlan ¹ <i>¹Faculty of Mechanical Engineering, Universiti Teknikal Malaysia Melaka, Malaysia.</i> <i>²Centre for Advanced Research on Energy, Universiti Teknikal Malaysia Melaka, Malaysia.</i>
	10:00-10:20	A - 2 - 4 Lubricated Wear Behaviour of Sic Reinforcement on Ti-6Al-4V Alloy Based on Taguchi Approach M. A. Maleque ¹ , L. H. Paijan ¹ , K. A. Bello ¹ , and M. Azwan ¹ <i>¹Department of Manufacturing and Materials Engineering, International Islamic University Malaysia, Malaysia.</i>	B - 2 - 4 The Effect of Pure Aluminium Pin on Steel Disc with Varies Speed and Constant Load A. M. S. Zuan ¹ , S. Syahrullail ¹ , and S. M. Azhar ¹ <i>¹Faculty of Mechanical Engineering, Universiti Teknologi Malaysia, Malaysia.</i>

MJTS 2016 Proceedings Book

Day	Time	Activities	
Day 2 [26 th Aug. 2016 (Fri.)]	10:20-10:40	Coffee break	
		General Session 3	
		Coating Materials (Room A) Session Chair: Dr. Nurin Wahidah binti Mohd Zulkifli	Fundamental (Room B) Session Chair: Prof. Dr. Prof. Toshi Wakabayashi
	10:40-11:00	A - 3 - 1 Tribological Behaviour of Surface Textured Hydrogenated Amorphous Carbon Coating in the Presence of PAO at Various Temperatures A. Arslan ¹ , H. H. Masjuki ¹ , M. A. Kalam ¹ , M. Varman ¹ , R. A. Mufti ² , M. H. Mosarof ¹ , and L. S. Khoung ¹ ¹ Center of Energy Sciences, University of Malaya, Malaysia. ² SMME, NUST, Islamabad, Pakistan.	B - 3 - 1 Tribological Properties of Plastic Materials Rubbed Against 6061-T6 Aluminum Alloy under High-Temperature Hydrogen Atmosphere T. Yasugi ¹ , T. Iwai ¹ , T. Ueda ¹ , and Y. Shoukaku ¹ ¹ Graduate School of Natural Science and Technology, Kanazawa University, Japan.
	11:00-11:20	A - 3 - 2 Friction Behavior of Polymer Overlays Containing Solid Lubricants Coated on the Micro-Textured Aluminum Substrate T. Doi ¹ , K. Enomoto ² , and H. Usami ² ¹ Division of materials science and engineering, Graduate school of Meijo University, Japan. ² Department of materials science and engineering, Meijo University, Japan.	B - 3 - 2 Analysis on the Early Stage of Contact Adhesion in Different Relative Humidity Z. A. Subhi ¹ , and K. Fukuda ¹ ¹ Department of Mechanical Precision Engineering, Malaysia Japan International Institute of Technology, Universiti Teknologi Malaysia, Malaysia.
	11:20-11:40	A - 3 - 3 Dry Sliding Wear Characterization of TIG Embedded Composite Coatings using Taguchi Based Grey Relational Analysis Approach K. A. Bello ^{1,2} , M. A. Maleque ^{1,2} , and A. Adebisi ¹ ¹ Department of Manufacturing and Materials Engineering, International Islamic University Malaysia, Malaysia. ² Department of Metallurgical and Materials Engineering, Ahmadu Bello University Zaria, Nigeria.	B - 3 - 3 Effects of Sliding Speed on Friction and Wear of Carbon Fiber Filled PTFE in Hydrogen T. Morita ^{1,2} , Y. Abe ³ , Y. Sawae ^{1,2} , and J. Sugimura ^{1,2,4} ¹ Faculty of Engineering, Kyushu University, Japan. ² International Institute for Carbon-Neutral Energy Research, Kyushu University, Japan. ³ Graduate School of Engineering, Kyushu University, Japan. ⁴ Research Center for Hydrogen Industrial Use and Storage, Kyushu University, Japan.
	11:40-12:00		B - 3 - 4 Time Dependent Change of Water Adsorption on Austenitic Stainless Steel N. D. A. Manaf ¹ , K. Fukuda ¹ , Z. A. Subhi ¹ , and M. F. M. Radzi ¹ ¹ Department of Mechanical Precision Engineering, Malaysia Japan International Institute of Technology, Universiti Teknologi Malaysia, Malaysia.
	12:00-13:00	Lunch	

MJTS 2016 Proceedings Book

Table of Content

“Title” , Authors	Pages
Bio-Medical Tribology	
“Frictional Characteristics of Highly Hydrated Hydrogel Artificial Cartilage” Y. Sawae, R. Baba, Y. Hong, T. Yamaguchi, and T. Morita	1-2
“Frictional Properties of Poly Vinyl Alcohol Hydrogel in Pseudo-Synovial Fluid Using A Pendulum-Type Friction Tester” C. Sawayama, T. Iwai, and Y. Syoukaku	3-4
“Formation Process of Protein Film Adsorbed on Joint Prosthesis Material” K. Nakashima, S. Kudo, Y. Sawae, and T. Murakami	5-6
Machining Technology	
“Surface Roughness of Hyper-Eutectic Al-Si A390 in High Speed Milling” K. Othman, J. A. Ghani, H. C. Haron, and M. S. Kasim	7-8
“Tribological Action and Cutting Performance of Lubricant Ester in MQL Machining” T. Wakabayashi	9-10
“The Difference of Dimple Structures Fabricated Using Turning And Milling Machines” M. N. A. B. M. Dali, J. A. Ghani, C. H. C. Haron, and S. Hassan	11-12
Composite Materials	
“Effect of Stir Casting Process Parameters on Tribological Performance of Al6061-SiCp Composite” A. A. Adebisi, M. A. Maleque, and K. A. Bell	13-14
“The Influence of Friction Force on the Higher-Order Structure of Filled Rubber” T. Iwai, K. Murata, and Y. Shoukaku	15-16
“Bearing Load Capacity of A Palm Kernel Activated Carbon-Epoxy Composite” D. N. F. Mahmud, M. F. B. Abdollah, N. A. B. Masripan, F. F. S. H. Amiruddin, and N. Tamaldina	17-18
“Lubricated Wear Behaviour of Sic Reinforcement on Ti-6al-4v Alloy Based on Taguchi Approach” M. A. Maleque, L. H. Paijan, K. A. Bello, and M. Azwan	19-20
Fluid Lubrication	
“Tribological Performance Evaluation of Palm Trimethylolpropane (Tmp) Ester as A Subsitute for Conventional Lubricant Base Oil” R. Zahid, M. B. H. Hassan, M. Varman, R. A. Mufti, M. A. Kalam, N. W. B. M. Zulkifli, and M. Gulzar	21-22

MJTS 2016 Proceedings Book

“Title” , Authors	Pages
“Performance Evaluation of Polyol Esters From Palm Oil as a Lubricant for Bentonite Suspension Drilling Fluid” D. Kania, R. Yunus, R. Omar, S. A. Rashid, and B. M. Jan	23-24
“Vibration Characteristic on Ball Bearing Operated with Hexagonal Boron Nitride (Hbn) Nanoparticle Mixed with Diesel Engine Oil” N. S. R. Apandi, R. Ismail, M. F. B. Abdollah, R. Ramlan	25-26
“The Effect of Pure Aluminium Pin on Steel Disc with Varies Speed and Constant Load” A. M. S. Zuan, S. Syahrullail, and S. M. Azhar	27-28
Coating Materials	
“Tribological Behaviour of Surface Textured Hydrogenated Amorphous Carbon Coating in the Presence of PAO at Various Temperatures” A. Arslan, H. H. Masjuki, M. A. Kalam, M. Varman, R. A. Mufti, M. H. Mosarof, and L. S. Khoung	29-30
“Friction Behavior o Polymer Overlays Containing Solid Lubricants Coated on the Micro-Textued Alminum Substrate” T. Doi, K. Enomoto, H. Usami	31-32
“Dry Sliding Wear Characterization of TIG Embedded Composite Coatings Using Taguchi Based Grey Relational Analysis Approach” K. A. Bello, M. A. Maleque, and A. Adebisi	33-34
Fundamental	
“Tribological Properties of Plastic Materials Rubbed Against 6061-T6 Aluminum Alloy Under High-Temperature Hydrogen Atmosphere” T. Yasugi, T. Iwai, T. Ueda, and Y. Shoukaku	35-36
“Analysis on The Early Stage of Contact Adhesion in Different Relative Humidity” Z. A. Subhi, K. Fukuda	37-38
“Effects of Sliding Speed on Friction And Wear of Carbon Fiber Filled PTFE in Hydrogen” T. Morita, Y. Abe, Y. Sawae, and J. Sugimura	39-40
“Time Dependent Change of Water Adsorption on Austenitic Stainless Steel” N. D. A. Manaf, K. Fukuda, Z. A. Subhi, and M. F. M. Radzi	41-42

FRICITIONAL CHARACTERISTICS OF HIGHLY HYDRATED HYDROGEL ARTIFICIAL CARTILAGE

Y. Sawae¹, R. Baba², Y. Hong², T. Yamaguchi¹, and T. Morita¹

¹Faculty of Engineering, Kyushu University, Japan.

²Graduate School of Engineering, Kyushu University, Japan.

1. INTRODUCTION

Natural synovial joints have fascinated many tribologist with their low friction and low wear nature. Articular cartilage is soft and hydrated tissue covering articulating surfaces of synovial joints and thought to be a key component in the sophisticated joint lubrication mechanism. Especially, several researchers have suggested that the highly hydrated nature of natural cartilage surface gives synovial joints unique lubrication mechanisms, i.e. biphasic lubrication [1] or hydration lubrication [2]. Based on these suggestions, the application of highly hydrated hydrogel as artificial cartilage in articulating surfaces of joint prosthesis has been proposed to mimic natural synovial joints and improve the lubrication mode and joint lifetime of artificial joints. In this study, poly(vinyl alcohol) (PVA) hydrogel was selected as an artificial cartilage material and its frictional characteristics are examined in reciprocating cylinder-on-plate test and hip joint simulator test. Subsequently, the contribution of water content of PVA hydrogel on the frictional behavior was discussed.

2. MATERIAL AND METHODS

PVA hydrogel used in this study was prepared by the repeated freeze-thawing method [3]. It was physically cross-linked polymer hydrogel and its elastic modulus and water content were 1.2 MPa and 79 wt%, respectively.

First, the frictional characteristics of PVA hydrogel was evaluated in the reciprocating cylinder-on-flat test. Reciprocating tests were conducted with two different specimen configurations. Schematics of two specimen configurations are shown in Fig. 1. In “Upper test” configuration, 2 mm thick PVA hydrogel sheet was glued on an acrylic cylinder with a radius of 11 mm and slid over a glass plate. On the other hand, a glass cylinder with a radius of 13 mm was slid over 2 mm thick flat PVA sheet glued on the stainless steel plate in “Lower test” configuration. In both configuration, the upper cylindrical specimen was fixed to the loading flange and loaded against the flat plate specimen which is immersed in a lubricant and reciprocated by a servo motor. The load was varied from 4.9 N to 10.8 N while the average speed and the stroke of reciprocating motion were set at 20 mm/s and 25 mm, respectively. All tests were conducted for 1500 cycles under room temperature and 30 vol% diluted fetal bovine serum was used as a lubricant.

Second, artificial hip models consists of a CoCrMo femoral head with 26 mm diameter and an acetabulum cup with 2

mm thick PVA hydrogel liner were prepared and their frictional characteristics were examined by a custom-made hip joint simulator under quasi-physiological kinematic conditions. A close-up view of the prepared hip joint model installed in the hip joint simulator was shown in Fig. 2. In this simulator, the femoral head was fixed to a swinging shaft and the acetabular component was mounted on the cradle. Then, the flexion-extension motion was applied to femoral head by a PC controlled servomotor while static or dynamic joint load within a physiological range was imposed to the hip joint model by hydraulic actuator. During the experiment, friction force exerted between CoCrMo head and PVA liner was monitored by a load cell which was connected to the cradle. Three acetabulum cups with different inner diameter of PVA liner, 26 mm, 26.2 mm and 26.6 mm, were prepared and the effect of nominal radial clearance on the frictional behavior was examined. All simulator tests were conducted under room temperature and 30 vol% diluted fetal bovine serum was also used as a lubricant in the simulator test.

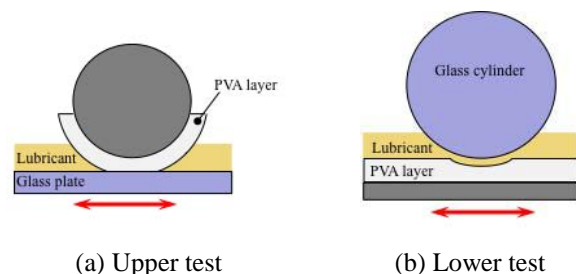


Fig.1 Specimen configurations in cylinder-on-flat test



Fig.2 Hip joint model installed in hip joint simulator

3. RESULTS AND DISCUSSIONS

3.1. Cylinder-on-flat test

The transitional behavior of friction coefficient in the reciprocating cylinder-on-flat tests was shown in Fig. 3. It was obviously observed that the friction coefficient was load- and time-dependent in the upper test except for the

6.86 N. The friction coefficient between PVA hydrogel and glass plate was initially around 0.1. However, it increased continuously during the sliding test and finally exceeded 0.3 in many cases.

On the other hand, the sliding pair of glass cylinder and PVA sheet did not show the load- and time-dependent behavior of friction in the lower test. The frictional behavior in the lower test was much better than that in the upper test and the friction coefficient around 0.1 could be maintained until the end of sliding tests under all loading conditions.

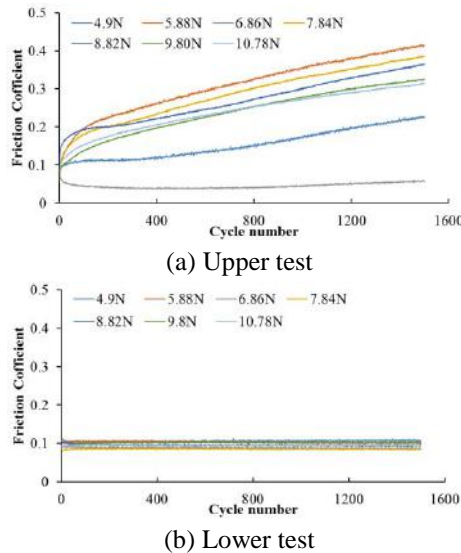


Fig.3 Transition of friction coefficient in reciprocating cylinder-on-flat test

The difference in the frictional behavior under the reciprocating motion observed in this test might be raised from the highly hydrated nature of PVA hydrogel. The biphasic lubrication mechanism was first proposed to describe the time-dependent frictional behavior of highly hydrated articular cartilage. In this theory, the hydrated cartilage was modeled as a biphasic material consists of solid phase and fluid phase and friction could be reduced as a large fraction of the contact load was supported by the pressurized fluid phase. In upper test, the contact load was always applied to the same position of PVA surface and the water contained in PVA was gradually squeezed out from the contact zone. Then PVA lost the load support by the interstitial water and subsequently friction coefficient increased. However, the contact point moved on the PVA surface continuously in the lower test. It allows PVA surface rehydrate after the contact with glass cylinder and maintain its water content. As a result, the friction coefficient could be level-off until the end of the sliding test.

The hip joint model consists of CoCrMo head and PVA liner also showed time-dependent frictional behavior and the friction coefficient increased with the progress of joint simulator test (Fig.4). The increasing rate of the friction coefficient depended on the inner diameter of PVA liner and PVA liner with the smallest inner diameter, 26.0 mm, resulted in the largest increasing rate while the largest inner

diameter, 26.6 mm, showed only slight increase in the friction coefficient.

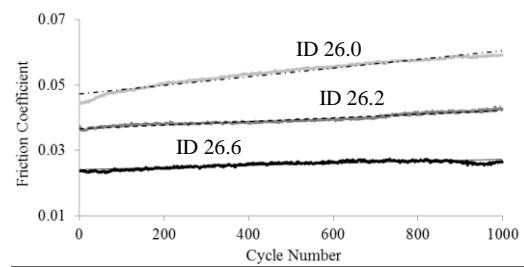


Fig.4 Transition of friction coefficient in hip joint simulator test

These results might also have linked to the hydrated nature of PVA hydrogel used in the articulating surface of the hip joint model. For the PVA liner with the inner diameter of 26.0, the radial clearance between head and liner become 0 and the contact patch reaches to the rim of the cup. In this case, the hip joint fall into the edge loading condition and elastohydro dynamic lubrication (EHL) film formation is restricted by the effect of starved condition [4]. Therefore, PVA surface could not be rehydrated under severe contact condition and the friction coefficient increased with decreasing the water content of PVA in the contact area. On the other hand, the 26.6 mm liner could have an enough inlet area and promote EHL film formation. Subsequently, the PVA liner surface could rehydrate by the lubricant entrained into the contact zone and the friction increase might be alleviated.

4. CONCLUSIONS

The frictional characteristic of highly hydrated PVA hydrogel was evaluated in the reciprocating cylinder-on-flat test and the hip joint simulator test to consider about its potential as an artificial cartilage for future joint prostheses. Results indicated that the hydrated nature and related intrinsic lubrication mechanisms play important role in the frictional behavior and PVA can keep low friction if it can be rehydrated by the lubricant.

REFERENCES

- [1] G.A. Ateshian, "The role of interstitial fluid pressurization in articular cartilage lubrication", *J Biomech*, Vol. 42, pp. 1163–76, 2009.
- [2] T. Murakami et al., "Effectiveness of adsorbed film and gel layer in hydration lubrication as adaptive multimode lubrication mechanism for articular cartilage", *Proc IMechE, Part J*, Vol. 225, No. 12, pp. 1174-1185, 2011.
- [3] Y. Sawae et al., "Lubrication property of total knee prostheses with PV A hydrogel layer as artificial cartilage", *JSME International Journal, Series C*, Vol. 39, No. 2. pp. 356-364, 1996.
- [4] Q. Meng, et al., "The lubrication performance of the ceramic-on-ceramic hip implant under starved conditions", *J Biomechanical Behavior of Biomedical Materials*, Vol. 50, pp. 70-76, 2015.

FRICTIONAL PROPERTIES OF POLY VINYL ALCOHOL HYDROGEL IN PSEUDO-SYNOVIAL FLUID USING A PENDULUM-TYPE FRICTION TESTER

C. Sawayama¹, T. Iwai¹, and Y. Syoukaku¹

¹Kanazawa University, Graduate School of Natural Science and Technology, Japan.

1. INTRODUCTION

The ultra-high molecular weight polyethylene used in conventional artificial joints causes prosthetic loosening or granuloma owing to the occurrence of wear debris caused by the mixed lubrication. Therefore polyvinyl alcohol hydrogel (PVA-H) has been proposed as an artificial cartilage material. PVA-H is expected to achieve fluid film lubrication that reduces friction and wear due to its high moisture content.

A pin-on-disk type tribometer has often been used as a friction test. PVA-H slides continually to the mating surface because the specimen is pin-shaped, whereas the cartilage of an actual human joint slides oscillatory. The purpose of this study is to clarify the frictional property of PVA-H by using a pendulum-type friction-tester which moves in a way that is similar to the movement of a human joint. In this study, saline and pseudo-synovial fluid including hyaluronic sodium were used as lubricants. The frictional properties of PVA-H in saline and pseudo-synovial fluid were compared.

2. EXPERIMENT

2.1. Experimental apparatus

A schematic diagram of the experimental apparatus is shown in Fig. 1. A concave piece made of PVA-H was rubbed to SUS304 stainless ball to oscillate the pendulum. The PVA-H was set in a water bath filled with a lubricant, either saline solution or pseudo-synovial fluid. To measure the frictional force, damped oscillation of the pendulum was detected. An inclinometer fixed to the pendulum was used to measure the amplitude angle of the pendulum. The experimental conditions are shown in Table 1.

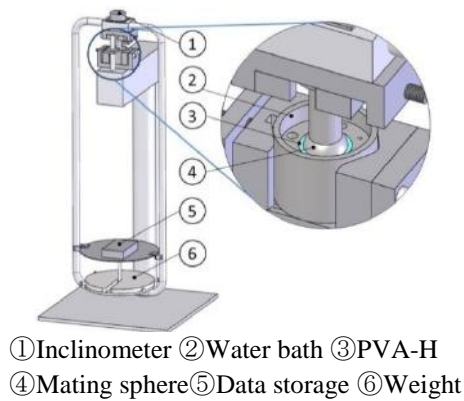


Fig. 1 Pendulum-type friction tester

Table 1 Conditions during friction test

Lubricant	saline solution, 0.5wt% NaHA with saline		
Mating sphere	SUS304		
Diameter of mating sphere, mm	35		
Load, N	200	300	400
Pendulum length, mm	465	635	715
Initial phase, °	-10		
Oscillation frequency, Hz	0.5		
Temperature, °C	23		

2.2. Specimen

The PVA-H used in this study was prepared by the repeated freezing-thawing method. Table 2 shows the specimen preparation conditions. Three types of PVA-H were used: unfilled PVA-H, tricalcium phosphate (α -TCP)-filled PVA-H, and laminated PVA-H. The PVA density of each PVA-H was 15 wt%, and 7 wt% α -TCP was introduced as a filled specimen in order to improve the mechanical properties. Unfilled PVA-H and filled PVA-H were layered to combine the lower frictional coefficient and higher mechanical properties.

Table 2 Conditions of specimen preparation

Specimen	Unfilled PVA-H	α -TCP filled PVA-H	Laminated PVA-H
PVA, wt%	15		
α -TCP, wt%	0	7	0, 3, 7
Freezing time, h	12		
Thawing time, h	12		
The number of freezing-thawing cycles	5		
Freezing temperature, °C	-23		
Thawing temperature, °C	3.5		
Radius of curvature, mm	17.5		
Thickness, mm	3		

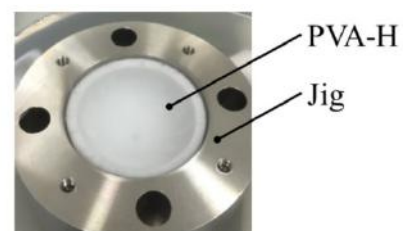


Fig. 2 PVA-H with spherical surface

2.3. Theory

The frictional coefficient calculated from the damped oscillation was deduced as follows¹⁾.

The frictional moment M of the pendulum was given by:

$$M = W \cdot r \cdot \mu \quad (1)$$

where W is the weight of the pendulum, r is the radius of curvature of the mating sphere, and μ is the frictional coefficient. The coefficient of mean resistance moment M/W was derived as:

$$\frac{M}{W} = l \cdot \frac{\theta_{n-1} - \theta_n}{4} \quad (2)$$

where l is the length between the center of oscillation and the center of gravity of the pendulum, and θ_n is the half-amplitude angle for the n th oscillation. By substituting eqn. (2) in eqn. (1), the frictional coefficient was as follows:

$$\mu = \frac{l \cdot \Delta\theta}{4r} \quad (3)$$

where $\Delta\theta$ is the difference between the half-amplitude angle for the n th oscillation and that for the $n-1$ th oscillation.

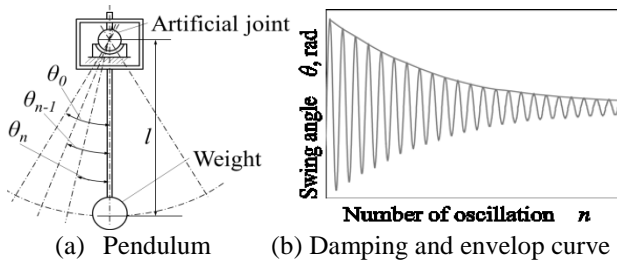


Fig. 3 Method of calculating frictional coefficient

3. RESULTS AND DISCUSSION

The experimental results are shown in Fig. 4-Fig. 7. Stribeck curves, e.g. the frictional coefficient as a function of $\eta U/W$, were introduced in which η is the viscosity of the lubricant, U is the sliding speed, and W is the normal load. The viscosity of the saline and pseudo-synovial fluid were set to 1.0 cP and 3590 cP, respectively. The frictional coefficient increased as the horizontal shaft increased and did so irrespective of the weight or specimen in saline.

When the unfilled PVA-H was rubbed in pseudo-synovial fluid, the frictional coefficient remained almost steady.

The difference in the frictional coefficient between unfilled and laminated PVA-H was small, and the frictional coefficient of α -TCP-filled PVA-H was slightly greater than those of the unfilled and laminated PVA-H in pseudo-synovial fluid. This difference was likely due to surface of laminated PVA-H being the same as that of unfilled PVA-H.

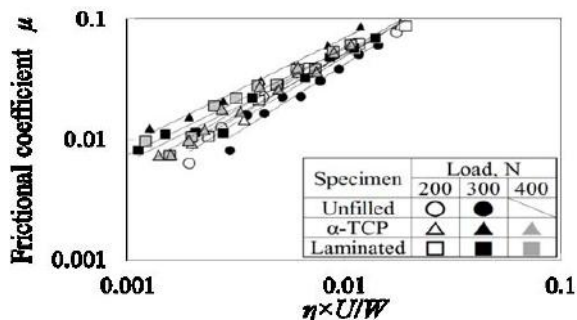


Fig. 4 Stribeck curve of PVA-H with saline solution

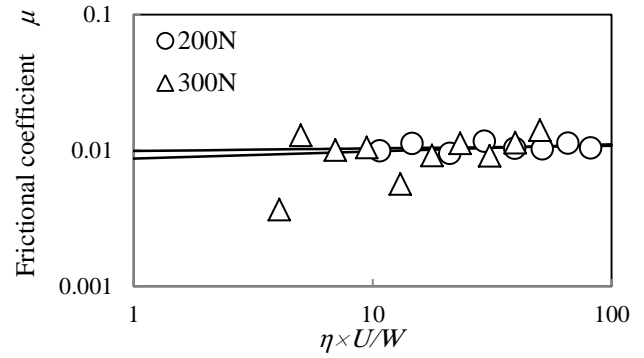


Fig. 5 Stribeck curve of unfilled PVA-H in pseudo-synovial fluid

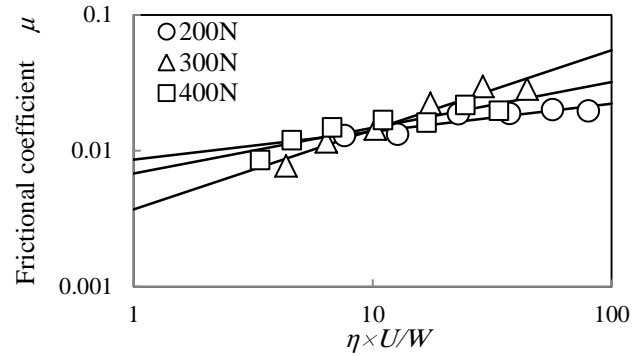


Fig. 6 Stribeck curve of α -TCP-filled PVA-H in pseudo-synovial fluid

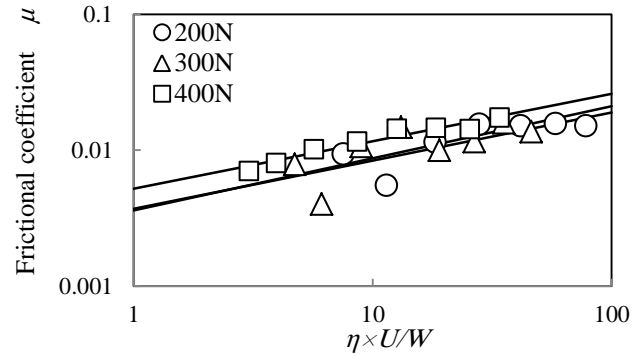


Fig. 7 Stribeck curve of laminated PVA-H in pseudo-synovial fluid

4. CONCLUSION

Experiments on a spherical surface made of PVA-H were conducted using a pendulum-type friction tester, and the results were as follows.

(1) The frictional coefficient increased as the horizontal shaft increased and did so irrespective of weight or PVA-H specimen in saline. In pseudo-synovial fluid, the frictional coefficient remained almost steady.

(2) The difference in the frictional coefficient between unfilled and laminated PVA-H was small, and the frictional coefficient of α -TCP-filled PVA-H was slightly greater than those of unfilled and laminated PVA-H in pseudo-synovial fluid.

REFERENCES

- [1] T. Sasada, K. Mabuchi and Y. Tsukamoto, *Bio-tribology*, Sangyo-tosyo, 1988 (Japanese)

FORMATION PROCESS OF PROTEIN FILM ADSORBED ON JOINT PROSTHESIS MATERIAL

K. Nakashima¹, S. Kudo¹, Y. Sawae¹, and T. Murakami²

¹Kyushu University, Japan, ²Teikyo University, Japan.

1. INTRODUCTION

Joint prostheses are implanted for patients who injured their own joints. The implants can release patients from pain, and improve their Quality of life (QOL). The longevity depends on the wear of rubbing material, ultra-high molecular weight polyethylene (UHMWPE). There are a lot of studies to improve the longevity by enhancing wear resistance of UHMWPE, or replacing rubbing material other materials. Authors have introduced artificial cartilage as rubbing material to change lubrication regime from boundary lubrication to adaptive multimode lubrication[1].

The artificial cartilage showed low friction, but it is considered that severe lubrication in human body will occur. Therefore wear property of artificial cartilage was investigated and resulted in low and high wear depending on protein concentration in lubricant. The adsorbed protein film showed low wear formed lamellar structure of bovine serum albumin (BSA) and human γ -globulin (HGG), but that showed high wear formed heterogeneous structure[2]. To understand the tribological properties of joint prosthesis, it is necessary to understand adsorbed proteins, because the adsorbed film showed a marked effect on tribological properties. In this study, the initial formation process of adsorbed film is discussed to clarify the origin of lowering wear depending on adsorbed protein film structure.

2. EXPERIMENTAL METHOD

Protein adsorption amount: BSA and HGG were employed as proteins included in natural synovial fluid. Lubricant was PBS (pH7.4) contained BSA or HGG. Frictional tests were performed in a reciprocating tribometer in a combination of glass plate and poly(vinyl alcohol) (PVA) hydrogel. The glass plate has thin gold layer (40 nm) with hydrophilic SAM (self assembled mono layer) to simulate hydrophilic PVA hydrogel surface. The adsorbed amount was measured in a Surface Plasmon Resonance (SPR). After rubbing, glass plate was set in the SPR and attached protein solution to investigate protein adsorption on adsorbed protein film to discuss protein formation process. Adsorbed HGG film thickness was analyzed in a ellipsometer.

Protein adsorption/desorption behavior: BSA and HGG will adsorb/desorb during rubbing. The electrochemical method was employed to investigate the adsorption property. The rubbing combination was UHMWPE (GUR1050) and CoCrMo alloy (ASTMF75) to measure the potential between lubricant and CoCrMo alloy by Callomel probe. The potential indicates surface oxidation/reduction during

rubbing. Therefore the method can measure adsorption property *in situ*.

3. RESULTS AND DISCUSSION

As shown in Fig.1, static adsorption amount of HGG was higher compared to BSA adsorption. Both of BSA and HGG showed increase of adsorption amount with increase of rubbing distance until 120m. BSA showed low adsorption amount compared with HGG adsorption. Therefore it is considered that HGG will remain compared to BSA molecules under rubbing condition. The HGG rich bottom layer under rubbing condition is similar to observation results of fluorescent technique[2]. Figure 2 shows protein adsorption amount on protein film constructed under rubbing condition (20 m). HGG adsorbed film showed adsorption of HGG molecules, but not of BSA molecules. BSA film constructed under rubbing condition adsorbed both of BSA and HGG molecules. In addition, longer sliding period showed little BSA molecules adsorption on BSA adsorbed film, but HGG adsorbed film showed HGG molecules adsorption as shown in Fig.4. It is considered that the difference of adsorption amount was due to surface property change by shear force of friction., and the surface property change induced by denature of protein molecules by shear. This indicates that HGG film grows on only HGG adsorbed film. These results of adsorption amount shows that BSA molecules are easily removed by shear force of rubbing, then HGG will remain on the hydrophilic substrate. BSA molecules can not readorb on HGG adsorbed film constructed under rubbing condition, but HGG molecules adsorb on HGG adsorbed layer.

The film thickness was less than 6 nm as shown in Fig.4. The theoretical thickness of adsorbed HGG without denature was estimated 6 nm from the aspect of native HGG molecule, so that adsorbed HGG film was thinned by rubbing. It indicates that adsorbed HGG molecule adsorbed under rubbing condition is denatured. The denature induces surface property change, and it resulted the difference of adsorption amount of BSA and HGG.

Protein adsorption behavior was obtained from potential transition as shown in Fig.5. BSA showed potential drop after starting rubbing, and it was about -0.1 V. On the other hand, potential drop of HGG was about -0.01 V. Potential drop indicates reduction of the surface, in this case, it means desorption of protein. Therefore it was shown that BSA was easily desorbed compared to HGG desorption from the *in situ* observation of protein adsorption/desorption behavior.

From above observation, protein adsorbed film formation process can be considered as following:

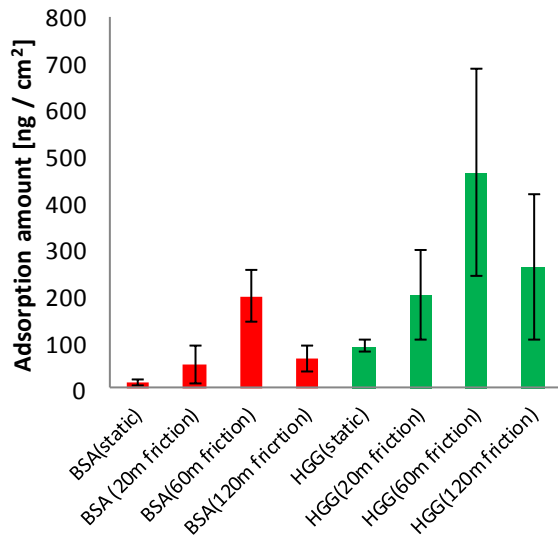


Fig.1 Protein adsorption amount under rubbing condition

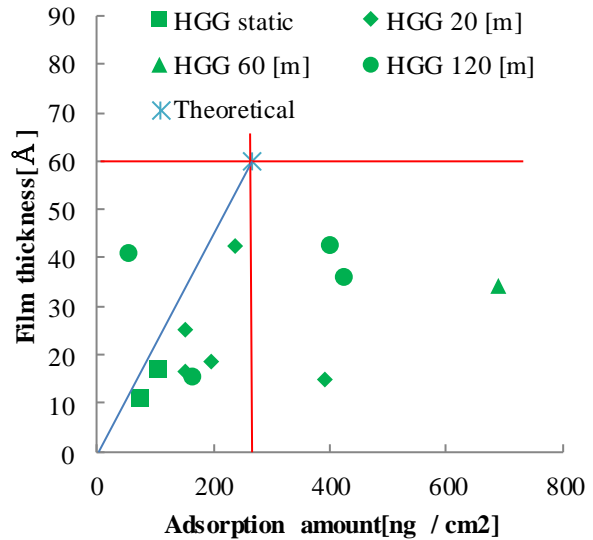


Fig.4 HGG adsorbed film thickness on glass plate

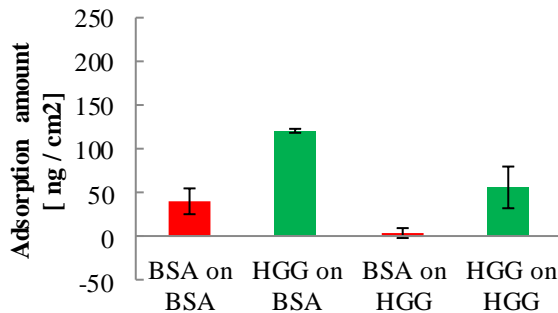


Fig.2 Protein adsorption amount on adsorbed protein film constructed under rubbing period 20 m

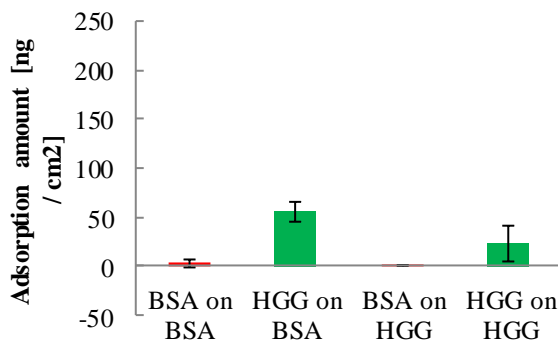


Fig.3 Protein adsorption amount on adsorbed protein film constructed under rubbing period 120 m

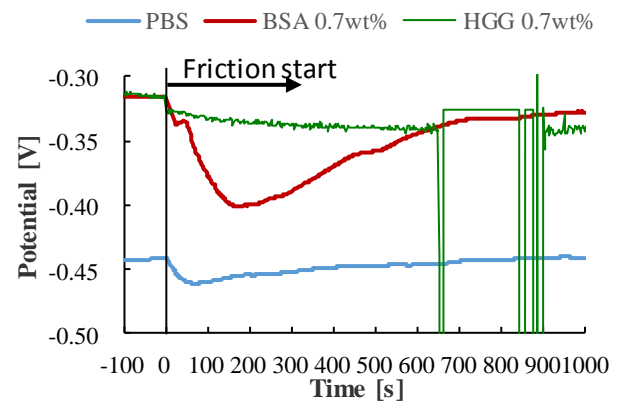


Fig.5 Potential transition in protein solution and PBS

The process can explain initial formation. Rich HGG film leads lamellar structure with low friction and wear.

4. CONCLUSIONS

Adsorption properties of proteins included in natural synovial fluid was observed. The initial process of protein adsorption under rubbing condition was clarified. Rubbing plays an important role to form bottom layer with rich HGG molecules.

A part of this work was supported by JSPS KAKENHI Grant Number 15K05765.

REFERENCES

- [1] T. Murakami, et. al., " The Adaptive Multimode Lubrication in Knee Prostheses with Artificial Cartilage during Walking," *Proceedings of the 23rd Leeds-Lyon Symposium on Tribology held in the Institute of Tribology*, Vol. 32, No. 6, pp. 371-382, 1997.
- [2] K. Nakashima, et. al., " Study on Wear Reduction Mechanisms of Artificial Cartilage by Synergistic Protein Boundary Film Formation," *JSME Int., Ser. C*, Vol. 48, No. 4, pp. 555-561, 2005.

1. BSA and HGG adsorb on the surface, but HGG amount is much compared with BSA adsorption amount
2. Adsorbed protein film is sheared by counter surface. BSA molecules are desorbed from surface, HGG rich layer is formed in the bottom.
3. Shear force makes HGG molecules denatured. The denatured HGG adsorbed film statically adsorbs HGG molecules included in lubricant.
4. HGG rich film is sheared again. Then HGG rich film grows in the bottom.

SURFACE ROUGHNESS OF HYPER-EUTECTIC AL-SI A390 IN HIGH SPEED MILLING

K. Othman¹, J. A. Ghani², C. H. Che Haron², and M. S. Kasim³

¹Production Technology Department, KT 3A, German Malaysian Institute, Jalan Ilmiah,
Taman Universiti, 43000 Kajang, Selangor.

²Department of Mechanical and Material Engineering,
Faculty of Engineering and Built Environment, Universiti Kebangsaan Malaysia,
43600 Bangi, Selangor, Malaysia.

³Department of Process, Faculty of Manufacturing Engineering,
Universiti Teknikal Malaysia Melaka, Hang Tuah Jaya, Melaka, Malaysia.

1. INTRODUCTION

A hypereutectic Al-Si alloy piston has great potential for use in the automotive industry, especially for engine components, due to its light weight, excellent castability, good thermal conductivity, high strength and excellent resistance to corrosion [1]. Due to its mechanical properties of light weight and high corrosion resistance, aluminum alloy is the main choice for piston in automotive application [2]. Aluminium-Si alloy can be divided into 3 categories, based on the percentage of silicon, i.e. 12-13 % of silicon (Si) is classified as eutectic, below 12 % is classified as hypoeutectic, and above 14 % is classified as hypereutectic Al-Si alloy, as explained by Lee [3]. Due to the high content of Si, machining of this type of material is very challenging. In this study milling of A390 at high cutting speed regime was carried out in order to evaluate the surface roughness obtained. The Si content for A390 is between 17-18%, which indicate this material is very abrasive and to achieve smooth surface in milling process is challenging.

2. METHODOLOGY

In this study the material A390 was utilized. The chemical composition of this material is shown in Table 1.

The cutting tool used was DL1000 grade from Sumitomo (diamond like coating (DLC) - aurora coating) with cutter diameter of 50 mm.

The experiment was performed with a high speed milling regime for milling aluminum alloy. The factors and level used is shown in Table 2.

The cutting speed (Vc), feed rate (Fz), and axial (Ap) depth of cut (Ae) used was suitable for a high speed machining regime of aluminum alloy. The cutting speed (Vc) was in the range of 900-1700m/min. The feed rate was 0.02-0.06 mm/tooth which is suitable for the finishing cut. The axial depth of cut was 0.2-0.4 mm, which is also suitable for the finishing cut.

The machine used was the Spinner VC450 Machining Centre with a capacity of 5.6 kW power and 23 Nm torque. The machining was carried out in a dry condition. A Mitutoyo Surftest SJ-310 surface roughness tester was used for measuring the roughness values of the machined surface.

The measurement was taken after the milling was performed and was repeated 3 times to find the average and standard deviation values.

Table 1 Chemical composition of work material of A390 in wt% [4]

Chemical composition (%)						
Al	Si	Cu	Mg	Fe	Ti	P
balance	17.51	4.12	0.43	0.28	0.06	0.06

Table 2 Factor and level used in the experiment

Factor/Level	0	1	2	3	4	5	6	7
Cutting Speed Vc (m/min)	900	1100	1200	1300	1400	1500	1600	1700
Feed Fz (mm/tooth)	0.02		0.04			0.06		
Axial depth -Ap (mm)	0.2		0.3		0.4			

3. RESULT AND DISCUSSION

Table 3 shows the result of average of Ra obtained in the experiment. It shows that for this range of milling conditions the $Ra \leq 0.5 \mu m$. This indicates very smooth surface finish can be achieved by implementing high speed machining concept even though the material is very abrasive.

Table 3 Average of Ra obtained in the experiment

Cutting speed Vc (m/min)	Feed rate (mm/tooth)	Axial Doc (mm)	Average Ra	Cutting speed Vc (m/min)	Feed rate (mm/tooth)	Axial Doc (mm)	Average Ra
900	0.02	0.2	0.15	1300	0.04	0.4	0.30
900	0.04	0.3	0.18	1300	0.06	0.2	0.31
900	0.06	0.4	0.18	1500	0.02	0.4	0.27
1100	0.02	0.3	0.18	1500	0.04	0.2	0.42
1100	0.04	0.4	0.27	1500	0.06	0.3	0.43
1100	0.06	0.2	0.35	1200	0.02	0.2	0.16
1300	0.02	0.4	0.19	1200	0.04	0.3	0.33
1300	0.04	0.2	0.35	1200	0.06	0.4	0.45
1300	0.06	0.3	0.36	1400	0.02	0.3	0.17

1000	0.02	0.2	0.21	1400	0.04	0.4	0.31
1000	0.04	0.3	0.29	1400	0.06	0.2	0.42
1000	0.06	0.4	0.36	1600	0.02	0.4	0.25
1200	0.02	0.3	0.14	1600	0.04	0.2	0.38
1200	0.04	0.4	0.21	1600	0.06	0.3	0.69
1200	0.06	0.2	0.34	1300	0.02	0.2	0.16
1400	0.02	0.4	0.16	1300	0.04	0.3	0.26
1400	0.04	0.2	0.30	1300	0.06	0.4	0.35
1400	0.06	0.3	0.50	1500	0.02	0.3	0.17
1100	0.02	0.2	0.18	1500	0.04	0.4	0.21
1100	0.04	0.3	0.20	1500	0.06	0.2	0.31
1100	0.06	0.4	0.32	1700	0.02	0.4	0.14
1300	0.02	0.3	0.15	1700	0.04	0.2	0.19
				1700	0.06	0.3	0.24

ANOVA for Response Surface Linear Model is shown in Table 4.

Table 4 ANOVA for Response Surface Linear Model

Source	Sum of Squares	DF	Square	Value	Prob > F
Model	0.32	3	0.11	16.57	< 0.0001
A	0.028	1	0.028	4.42	0.0418
B	0.29	1	0.29	44.96	< 0.0001
C	2.128E-003	1	2.128E-003	0.33	0.5667
Residual	0.26	41	6.380E-003		
Cor Total	0.58	44			

The Model F-value of 16.57 implies the model is significant. There is only a 0.01% chance that a "Model F-Value" this large could occur due to noise.

Final Equation in Terms of Coded Factors:

$$Ra = 0.28 + 0.046 * A + 0.098 * B - 8.422E-003 * C$$

This equation indicates that the Ra increases with the cutting speed and feed rates, whilst the effect of depth of cut is considered negligible. This relationship is supported by the 3D surface plot using Design Expert 6 as shown in Fig. 1.

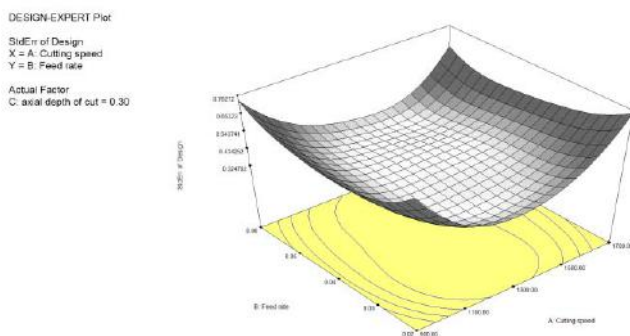


Fig. 1 3D surface plot

Fig. 2 shows the normal plot of the residuals that indicate the model is adequate.

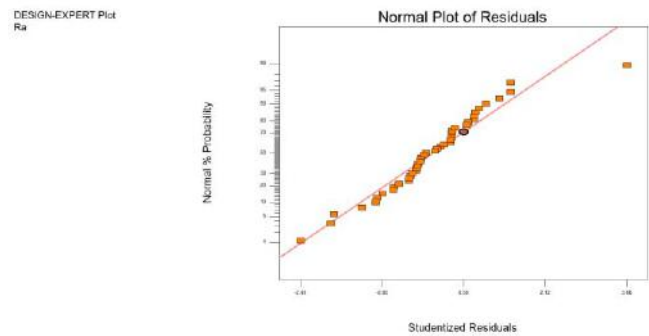


Fig. 2 Normal plot of the residuals

4. CONCLUSIONS

Smooth surface finish of less than 0.5 μm can be achieved by machining at high cutting speed with very low feed rate and depth of cut for abrasive A390 material. ANOVA found that cutting speed and feed rate are the most influential factors that affecting the Ra produced.

REFERENCES

- [1] Alireza Hekmat-Ardakan, Frank Ajersch, "Thermodynamic evaluation of hypereutectic Al-Si (A390) alloy with addition of Mg," Acta Materialia, vol.58, pp.3422-3428, 2010.
- [2] Muzaffer Zeren. "The effect of heat-treatment on aluminum-based piston alloys". Material and design 28 (2007) 2511-2517.
- [3] Jonathan A. Lee. "Cast aluminum alloy for high temperature application". The 132nd TMS Annual Meeting & Exhibition San Diego Convention Centre, San Diego, CA. 2003.
- [4] Guoji Cha, Jianguo Li, Shoumei Xiong, Zhiqiang Han, "Fracture behaviors of A390 aluminum cylinder liner alloys under static loading," Journal of Alloys and Compounds, vol.550, pp.370-370, 2013.

TRIBOLOGICAL ACTION AND CUTTING PERFORMANCE OF LUBRICANT ESTER IN MQL MACHINING

T. WAKABAYASHI¹

¹Kagawa University, Takamatsu, 761-0396, Japan.

1. INTRODUCTION

Minimal quantity lubrication (MQL) machining has already been well recognized as representative environmentally friendly machining in a number of practical applications [1]. In order to achieve successful MQL machining, cutting lubricants would play a significant role because they should be supplied to the cutting zone in a very small amount. Under the circumstances, a synthetic biodegradable polyol ester, rather than vegetable based oils, has presented the optimal characteristics as a cutting lubricant [2, 3]. If an ester works as an effective lubricant, its tribological action is usually resulted from the formation of an excellent lubricating film by means of some strong chemical adsorption onto sliding surfaces. This paper therefore discusses the tribological action of the lubricant ester in connection with its cutting performance encountered in practical MQL machining.

2. EXPERIMENTAL METHODS

2.1. Controlled Atmosphere Cutting Apparatus

Fig. 1(a), illustrates a high vacuum cutting apparatus (setup A) consisting of a cutting chamber, a quadrupole mass spectrometer, a cutting force dynamometer, a workpiece assembly, a cutting tool and two gas leak valves. The atmosphere in the chamber can be maintained at the vacuum level of 5×10^{-5} Pa by two turbo molecular pumps. A mass spectrometer monitors the ion currents of gases in the chamber. Two different gases can be supplied into the chamber through individual leak valves. Each gas was introduced to make its ion current equivalent to the pressure of 0.01 Pa.

Fig. 1(b) shows a normal atmosphere cutting apparatus (setup B) which has the same cutting configuration as that of setup A. This apparatus was prepared to examine the cutting performance in actual MQL machining with various carrier gases. The specifications of the synthetic polyol ester used in MQL machining are listed in Table 1 and this ester has been developed as an optimal MQL lubricant [2, 3]. MQL mists were supplied externally and close to the cutting interface by a pressurized gas of 0.2 MPa.

The machining process used for both setups was orthogonal using metal disks with the width of 1.2 mm. The rotational speed of the disk and the feed rate of the tool were adjusted synchronously to maintain the constant cutting speed and depth of cut. Table 2, presents the cutting conditions of the tests using the above setups A and B.

Table 1: Specifications of synthetic polyol ester

Density (15 °C)	0.95 g/cm ³
Kinematic Viscosity (40 °C)	19.1 mm ² /s
Biodegradability (CEC L-33-A-93)	100 %

Table 2: Cutting conditions of the tests for setups A and B

	Setup A	Setup B
Cutting speed	12 m/min	60 m/min
Tool feed	0.02 mm/rev.	0.06 mm/rev.
Workpiece	JIS* SCM435 steel	JIS* S45C steel
Tool	Uncoated cemented carbide insert	

* Japanese Industrial Standard

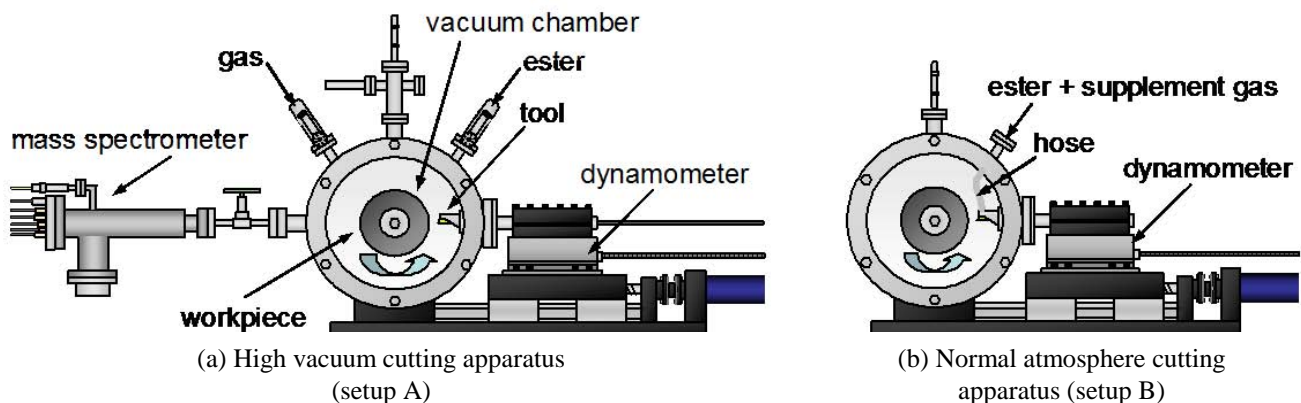


Fig. 1: Experimental setups of controlled atmosphere cutting apparatus

2.2. Adsorption Activity Measurement

In the test using the setup A, the experimental procedures of measuring adsorption activity are as follows. After inlet and outlet gas flows are balanced, the introduced gas pressure becomes constant. Then, the tool starts machining the steel disk specimen at a given cutting speed and a feed rate to create a clean surface of the metal. If the introduced gas adsorbs onto, or reacts with, this freshly cut metal surface, its pressure decreases. According to Mori's method [4], a linear relationship can be obtained on semi-logarithmic diagram. The adsorption activity of the gas component can readily be calculated as an absolute value from the slope of this relation. It should be noted that this calculation provides the same slope even if ion current is used instead of pressure because of the linear relation between them. The adsorption activity is a quantitative measure of gas molecule's affinity for the clean metal surface.

3. RESULTS AND DISCUSSION

3.1. Adsorption Activity Evaluation with Setup A

Fig. 2 compares the adsorption activity of methyl propionate, a model ester, with that of n-Hexane representing hydrocarbons. Methyl propionate shows relatively high adsorption activity in both cases with argon and oxygen. Here, chemically inactive argon is introduced to make the partial pressure of the ester in the chamber same as that when the ester and oxygen are introduced together. n-Hexane shows no significant adsorption because hydrocarbons have no polar group to adsorb on the metal surface. It is considerably interesting that the adsorption activity of methyl propionate is increased if oxygen is present. This result suggests that oxygen can enhance the adsorption ability of ester. This situation may be very similar to the behavior of a lubricant in MQL cutting because, even near the cutting point, the lubricant particles are surrounded by a large amount of air containing oxygen.

In MQL cutting, therefore, the reactivity of the lubricant ester is supposed to be intensified by atmospheric oxygen, leading to the formation of a robust and tribologically effective lubricating film. As a matter of fact, the cutting force evaluated for the ester with oxygen was somewhat lower than that for the ester with each of inert gases. However, the degree of cutting force reduction was only several %, probably because the length of alkyl chain provided by methyl propionate was not enough to form a robust lubricating film. Thus, the influence of oxygen on the cutting performance of synthetic ester should further be discussed in the case of actual MQL machining with the setup B.

3.2. MQL Cutting Performance with Setup B

In actual MQL machining with the setup B, synthetic polyol ester of Table 1 was applied as MQL media and the influence of different carrier gases on the cutting force was

investigated using nitrogen, air and oxygen. Fig. 3 shows the resultant cutting force obtained in this MQL machining, obviously demonstrating the better cutting performance in the order of higher oxygen concentration in the carrier gas.

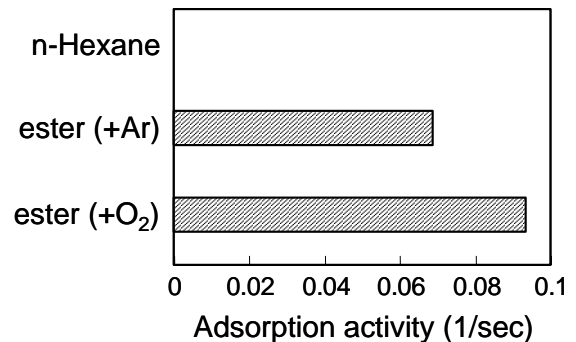


Fig. 2: Values of measured adsorption activity

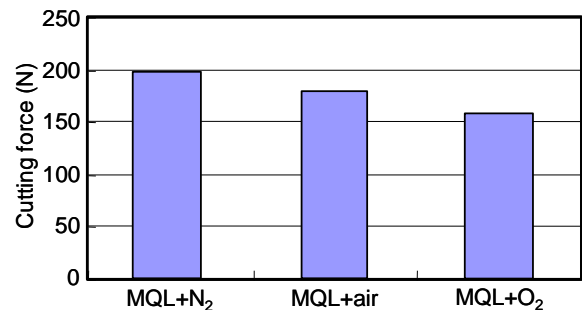


Fig. 3: Cutting force obtained in MQL machining with different carrier gases

4. CONCLUSIONS

Using the controlled atmosphere machining apparatus, this study presented the adsorption characteristics of a model ester and oxygen were complementary and, further, the ester and oxygen were likely to enhance mutually their adsorption activities. The experimental facts obtained by normal atmosphere cutting apparatus demonstrated that an optimal synthetic ester for MQL machining provided the better cutting performance in the order of higher oxygen concentration in the carrier gas. These results suggested that the cutting phenomena could tribologically be in good connection with the adsorption behavior of the ester and atmospheric gases.

REFERENCES

- [1] K. WEINERT *et al.*, "Dry Machining and Minimum Quantity Lubrication," *CIRP Annals*, Vol.53, No.2, pp.511-537, 1976.
- [2] S. Suda *et al.*, "A synthetic ester as an optimal cutting fluid for minimal quantity lubrication machining," *CIRP Annals*, Vol.51, No.1, pp.95-98, 2002.
- [3] T. Wakabayashi *et al.*, "Tribological characteristics and cutting performance of lubricant esters for semi-dry machining," *CIRP Annals*, Vol.52, No.1, pp.61-64, 2003.
- [4] S. MORI *et al.*, "Chemisorption of Organic Compounds on a Clean Aluminum Surface Prepared by Cutting under High Vacuum," *ASLE Trans.*, Vol.25, No.2, pp.261-266, 1982.

THE DIFFERENCE OF DIMPLE STRUCTURES FABRICATED USING TURNING AND MILLING MACHINES

M. N. A. B. M. Dali^{1,2}, J. A. Ghani², C. H. C. Haron², and S. Hassan^{1,2}

¹*Politeknik Ungku Omar, Jalan Raja Musa Mahadi,
31400 Ipoh, Perak, Malaysia.*

²*Department of Mechanical and Material Engineering,
Faculty of Engineering and Built Environment, Universiti Kebangsaan Malaysia,
43600 Bangi, Selangor, Malaysia.*

ABSTRACT

Dimple structure geometries like shape, size, depth, area ratio and array are among the important issues as the main role for micro lubricating reservoir and minimizing friction and wear rate during sliding of mechanical components. Turning and milling processes were used in this research to produce various geometries of dimple structure resulted in turning process was able to produce three shapes of dimple structure (spherical, short drop and long drop), whereas milling process was able to produce circle shape. The range of sizes of dimple structures produced were width (153 μm - 999 μm), length (964 μm - 3261 μm), diameter (15 - 30 μm), depth (37 μm - 155 μm) and area ratio (2.7 - 13.8 %). These range of sizes, depths, area ratios and array produced were within the limit obtained by earlier researchers which will minimize the friction and wear for sliding mechanical components.

1. INTRODUCTION

The issue of friction and wear particularly on sliding components is the problem that has long existed in manufacturing, automotive and aerospace industries. Surface treatment process or dimple structure especially on mechanical components is one of the methods to overcome this problem in order to avoid the occurrence of system failure [1]. The distribution of micro dimples in relation to textured surfaces acts as a lubrication reservoir and is able to reduce friction by 30% [2]. Various methods exist and have drawn the attention of researchers especially tribology members to search for the effective and efficient method in the dimple structure fabrication. Processes like etching, laser beam, laser coating, photochemical, and many more. From the stated processes, chemical based process or energy beam process is effective in dimple structure production but there arise several negative issues like environmental effect, flexibility, cost and production rate [3]. However the accuracy as well as the efficient fabrication of micro structure as textured surface are still the major challenges in research world [4]. Therefore, as a selection of an alternative process, machining process is the best judgement to produce dimple structure [3,6]. This view is in line that machining process has the absolute advantage in terms of cost, lower energy and time too [5]. Geometries like area ratio, depth and diameter are the main parameters than can affect tribology attributes [7]. Based on the

importance of various structure geometries that were studied by earlier researchers, therefore through this research, turning and milling processes were selected as methods to produce dimple structure. It is also based on the potential of the machining itself which able to produce multiple sizes, shapes, depth, area ratios and dimple structure arrays. In addition, the difference in dimple structure geometries produced from both processes were studied, analyzed and compared.

2. METHODOLOGY

Experiments were conducted using CNC Lathe Colchester Tornado and Sajo UF-52 Vertical Milling with assisted toolings developed in house for generating vibration on the cutting tool in both machining processes. The following is the simple flowchart of the research which covers determination of important parameters, the development of assisted tooling, experiment procedure, analysis and evaluation procedure.

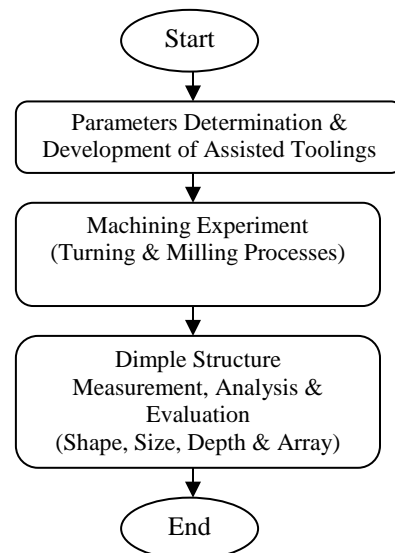


Fig. 1 Flowchart

3. RESULT AND DISCUSSION

By using Design of Experiment (Taguchi) in conducting experiment, four shapes of dimple were produced (turning

and milling processes) i.e. spherical, short drop, long drop and circle with the array approaching square, hexagon and square.

Table 1 Shapes with the arrays (Turning Process)

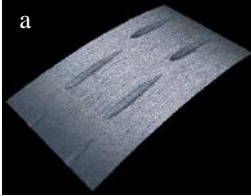
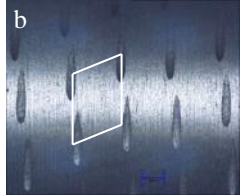
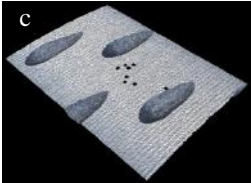

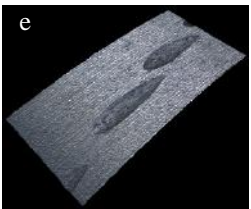
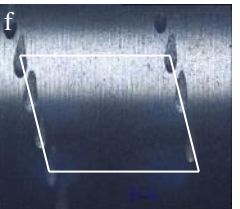
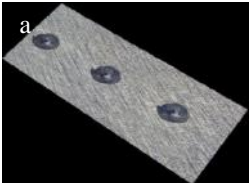
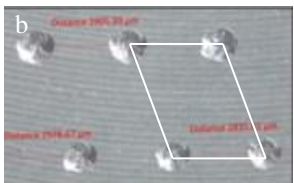
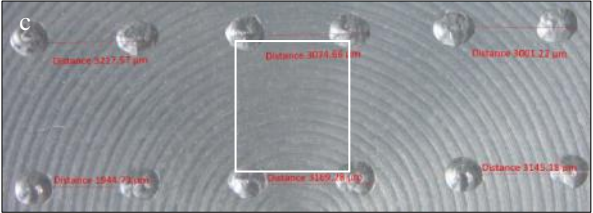
3D view	Array	Shapes
		Long drop
depth = 64 μm , width = 397 μm , length = 3261 μm , area ratio = 9 %		
		Spherical
depth = 155 μm , width = 999 μm , length = 2800 μm , area ratio = 13.8 %		
		Short drop
depth = 66 μm , width = 560 μm , length = 2420 μm , area ratio = 8.5 %		

Table 2 Circle shape with arrays (Milling Process)

3D view	Array
	
	
depth = 45 μm , diameter = 69 μm & area ratio = 6.5 %	

There are some differences between dimple structures produced using milling and turning processes i.e. in the form of shape and array. Turning process was able to produce more shapes by using various cutting tool

geometries. Similarly for the arrays, hexagon and almost square arrays were obtained. On the other hand, for milling process, dimple shape produced was limited to one type only. This was due limited to one rotating condition of the cutting tool during machining which would only form a circle shape. But various arrays could be produced since it can be controlled during the machining process. Based on shapes and area ratio derived i.e. width range (153 μm - 999 μm), length (964 μm - 3261 μm), diameter (110 - 890 μm), depth (37 μm - 155 μm) and area ratio (2.7 - 13.8 %) they were within the range studied and derived by earlier researchers i.e. equivalent diameter (20 μm - 4 mm), area ratio (7 - 40 %) and depth (200 nm - 100 μm) as reported [6]. The outcome was in line with the research done [8] that tested shape and area ratio of dimple structure of 3 shapes i.e. circle, long drop and short drop with width geometry (500 - 800 μm), length (800 - 1600 μm), depth (55 - 60 μm) and area ratio (7.5 - 20 %). Circle shape and long drop shape could minimize coefficient of friction more than short drop shape. Overall, dimple geometry structure derived has the potential in minimizing coefficient of friction and wear on mechanical component plus upgrading tribology attributes.

4. CONCLUSION

There are some differences between dimple structures produced using milling and turning processes i.e. turning process was able to produce more shapes but for milling process was limited to one type only.

REFERENCES

- [1] A. Amanov, I.S. Cho, Y.S. Pyoun, C.S. Lee, I.G. Park. 2012. "Micro-dimpled surface by ultrasonic nanocrystal surface modification and its tribological effects". *Wear*, 286-287, 136-144.
- [2] A.A.G. Bruzzone, H.L. Costa, P.M. Lonardo, and D.A. Lucca. 2008. "Advances in engineered surfaces for functional performance". *CIRP Annals: Manufacturing Technology*, Vol. 57, pp.750-769.
- [3] T. Matsumura, M. Serizawa, T. Ogawa, M. Sasaki. 2014. "Surface Dimple Machining in Whirling". *Journal of Manufacturing System xxx(2014) xxx-xxx* article in Press.
- [4] P. Guo, K. F. Ehmann, 2013, "Development of a Tertiary Motion Generator for Elliptical Vibration Texturing", *Precision Engineering*, vol. 37, pp. 364-371.
- [5] R. Zhang, P. Steinert, A. Schubert. 2014. "Microstructuring of surface by two-stage vibration-assisted turning," 6th CIRP International Conference on High Performance Cutting, HPC2014, vol.14, pp. 136-141.
- [6] T. Roy, D. Choudry, A. B. Mamat, B. P. Murphy. 2014. "Fabrication and Characterization of Micro-dimple Array on Al_2O_3 Surfaces by Using a Micro-tooling", *Ceramic International* 40, 2381-2388.
- [7] H. Yu, W. Huang and X. Wang, "Dimple patterns design for different circumstances". *Lubrication Science* (2011).Published online in Wiley Online Library. DOI: 10.1002/ls.168
- [8] L. Galda, P. Pawlus, Jaroslaw Sep. 2009. "Dimples shape and distribution effect on characteristics of Stribeck curve". *Tribology International* 42, 1505-1512

EFFECT OF STIR CASTING PROCESS PARAMETERS ON TRIBOLOGICAL PERFORMANCE OF Al6061-SiC_p COMPOSITE

A. A. Adebisi¹, M. A. Maleque¹, and K. A. Bello¹

¹International Islamic University Malaysia,
Faculty of Engineering, Department of Manufacturing and Material Engineering,
53100 Kuala Lumpur, Selangor, Malaysia.

1. ABSTRACT

In this study, the tribological performance of Al6061-SiC_p composite is investigated considering the influence of stir casting process parameters. The wear and frictional characteristics were studied using the dry reciprocating wear testing machine. Experimentation is generated through the central composite design (CCD) using a four factor five level design plan. The process parameters (reinforcement fraction *wt%*, stirring speed *rpm*, processing temperature °C and processing time *s*) are examined using ANOVA and multiple objective optimization (MOO) analysis. The result shows that stirring speed has the most significant contribution in controlling the wear and friction characteristics. Confirmation test is also conducted to verify and validate the process parameters in order to optimize the tribological output. Moreover, characterization of the composite wear scar mechanism is performed using scanning electron microscope. This study provides an effective method of minimizing the tribological properties of Al6061-SiC_p composite by optimizing the stir casting process parameters.

2. INTRODUCTION

The demand for superior performance and light weight materials for tribological applications in the automotive and aerospace industries has led to the development of advanced materials. Due to these requirements, metal matrix composite (MMC) have become attractive and are increasingly preferred over monolithic materials due to their high strength to weight ratio, toughness and tribological characteristics [1]. As a result, aluminium based particulate reinforced MMC has attracted much attention by researchers owing to its low density, high thermal conductivity, low melting point and the ability to be reinforced by a wide variety of reinforcement phases [2]. Moreover, numerous processing technique such as powder metallurgy, squeeze casting, liquid infiltration and stir casting can be employed in developing MMC. However, studies [3] have shown that stir casting process possesses a simple and cost effective route to fabricate particulate reinforced composite. With this, achieving optimal AMC properties has been major challenge due to the influence of several processing factors considered.

As a result, it is of utmost necessity to consider the simultaneously interaction of these factors. This is because when two or more factors are investigated together, the

effect of one factor on response depends on the level of the other factor. CCD has been a preferred method because it is a very efficient method to reduce the number of experiments with a large number of factors and levels. It provides high quality predictions in studying linear, quadratic and interaction effects of factors influencing the response [4]. It is also capable of achieving optimum conditions required to attain the best characteristic properties. Most studies conducted with experimental design are conducted using powder metallurgy route, however very limited report have been made on stir casting technique with CCD. Therefore, the aim of this study is to utilize the CCD to achieve optimal tribological performance of Al6061-SiC_p composite. Crucial parameters considered for the stir casting process include the reinforcement fraction *wt%*, stirring speed *rpm*, processing temperature °C as well as the processing time *s*.

3. METHODOLOGY

The CCD of response surface methodology (RSM) accommodates five levels of each factors comprising of factorial, axial and center points as shown in Table 1

Table 1 Factors and levels in CCD plan

Factors	Levels				
	-2	-1	0	+1	+2
RF: Reinforcement fraction (<i>wt %</i>)	5	10	15	20	25
SS: Stirring speed (<i>rpm</i>)	200	300	400	500	600
PT _{emp} : Processing temperature (°C)	700	750	800	850	900
PT: Processing time (<i>secs</i>)	60	90	120	150	180

Wear test is conducted with a dry reciprocating wear and friction monitor according to ASTM D 6079-97/EN 590. The test utilized an applied load of 50 *N* at 600 *rpm* for 30 *mins* for each of the cast AMC from the design plan. The wear characteristics is calculated as expressed in the eq. (1):

$$w_r = \frac{\Delta m}{\rho t} \quad (1)$$

Δm = mass loss, ρ = density, t = time

4. RESULTS AND DISCUSSION

According to ANOVA, the response (wear rate w_r and friction coefficient μ) output indicates a quadratic relationship based on regression analysis with the processing factors. The tribological performance models suggested are dependent on the significant terms with p

values < 0.05 . To improve the model and also optimize the results insignificant terms are eliminated. The fitness and adequacy of the tribological output ($w_r = 0.19$, $\mu = 0.15$) is confirmed by ensuring the R^2_{pred} and R^2_{adj} has a difference of < 0.2 . The factor with the most influencing impact in order of importance on w_r are SS, PT_{emp} and RF. Fig. 1 shows the 3D surface plot of the process parameters interaction on w_r . Fig. 1(a) depicts the influence of SS and PT_{emp} which achieved a minimum w_r of $1.21 \times 10^{-5} \text{ mm}^3/\text{min}$ at 530 rpm and 825 °C. Also, Fig 1(b) shows that SS and RF which attained minimum w_r of $1.22 \times 10^{-5} \text{ mm}^3/\text{min}$ at 520 rpm and 16 wt%.

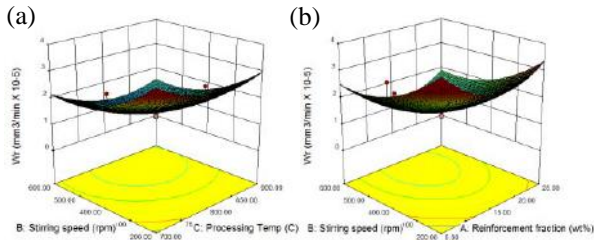


Fig. 1 3D surface plot of w_r performance considering (a) SS and PT_{emp} (b) SS and RF

For μ , SS and RF are the only factors which influences the output performance. Stable μ (0.39-0.41) is attained within the range of 500-540 rpm and 13-18 wt% respectively as shown in Fig. 2.

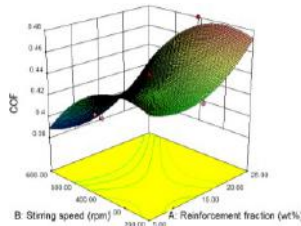


Fig. 2 3D surface plot of w_r performance for SS and RF.

In optimization analysis, the condition required is to minimize the w_r and μ properties. Therefore, the MOO is used to achieve a set of process factors which simultaneously optimizes the tribological performance. Table 2 shows the optimal generated desirability of the response with solution No. 1 selected as the predicted optimal by 84 % desirability.

Table 2: Optimal solution generated for response

RF	SS	PT_{emp}	PT	w_r	μ	Desir.	
14.283	500.000	827.747	150.000	0.974	0.405	0.838	Selected
14.300	499.999	828.556	150.000	0.974	0.405	0.838	
14.240	500.000	828.217	150.000	0.976	0.405	0.838	

Confirmation test were conducted three times to validate the predicted optimal process parameters in order to verify the MOO analysis. Fig. 3 shows that the percentage error of the response (w_r , μ) are within the range of 1.2 to 3.5%. The topography of the worn surface is characterized as relatively smooth mild wear without formation of cracks and craters. Also, the formation of oxide layer on the wear

surface is represented as a brownish dark layer on AMC sample. However, it is viewed as the whitish scale profile as seen in Fig. 4 (a).

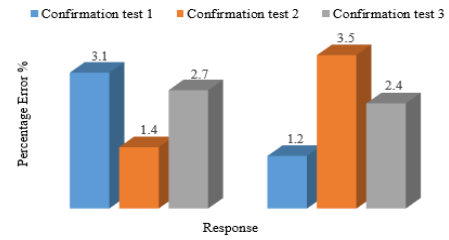


Fig. 3 Percentage error analysis between predicted and actual response

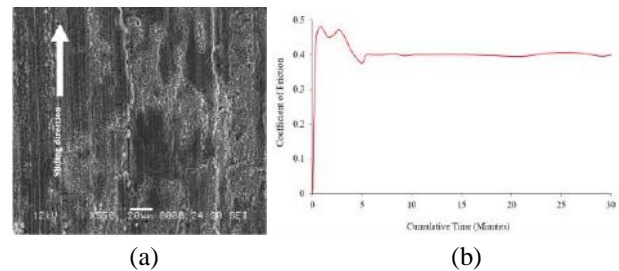


Fig. 4 (a) Wear surface morphology and (b) frictional performance for optimized Al6061-SiC_p composite

This layer serves as a protective surface which improves the abrasion and adhesive resistance. Moreover, the layer acts as a coating shield protecting against excessive wear and also stabilizes frictional performance as shown in Fig. 4(b).

5. CONCLUSIONS

The optimum input process factor that achieved optimized tribological performance of Al6061-SiC_p composite are 14 wt% RF, 500 rpm SS, 828 °C PT_{emp} and 150 s PT. These conditions achieved a w_r of $0.974 \times 10^{-5} \text{ mm}^3/\text{min}$ and μ of 0.41 with a desirability value of 84%.

6. REFERENCES

- [1] A. A. Adebisi, M. A. Maleque and M. Y. Ali, "Wear characteristics of multiple particle size silicon carbide reinforced aluminium composite," *Adv. Mater. Res.*, Vol. 1115, pp. 174-177, 2015.
- [2] Hariprasad T, Varatharajan K, Ravi S., "Wear characteristics of B₄C and Al₂O₃ reinforced with Al-5083 metal matrix based hybrid composite," *Procedia Eng*, Vol. 97, pp. 925-929, 2015.
- [3] Sozhamannan G.G., Balasivanandha S.P., "Effect of processing parameters on metal matrix composites: stir casting process," *J Surf Eng Mater Adv Technol*, Vol. 2, pp. 11-15, 2012.
- [4] Suresh S., Moorthi N.S.V., Vettivel S., Selvakumar N., "Mechanical behavior and wear prediction of stir cast Al-TiB₂ composites using response surface methodology," *Mater. and Des*, Vol. 59, pp. 383-396, 2014.

THE INFLUENCE OF FRICTION FORCE ON THE HIGHER-ORDER STRUCTURE OF FILLED RUBBER

T. Iwai¹, K. Murata¹, and Y. Shoukaku¹

¹College of Science and Engineering, Kanazawa University, Japan.

1. INTRODUCTION

Fuel efficiency tires are developed due to the recent rise in the environmental problems. Carbon black (CB) are usually used as the reinforcing filler for tread rubber of general tires. On the other hand, Silica (Si) was used as the reinforcing filler for fuel efficiency tire. It is well known that silica-filled rubber decrease in rolling resistance of tire. However, the wear of silica-filled rubber as compared with that of carbon black-filled rubber is thought to be either larger or lower. The rubber mixed with CB and Si forms three-dimensional network structure. The molecular chains of rubber react with CB and silica physicochemically. The bound molecular chain on the filler surface is called bound rubber and constrained rubber inside filler aggregates is defined occluded rubber. The higher-order structure of filled rubber consists of bound rubber, occluded rubber, and unconstrained rubber. Some reports said that the decrease in the repeated stress occurred owing to the change in restrained rubber after the wear test. However, the influence of friction force on the higher-order structure of filled rubber are not clearly understood.

The purpose of this study is to clarify the change in the higher-order structure of the carbon-black filled and the silica-filled rubber using atomic force microscope

2. EXPERIMENTAL

2.1. Specimens

The main formulation of rubber specimens were shown in Table 1. 103.13 phr (parts per hundred parts of rubber) styrene butadiene rubber mixed with 25 phr butadiene rubber was used. The mixture amount of Si and CB varied from 0 phr to 25 phr respectively, whereas the total amount of fillers was fixed 25 phr. Unfilled specimen was also studied for the comparison. Stainless metal gauze was used as the mating surface for the friction test.

2.2. Apparatus and method

A pin-disk type tribometer was used for the friction test. The schematic diagram of the apparatus is shown in Fig. 1.

Table 1 Main formulation of rubber specimen
 phr: parts per hundred parts of rubber

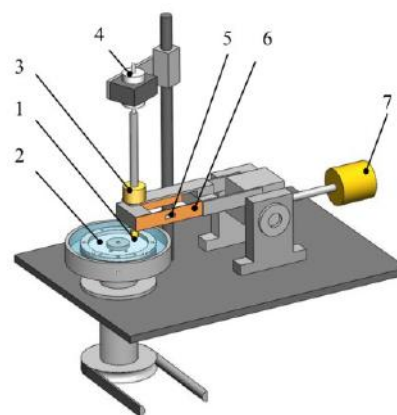
A rubber pin specimen was rubbed to the mating stainless gauze fixed on the rotating disk. Friction force was detected by strain gauges affixed to the parallel leaf springs and wear depth was measured by a differential transducer as the decrease in the thickness. The dimensions of the rubber specimen were 3 x 3 x 1 mm. The normal load was 1.8N (0.2MPa) for filled rubber and 0.49N (0.06MPa) for unfilled rubber. The sliding speed was 10 mm/s.

The higher-order structure in the rubber specimen was observed using an intermittent contact mode of atomic force microscope (AFM). This mode detected the phase change of the cantilever oscillation due to the hardness of the contact point. Harder substance such as bound rubber and filler is represented brighter area in the phase image obtained by the observation, though the unrestricted rubber is displayed darker tone.

AFM observation is conducted at the worn surface and at the cross-section immediately under the worn surface. In addition, rupture surface of tensile specimen after the tensile test was also observed for comparison.

3. RESULTS AND DISCUSSIONS

Optical micrograph of the worn surface were shown in Fig.2. Abrasion patterns perpendicular to the sliding direction were formed. It was clearly understood that rubber surface was severely damaged by the friction force. Figure 3 represents the AFM phase images of the rubber specimen before the experiment. The size of each observing area was 5μm x 5μm. A lot of small bright spots were distributed in



1; rubber specimen, 2; metal gauze, 3; dead weight, 4; differential transducer, 5; strain gauge, 6; parallel leaf spring, 7; counterbalance

Fig. 1 Schematic diagram of the apparatus

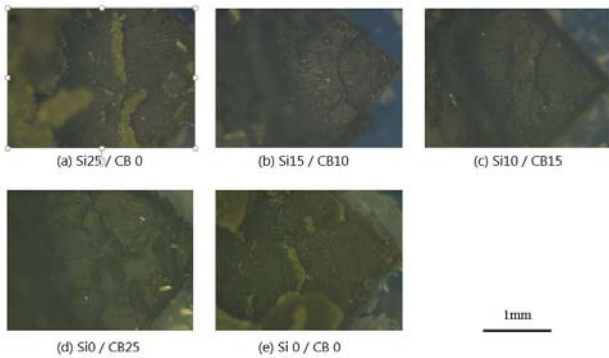


Fig.2 Optical micrograph of worn rubber surface

the observed area of filled rubber irrespective of CB contents. On the contrary, no bright spots were observed in the unfilled rubber. Consequently it was confirmed that these small light spots represent the restricted rubber, bound rubber and occluded rubber, or filler. Although two types of fillers were introduced, no differences in the phase lag and in the shape were seen. In consequence, the difference between the filler types were hardly distinguished.

The AFM phase images of worn surface after the experiment were shown in Fig. 4. It was found that the bright spots representing restricted rubber were fragmented as compared with the image obtained before the experiment. It seems the higher-order structure of filled rubber were destroyed by friction force. The cross-section of immediately under the worn surface were investigated to understand the extent of the destruction of restricted rubber by the friction force

Figure 5 represents the phase image in the vicinity of the worn surface. As a result, both the phase lag and the spot size were as the same as that of the initial situation. Accordingly, it is probably said that the extent of destruction of the restricted rubber influenced by the friction force is limited to the worn surface. Assuming the crack propagating on the surface when the rubber was worn by the friction, the restricted rubber was thought to be influenced by the crack propagation. Therefore the ruptured rubber surface of tensile test was also observed to confirm

the relation between crack propagation and fragment of restricted rubber. As compared with the initial specimen, the phase lag and bright spot size of the restricted rubber in the ruptured surface was identical. As a result, it was found that the restricted rubber such as bound rubber or occlude rubber were destroyed directly by frictional force, however, the restricted rubber was kept steady when frictional force acted indirectly to the restricted rubber or crack propagation region.

4. CONCLUSIONS

The higher-order structure of rubber at the worn surface was fragmented as compared with the initial state before the experiment. On the other hand, the higher-order structure immediately under the worn surface after the experiment and of the fracture surface after the tensile test were unchanged.

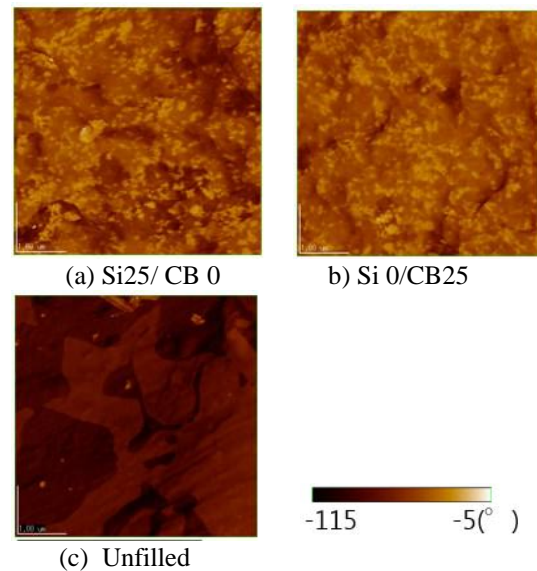


Fig.4 AFM phase image of worn rubber surface

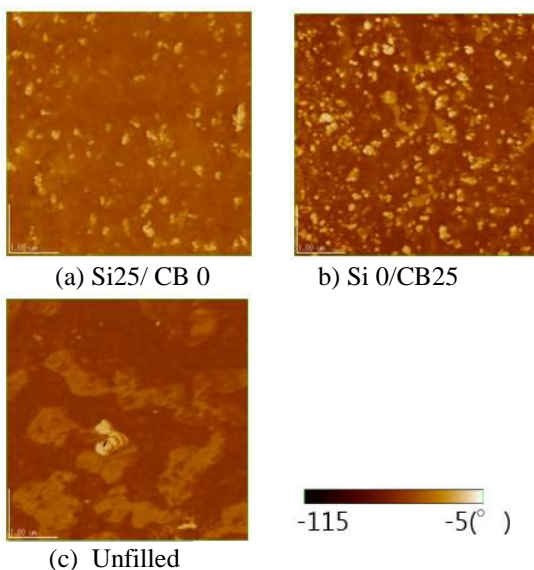


Fig.3 AFM phase image before the experiment

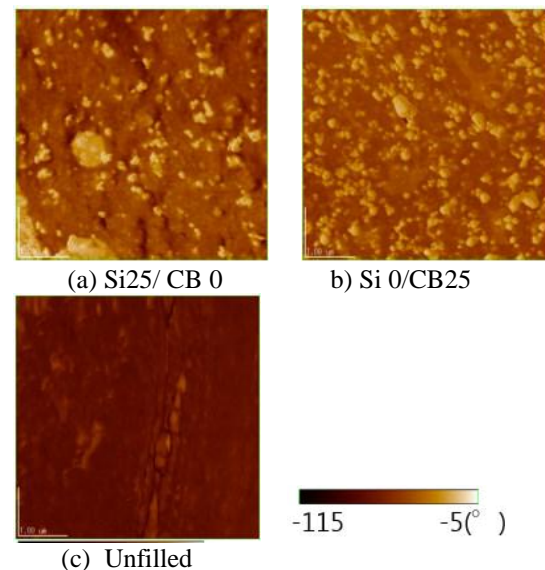


Fig.5 AFM phase image immediately under worn surface

BEARING LOAD CAPACITY OF A PALM KERNEL ACTIVATED CARBON-EPOXY COMPOSITE

D. N. F. Mahmud¹, M. F. B. Abdollah^{1,2}, N. A. B. Masripan^{1,2}, F. F. Shuhimi¹, H. Amiruddin^{1,2}, and N. Tamaldin^{1,2}

¹Faculty of Mechanical Engineering, Universiti Teknikal Malaysia Melaka, Hang Tuah Jaya, 76100 Durian Tunggal, Melaka, Malaysia.

²Centre for Advanced Research on Energy, Universiti Teknikal Malaysia Melaka, Hang Tuah Jaya, 76100 Durian Tunggal, Melaka, Malaysia.

1. INTRODUCTION

From previous studies, many researchers established that different types of solid lubricants can be applied in tribological applications such as material coating or reinforcement [1]. Hence, the development and formation of this tribolayer on sliding surfaces can affect the material tribological behaviour characteristics such as thickness, hardness, fracture, and materials composition [2]. The potential usage of local waste products as reinforcement substitute in the manufacturing of lightweight materials such as metal and polymer matrix composites has gained attention due to its self-lubricating properties and zero waste approach at an affordable cost [3]. Some research cases found that porous carbon, such as Palm Shell Activated Carbon (PSAC) have displayed capability to turn into a self-lubricating material when reinforced with aluminium alloy which can considerably improve wear resistance by increasing PSAC content up to 10 wt.% [4]. In the recent decade, studies regarding on Palm Kernel Activated Carbon (PKAC) have been widely conducted by numerous researchers due to its remarkable properties in the tribology field. Developed from waste materials of palm oil extraction process, it contains carbon properties and residual oils (natural lubricant) which can change into a new self-lubricating material with a low friction coefficient and high wear resistance. Thus, potential for zero waste strategy and improving tribological properties at an affordable cost can be attained by applying carbon materials formulated from agriculture wastes as a new reinforcement substitutes in the fabrication of polymer matrix composites [5]. Since there are a limited number of studies conducted regarding on the effects of applied load on PKAC materials as solid lubricants in polymer matrix composites, the aim of this project is to determine the load bearing capacity of PKAC-E composite under a dry sliding condition.

2. METHODOLOGY

In this research, PKAC were used as a self-lubricating material with high-density epoxy [West system 105 epoxy resin (105-B) and West system 206 slow hardener (206-B)]. The fine powder of PKAC was prepared using a crusher machine and sieved into particle sizes of 250 μm using a sieves shaker. The 60 wt% PKAC powder was then mixed

with 40 wt% epoxy of resin to hardener ratio 4:1. The mixture of PKAC and epoxy was then placed into a mould with a layer of wax before compressing it using a hot-press machine. The equipment was used at a working temperature and pressure of 80°C and 2.5MPa respectively

The sample was compressed in 10 minutes and then cooled down to room temperature for another 15 minutes before extracting it out from the mould. The completed disc specimens of 74mm in diameter and 5mm thickness were left to be cured at room temperature for one week. This can be seen in Fig. 1. The densitometer and shore hardness tester (Type D), were used to measure density and hardness respectively. Mechanical properties of the disc specimens and steel ball are shown in Table 1. The dry sliding test was conducted at a constant 60 wt% of PKAC using a ball-on-disc machine with according to standard ASTM G99-05 (2010). All tests were performed at speed 500 rpm and 3000m sliding distance with applied load between 20-100N. The morphology of the particles and worn surfaces were observed and analysed using a scanning electron microscope (SEM). Fig. 2 shows the schematic diagram of ball-on-disc tribometer.

Table 1: Mechanical properties of the ball and disc materials before testing

Properties	Disc (60 wt% PKAC + 40wt% epoxy)	Ball (carbon chromium steel)
Hardness (H), HRC	8.36	61
Density, ρ [g/cm ³]	1.4	7.79
Surface roughness (Ra), μm	0.4	0.022



Fig. 1 Sample of PKAC-E composite disc.

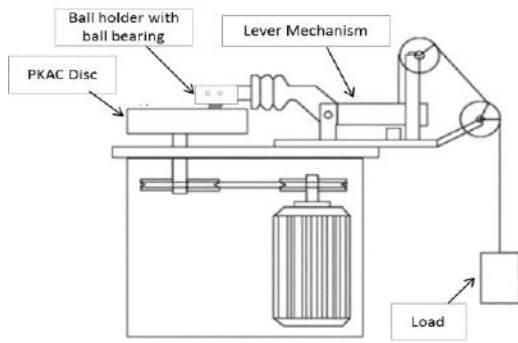


Fig. 2 Schematic diagram of ball on disc tribometer

3. RESULTS AND DISCUSSION

Fig. 3 shows the coefficient of friction, COF results of PKAC-E composite sliding against carbon chromium ball steel from the ball on disc test with increasing operating load. The tests were divided into three stages for a better understanding of tribological behaviour relating to contact mechanisms during the experiment process. As illustrated in Fig. 4, the first stage (Stage I) shows the COF value decreased dramatically. This could imply that when applied load is increased, the real surface contact area increases as well which in return causing more plastic deformation or damaging of asperities. As a result, surface roughness will diminish and would lead to decrease value of COF. Second stage test (Stage II) shown to have similar results which suggest that there are no significant differences statistically where the value of COF remains steady about 0.11. The result mentioned could be explained by the fact that the tribolayer generated from the preferential wear of the soft carbon material is caused by a carbon-based tribofilm adhering onto the counter surface which breaks the adhesive joints between the asperities [6]. Fig. 4(a) shows that the transfer layer of the PKAC-E material is formed on the counter surface thus helps to stabilise COF due to the surface contact change from PKAC-steel to PKAC-PKAC. This correlates with the results established by Mat Tahir et al. [5] in 2016. In the final stage (Stage III), the COF value significantly, where more friction is generated and abrasive wear occurred. Because of that, the transfer layer deteriorates making the ball bearing no longer have a protective layer to act as self-lubricant. This also means that the contact surface experienced high abrasion due to the ploughing of harshness between contacting surfaces which might influence on the increment of friction force [7]. Fig. 4(b) visualise a higher magnification micrograph of damaged regions and the formation of debris. From the above discussion, the overall results show that when the applied load exceeds 80N, the value of COF will increase again due to the breaking of the protective transfer layer. Therefore, the load bearing capacity for PKAC-E composite is proposed to be 80N.

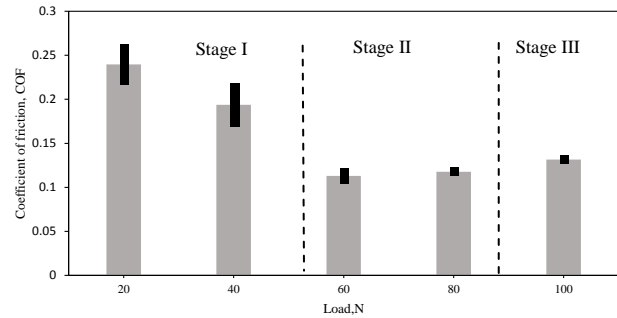


Fig. 3 Average steady state COF of the PKAC-E composite at different load. The error bar is for standard deviation.

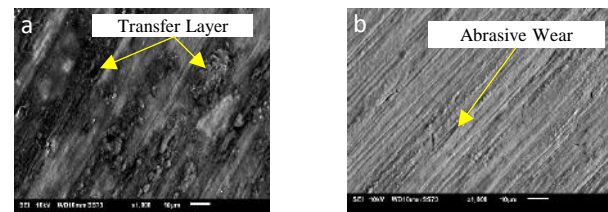


Fig. 4 SEM micrograph at (a) 60 N (b) 100 N of the PKAC-E composite.

4. CONCLUSION

In a nut shell, high load ball-on-disc experiment has been successfully carried out to stimulate tribological behaviour of PKAC-E composite. Overall, it can be said that the COF value from Stage I to Stage III decreases and increases from a low to high bearing load respectively with Stage II being considered as the optimum load range for the specimen. Hence, this study suggests that the load bearing capacity for PKAC-E composite is 80N.

REFERENCES

- [1] A. Erdemir, O.L. Eryilmaz, And G. Fenske, "Synthesis of diamondlike carbon films with superlow friction and wear properties", *Journal of Vacuum Science & Technology A*, 18(4), pp.1987-1992, 2000.
- [2] A. Baradeswaran, and A.E. Perumal, "Wear and mechanical characteristics of Al 7075/graphite composites." *Composites Part B: Engineering*, 56, pp.472-476, 2014
- [3] Z. Yusoff, S.B. Jamaludin, M. Amin, and N.H.A. Zaidi, "Sliding wear properties of hybrid aluminium composite reinforced by particles of palm shell activated carbon and slag", *Journal of Science and Technology*, 2(1), 2010
- [4] M. Bakry, M.O. Mousa, and W.Y. Ali, "Friction and wear of friction composites reinforced by natural fibres", *Materials Science and Engineering Technology*, 44, 21-28, 2013.
- [5] N.A. Mat Tahir, M.F.B. Abdollah, R. Hasan, H. Amiruddin, "The effect of sliding distance at different temperatures on the tribological properties of a palm kernel activated carbon-epoxy composite", *Tribology International*, 94, 352-359, 2016.
- [6] Luo Q, "Tribofilms in solid lubricants", *Encyclopedia of Tribology*, Springer; 2013.
- [7] M.A. Chowdhury, and M. Helali, "The effect of amplitude of vibration on the coefficient of friction for different materials", *Tribology International*, 41(4), pp.307-314, 2008.

LUBRICATED WEAR BEHAVIOUR OF SiC REINFORCED COMPOSITE COATED Ti-6Al-4V ALLOY BASED ON TAGUCHI APPROACH

M. A. Maleque¹, H. Lailatul¹, K. A. Bello¹, and M. Azwan¹

¹Department of Manufacturing and Materials Engineering, International Islamic University Malaysia, Malaysia.
maleque@iium.edu.my, Laila_7164@yahoo.com, bellkamm@gmail.com, azwanmuhd92@gmail.com

1. INTRODUCTION

Titanium alloy grade 5 (Ti-6Al-4V) is widely used in engineering industries. Ti-6Al-4V also has been known to show good mechanical properties, excellent corrosion resistance and having low density [1]. However, the grade 5 titanium alloys have poor tribological properties since it has poor wear resistance, low hardness and high coefficient of friction. Therefore, the improvement of surface properties are required to increase the performance of the parts. Previous research work by Adeleke & Maleque [2] studied the surface alloying of commercial purity titanium (CP-Ti) using preplaced Fe-C-Si powder by TIG technique. The surface modified CP-Ti alloy exhibited hardness values ranging from 600 Hv to 800 Hv which was 3 times higher than base material hardness. The main aim of this study is to improve the tribological properties of grade 5 (Ti-6Al-4V) under lubricated condition based on Taguchi approach. The substrate alloy was preplaced with silicon carbide (SiC) powder and tungsten inert gas (TIG) torch surface melting technique was applied for composite coating on Ti-6Al-4V alloy.

2. EXPERIMENTAL DETAILS

The material used for this study is titanium alloy grade 5 (Ti-6Al-4V) with the dimension of 17 mm x 40 mm x 15 mm as the substrate material. The SiC powder preplacement with different sizes of 20, 40 and 60 μm was used for surface modification. The SiC powder weighed of 0.5 mg per millimeter square was mixed with a small amount of polyvinyl acetate (PVA) binder and agitated to form a paste with the aid of distilled water and alcohol. The addition of binder is to keep the powder on the surface under the flow of the shielding gas. The Ti-6Al-4V substrate with preplacement reinforcement of SiC was carried out using TIG torch melting technique to produce a series of tracks. The wear testing under lubricated condition was conducted using ball-on-disc sliding machine with load of 30 N and frequency of 10Hz for 30 minutes. In this research, L9 orthogonal array of the Taguchi experimental design was used in designing and analyzing the effect of TIG process parameters on the wear rate and coefficient of friction (CoF) of the TIG-processed SiC reinforced composite coated Ti-6Al-4V under lubricated condition. The design matrix for the experiment is shown in Table 1.

Table 1 Design matrix for TIG-processed SiC coating

Current (A)	Speed (mm/s)	Voltage (V)	SiC powder sizes (μm)	Wear rate ($\mu\text{m}^3/\text{s}$)	Coefficient of friction
70	1.0	20	20		
70	1.5	25	40		
70	2.0	30	60		
80	1.0	25	60		
80	1.5	30	20		
80	2.0	20	40		
90	1.0	30	40		
90	1.5	20	60		
90	2.0	25	20		

3. RESULT AND DISCUSSION

3.1. Wear rate analysis

The wear rate of silicon carbide reinforced composite coated Ti-6Al-4V alloy for each experimental run of L9 orthogonal array is listed in Table 2. In Taguchi method, the wear rate of the TIG processed coating is analyzed with S/N ratio using the smaller the better criterion. The signal-to-noise ratio is calculated in decibel scale (dB) using equation 1 [4].

$$S/N \text{ (STB)} = -10 \log^*(\sum (Y^2)/n) \quad (1)$$

Where Y is the experimental data and n is the number of experiment. The wear rate value and their corresponding S/N ratio obtained for each of L9 experiment is shown in Table 2. The computation and analysis of S/N ratio is done using Minitab 17 statistical software package.

Table 2 Experimental results for wear with S/N ratio

Exp. runs	Wear rate ($\mu\text{m}^3/\text{s}$)	S/N ratio (dB)
1	0.4212	-12.490
2	0.1975	-5.911
3	0.3160	-9.994
4	0.1711	-4.665
5	0.4081	-12.215
6	0.3028	-9.623
7	0.2370	-7.495
8	0.3555	-11.017
9	0.3291	-10.347

The S/N response analysis is obtained from the experiment results by calculating the average of S/N ratio for each level

of selected process factor or parameter. The mean responses for S/N ratio of wear rate is shown in Table 3. From the obtained result, the rank '1' and rank '2' in Table 3 indicates that the TIG voltage and SiC powder size have a stronger effect on the TIG process. Rank '3' in the same table shows that welding speed has a strong effect on the process followed by Rank '4' which means that welding current has the minimum effect on the process.

Table 3 Mean responses for S/N ratio of wear rate

Levels	Current (A)	Speed (mm/s)	Voltage (V)	SiC powder sizes (μm)
1	-9.465	-8.217	-11.043	-11.684
2	-8.834	-9.714	-6.974	-7.676
3	-9.619	-9.988	-9.901	-8.559
Delta	0.785	1.771	4.069	4.007
Rank	4	3	1	2

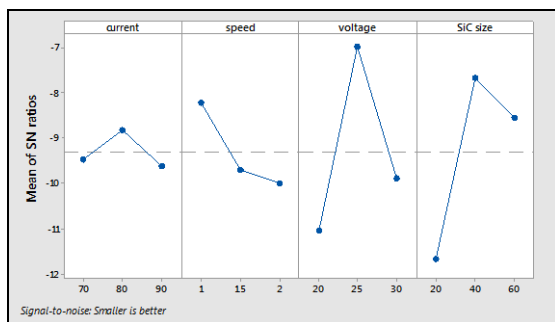


Fig. 1 Main effect plot for the wear rate of SiC coated Ti-6Al-4V.

The effect of process factor on the mean S/N response for wear rate is shown in Fig. 1. From the main effect plot in Fig. 1, the inclination of the plot is used to determine the significance of each parameter. The parameter with the highest inclination line has most effect on the wear rate of the material. Hence, the optimum value to obtain the minimum wear rate in the composite coated was at current level of 80A, speed at 1.0 mm/s, voltage of 25V and SiC powder size of 40 μm . However, the confirmation test is needed to fulfill the requirement of the Taguchi design matrix.

3.2. Coefficient of friction (CoF) analysis

The CoF value and corresponding S/N ratio for all experimental runs is shown in Table 4. The mean of S/N ratio for CoF is given in the response table of Table 5. The ranking which gives the order of importance of the TIG process factors indicates that CoF is influenced by welding voltage, SiC size, speed and current in that order. Interestingly, this trend is similar to what was obtained for wear rate response in this study. Fig. 2 shows the response plots for CoF. The optimum combination of process parameters is current level of 80A, speed at 2 mm/s, voltage of 25 V and SiC powder size of 40 μm . However, the confirmation test is needed to fulfill the requirement of Taguchi design matrix.

Table 4 Experimental results for CoF with S/N ratio

Exp. runs	Coefficient of friction	S/N ratio (dB)
1	0.76740	-17.700
2	0.14203	-3.048
3	0.23409	-7.388
4	0.109033	-0.751
5	0.75285	-17.534
6	0.18091	-5.149
7	0.17353	-4.788
8	0.87323	-18.823
9	0.21043	-6.462

Table 5 Mean responses for S/N ratio of CoF

Levels	Current (A)	Speed (mm/s)	Voltage (V)	SiC powder sizes (μm)
1	-9.379	-7.746	-13.891	-13.899
2	-7.812	-13.135	-3.420	-4.328
3	-10.024	-6.333	-9.903	-8.987
Delta	2.213	6.802	10.470	9.571
Rank	4	3	1	2

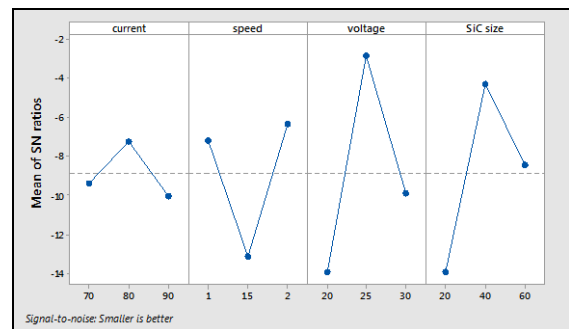


Fig. 2 Main effect plot for CoF of SiC coated Ti-6Al-4V.

4. CONCLUSIONS

- 1) The influence of the process parameter for SiC reinforced composite coated Ti-6Al-4V is similar for both wear rate and friction behavior. The voltage and SiC powder sizes are the prominent factor influencing the process.
- 2) SiC with 40 μm preplaced powder on Ti-alloy surface exhibited lower wear rate under lubricated condition.

REFERENCES

- [1] M. Dewidar, "Improvement of Hardness and Wear Resistance of Ti-6Al-4V Alloy by Thermal Oxidation for Biomedical Application," *Journal of Engineering Sciences*, Vol. 34, pp. 1941-1951, 2006.
- [2] S.A. Adeleke, & M.A. Maleque, "TIG Melted Surface Modified Titanium Alloy For Cylinder Liner Application," *International Journal of Automotive Engineering and Technologies*, Vol. 4, pp. 130-138, 2015.
- [3] K.A. Bello, M.A. Maleque and Z. Ahmad, "Optimization of Hardness Behaviour of TIG Surface Modified LAS Based on Taguchi Approach," *Advanced Material Research*, Vol. 115, pp. 238-242, 2015.

TRIBOLOGICAL PERFORMANCE EVALUATION OF PALM TRIMETHYLOLPROPANE (TMP) ESTER AS A SUBSTITUTE FOR CONVENTIONAL LUBRICANT BASE OIL

R. Zahid^{1,2}, M. B. H. Hassan¹, M. Varman¹, R. A. Mufti¹, Md. Abul Kalam¹, N. W. B. M. Zulkifli¹, and M. Gulzar¹

¹Center for Energy Sciences, Department of Mechanical Engineering, University of Malaya, 50603, Kuala Lumpur, Malaysia.

²School of Mechanical and Manufacturing Engineering, National University of Sciences and Technology, Sector H-12, 44000, Islamabad, Pakistan.

1. ABSTRACT

In this paper, effectiveness of non-additivated and additivated versions of palm trimethylolpropane (TMP) ester containing glycerol mono-oleate (GMO), molybdenum dithiocarbamate (MoDTC) and zinc dialkyldithiophosphate (ZDDP), in enhancing tribological performance of steel/cast iron contact has been investigated. Friction and wear results obtained with TMP-based lubricants are then compared with those of PAO-based ones to evaluate the compatibility of bio-lubricant with conventional additives. In addition to that, mechanisms involved in a particular tribological behavior are investigated using scanning electron microscope (SEM) and energy dispersive x-ray (EDX).

2. INTRODUCTION

The main constituents of commercially available lubricants are base oils and additives packages. About 85% of the lubricants consumed worldwide are derived from non-renewable and non-biodegradable sources such as petroleum whereas rest of them are either synthetic or bio-based [1]. In order to meet the energy needs of rapidly developing world, fossil fuel reserves are depleting at a rapid pace and are at the verge of scarcity [2]. Moreover, there are many environmental and health issues associated with the excessive usage of petroleum-based fuels and lubricants. Therefore, there is a need to reduce reliance on conventional lubricants and shift to environmentally sustainable, renewable and biodegradable ones.

Chemically modified vegetable oils such as palm TMP ester are one of the potential candidates for alternate lubricant base oils due to their extraordinary lubricating properties. Since, conventional lubricant additives are optimized for conventional base oils; therefore, there is a need to evaluate the effectiveness of these additives in bio-based oils.

In this research work, viability of palm TMP ester as a substitute for conventional base oils has been investigated by analyzing its tribological compatibility with most widely used lubricant additives (GMO, MoDTC and ZDDP) in combination with steel/cast iron contact.

3. METHODOLOGY

Reciprocating sliding tests were conducted using universal wear testing machine (Cameron Plint TE99) with pin-on-plate geometric configuration. AISI 52100 steel rectangular plates were used as flat surfaces whereas BS 1452 cast iron pins were used as counterbody. Tribotest conditions were selected in such a way that they replicate cam/tappet interface of a commercial automotive engine Table 1. Additivated version of bio-lubricant was synthesized by mixing 1.0 wt% of each additives in palm TMP ester. For reference, PAO was used as conventional base oil, with and without additives. In order to investigate the mechanisms responsible for a particular tribological behavior, wear tracks on cylindrical pins were analyzed by field emission scanning electron microscope (FESEM) and energy dispersive x-ray (EDX).

Table 1: Tribotest conditions

Physical Quantities	Specifications
Temperature	90 °C
Speed	0.04 m/s
Duration	120 min
Stroke length	10 mm
Load	615 N
Maximum hertzian contact	700 MPa
Total sliding distance	288 m

4. RESULTS AND DISCUSSION

Average friction coefficients of steel/cast iron contacts in combination with non-additivated and additivated versions of PAO and TMP are shown in Fig. 1 whereas wear coefficient of pins are presented in Fig. 2. Among the base oils, TMP showed superior friction behavior compared to PAO. This improved friction characteristic of TMP can be attributed to its polar nature due to which it adsorbs on the interacting surface whereas no such behavior can be seen in case of PAO due to its non-polar chemical structure. A significant improvement in friction behavior was observed when additivated lubricants were used instead of non-additivated ones.

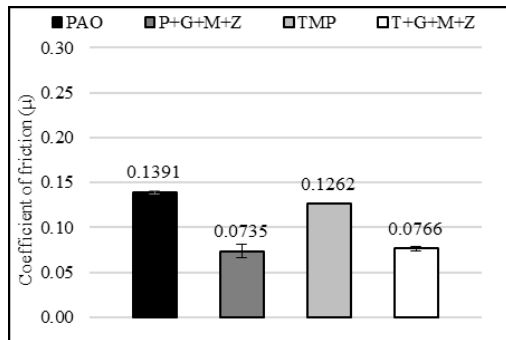


Fig. 1 Average friction coefficient values of steel/cast iron contacts

Contrary to friction results, high values of wear coefficient of pins were observed with TMP compared to PAO. This can be attributed to ineffectiveness of TMP in providing boundary lubrication and preventing the asperities of interacting surfaces from coming into direct contact with each other. Mixing of base oils with additives substantially improved the wear characteristics. Additivated lubricants were proved to be very effective and reduced the wear coefficients of pins to almost one-hundredth irrespective of base oil used. Among additivated lubricants, T+G+M+Z proved to be the most effective lubricant in preventing the pin from excessive wear.

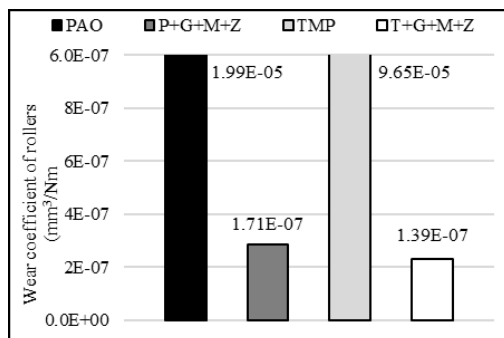


Fig. 2 Wear-coefficients of cast iron pin

Atomic percentage of elements deposited on cast iron pins after 2 hours of sliding against AISI 52100 steel plates are presented in Table 2. Lowest value of composite wear observed with T+G+M+Z can be attributed to the formation of ZDDP-derived tribofilm on the contact which prohibits surfaces from excessive wearing. MoDTC-derived tribofilm composed of molybdenum oxide and molybdenum disulfide were observed on cast iron pins which resulted in improvement in friction performance.

Table 2: Atomic percentage of elements found on cast iron pins after 2 hours of sliding using EDX

Lubricants	Elements						
	C	P	S	Mo	Zn	Fe	O
TMP	29.5	-	-	-	-	58.2	12.3
PAO	20.7	-	-	-	-	53.1	26.3
T+G+M+Z	51.8	0.2	0.9	1.3	1.3	22.9	21.5

P+G+M+Z 18.2 0.4 0.7 4.3 1.4 57.1 17.9

SEM micrographs of cast iron pins are presented in Fig. 3. When non-additivated lubricants were used, severe cracks, wear debris, deep grooves and structural disintegration was observed on pin surface which resulted in extremely high wear coefficients whereas no such effect was seen with additivated lubricants. This surface deterioration was more eloquent when non-additivated TMP was used and wearing-out of cast iron pin was 5 times more compared to PAO.

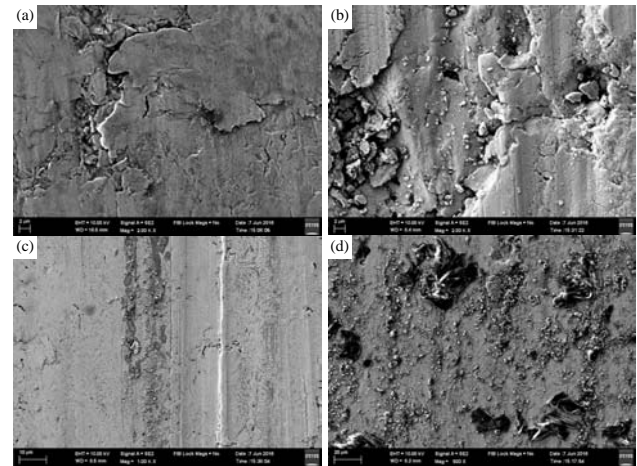


Fig. 3 SEM micrographs of cast iron pins in case of steel/cast iron contacts in combination with (a) PAO, (b) TMP, (c) P+G+M+Z and (d) T+GM+Z

5. CONCLUSION

In non-additivated form, palm TMP ester proved to be more effective in enhancing friction performance of steel/cast iron contact compared to PAO. Lowest value of wear coefficient was observed with T+G+M+Z which shows that conventional additives which are actually optimized for conventional base oils such as PAO are also effective in augmenting tribological characteristics of palm TMP ester. From these observations, it can be concluded that TMP ester has a potential to be used as base oil in automotive lubricants in combination with PAO.

6. ACKNOWLEDGEMENT

The authors would like to acknowledge University of Malaya for funding this research through High Impact Research grant project titled "Clean Diesel Technology for Military and Civilian Transport Vehicles" (UM.C/HIR/MOHE/ENG/07)

REFERENCES

- [1] L. Pop, et al., "Basestock Oils for Lubricants from Mixtures of Corn Oil and Synthetic Diesters," *Journal of the American Oil Chemists' Society*, Vol. 85, No. 1, pp. 71-76, 2007
- [2] H. M. Mobarak, et al., "The prospects of biolubricants as alternatives in automotive applications," *Renewable and Sustainable Energy Reviews*, Vol. 33, pp. 34-43, 2014

PERFORMANCE EVALUATION OF POLYOL ESTERS FROM PALM OIL AS A LUBRICANT FOR BENTONITE SUSPENSION DRILLING FLUID

K. Dina ¹, Y. Robiah ¹, R. Omar ¹, S. A. Rashid ², and B. M. Jan ³

¹Department of Chemical and Environmental Engineering, Faculty of Engineering, Universiti Putra Malaysia

²Institute of Advanced Technology, Universiti Putra Malaysia, Malaysia.

³Department of Chemical Engineering, Faculty of Engineering, University of Malaya, Malaysia.

ABSTRACT

This study examined the potential use of three polyol esters (POEs) derived from palm oil as a lubricant in bentonite suspension drilling fluid. It was revealed that the POEs investigated reduced the coefficient of friction in bentonite suspension by more than 80%. However, trimethylolpropane (TMPE) and neopentylglycol ester (NPGE) undesirably altered the gel texture of the suspension. Pentaerythritol (PEE) shows the best performance as it produced the highest lubricity and the lowest effect on the suspension texture.

Keywords—drilling fluid; bentonite suspension; polyol ester lubricant; mud lubricity

1. INTRODUCTION

High lubricity drilling fluids or muds are always desired in oil and gas drilling operation. They can minimize the friction between the drill pipes and the wellbore wall, increase the penetration rate, and prevent drilling problems such as stuck pipe, wear and tear. Lubricants are usually added to the mud to increase the lubricity [1, 2]. Research into the potential use of polyol ester (POE) as drilling mud lubricants has not been given a great attention [3], despite their high performance and biodegradability in general lubricant application [4]. In this study, the lubricating effect of different kind of polyol esters on bentonite suspension is reported. Bentonite suspension was chosen as the base drilling mud because this type of mud has poor lubricity but economical. It simply comprises of bentonite and water. POEs are hygroscopic lubricants (i.e. they absorb water), which makes them theoretically compatible for water-based mud. The finding in this study would be useful as a preliminary data for future applications of POE in wider mud formulation.

2. EXPERIMENTAL

2.1. Polyol ester lubricants

Three different high viscosity POEs, which are pentaerythritol ester (PEE), trimethylolpropane ester (TMPE), and neopentylglycol ester (NPGE), were used as lubricant additives for separate mud samples. The viscosity of PEE, TMPE, and NPGE, are 68.4, 45.7, and 21 cSt at 40°C, respectively.

2.2. Bentonite suspension preparation

The bentonite suspension was prepared by mixing 7.5% (w/v) of bentonite in distilled water using a Silverson mixer at 6000 rpm for 30 minutes. The mud was then being static aged at 90°C for 16 hours. After that, distilled water was added while mixing until the resultant mud had the apparent viscosity in the range of 15 ± 1 centiPoise, which was a good mud viscosity for general drilling purposes [5]. One type of lubricant was added accordingly while being stirred.

2.3. Lubricity measurement

Lubricity was measured using a Fann Model 212 lubricity tester. The force of 150 inch-pounds was applied to the test block that ran at 60 RPM. The torque reading was recorded and the mud lubricity was expressed as coefficient of friction (COF).

2.4. Foaming test

It is common for lubricants to foam in mud [2, 6]. Foaming tendency caused by POE were evaluated by measuring the mud weight using a mud balance and visual inspection.

3. RESULTS AND DISCUSSIONS

3.1. Effect of different lubricant on mud lubricity

At a low concentration of 0.5%, PEE, TMPE, and NPGE reduced the COF of the mud by 86.8%, 82.4%, and 80%, respectively. Increasing the lubricant concentration to 1% appeared to not improve the lubricity any further. The COF reduction by 1% of PEE, TMPE, and NPGE are 87.5%, 82.8%, and 80.4%. This is mainly attributed to the strong attraction between the high polar POE molecules and metal surfaces, even at a very low concentration [1, 7]. A small quantity of POE possibly sticks to the metal surface of lubricity tester, creates a lubricant film, and stays in the contact area.

In Fig. 1, PEE is shown to have the highest COF reduction, compared to TMPE and NPGE. The viscosity of PEE, which is the highest among other lubricants, might play the essential role in resulting thicker lubricant film.

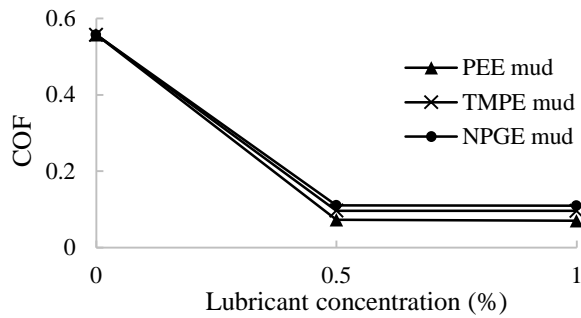


Fig. 1 Coefficient of friction of bentonite suspensions containing lubricants.

3.2. Foaming tendency

The density of the mud containing TMPE and NPGE decreased, compared to the base mud, as reported in Table 1. The density reduction of the mud indicates there is foam/bubbles presence in the mud. Meanwhile, the density of the mud containing 0.5% of PEE was relatively the same with the base. The results also show that increasing the lubricant concentration to 1% increases the tendency to foam which is shown by further reduction of density.

Table 1: The density (pound per gallon, ppg) of the bentonite suspensions with the presence of 0.5% and 1% of lubricants

Conc. (%)	Base mud	NPGE mud	TMPE mud	PEE mud
0.5	8.6	8.1	7.9	8.55
1	8.6	7.6	7.2	8.1

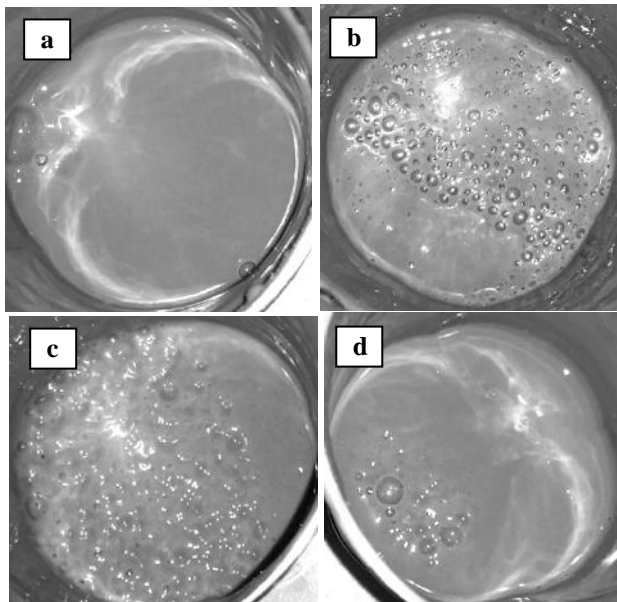


Fig. 2 The different texture of (a) base mud, (b) NPGE added mud, (c) TMPE added mud, and (d) PEE added mud.

The texture of the mud after the addition of lubricants is presented in Fig. 2. Mud containing TMPE demonstrated the worst appearance in terms of numerous bubbles formed, gel-like texture, and density reduction, while mud containing

NPGE showed a better properties. The bentonite particles seem flocculated in the presence of TMPE. Mud with NPGE also had much bubbles trapped inside, but since it did not gel up and partial bubbles could be easily released. Meanwhile, mud with PEE appeared thick and smooth, very similar with the base mud. Regardless, the difference in ester linkages and chain length of lubricant used in this study affect its compatibility with bentonite suspension. Since both of TMPE and NPGE changed physical properties of the mud, the usage of both lubricants might not be favourable, especially when the application of bentonite suspensions mostly depends on its viscosity and gel characteristics. Montmorillonitic clay, the main component of bentonite, possibly has a negative nature towards TMPE and NPGE.

4. CONCLUSIONS

High polar polyol esters investigated in this study, which are PEE, TMPE, and NPGE, were able to reduce the friction in bentonite suspension by more than 80% at a concentration of 0.5%. On the basis of current results, PEE performed better compared to TMPE and NPGE, as it resulted in highest COF reduction and did not have significant foam tendency. TMPE and NPGE also caused texture alteration of the mud. The use of TMPE and NPGE might not be desirable for bentonite suspension application. Unfortunately, there is no systematic understanding of the interaction between bentonite with the lubricants in the present study.

In the future, it is encouraged to study the lubricity performance and compatibility of POE on a water-based mud, which consist of other mud additives, apart from bentonite alone.

REFERENCES

- [1] Amorim, L.V., et al., *Evaluation of the Behavior of Biodegradable Lubricants in the Differential Sticking Coefficient of Water Based Drilling Fluids*. Brazilian Journal of Petroleum and Gas, 2011. 5(4): p. 197-207.
- [2] Dong, X., et al., *Effect of ester based lubricant SMJH-1 on the lubricity properties of water based drilling fluid*. Journal of Petroleum Science and Engineering, 2015. 135: p. 161-167.
- [3] Kania, D., et al., *A review of biolubricants in drilling fluids: Recent research, performance, and applications*. Journal of Petroleum Science and Engineering, 2015. 135: p. 177-184.
- [4] Aldrich, H.S., et al., *Polyol ester compositions with unconverted hydroxyl groups*. 1998, US Patent EP0835922 A1.
- [5] Abdou, M.I., A.M. Al-sabagh, and M.M. Dardir, *Evaluation of Egyptian bentonite and nano-bentonite as drilling mud*. Egyptian Journal of Petroleum, 2013. 22(1): p. 53-59.
- [6] Sönmez, A., M. Verşan Kök, and R. Özel, *Performance analysis of drilling fluid liquid lubricants*. Journal of Petroleum Science and Engineering, 2013. 108: p. 64-73.
- [7] Rudnick, L.R., *Synthetics, Mineral Oils, and Bio-Based Lubricants: Chemistry and Technology*. 2013: CRC Press.

VIBRATION CHARACTERISTIC ON BALL BEARING OPERATED WITH HEXAGONAL BORON NITRIDE (hBN) NANOPARTICLE MIXED WITH DIESEL ENGINE OIL

N. S. R. Apandi¹, R. Ismail¹, M. F. B. Abdollah^{1,2}, and R. Ramlan¹

¹ Faculty of Mechanical Engineering, Universiti Teknikal Malaysia Melaka,
Hang Tuah Jaya, 76100 Durian Tunggal, Melaka, Malaysia.

² Centre for Advanced Research on Energy, Universiti Teknikal Malaysia Melaka,
Hang Tuah Jaya, 76100 Durian Tunggal, Melaka, Malaysia.

1. ABSTRACT

This paper presents the investigation on vibration characteristic on ball bearing operated with hexagonal boron nitride (hBN) nanoparticle mixed with diesel engine oil. Machine components including gears and bearings operates at high speed and high load condition. These extreme condition will lead to the high pressure and vibration on the working system. Thus, lubricant is needed to overcome the increase in pressure, temperature and also vibration. In this paper, the hBN nanoparticle was added as an additive into the SAE 15W40 diesel engine oil. Comparison study is also carried out with based engine oil and nanoparticles hBN mixed engine oil for different concentration. From this proposed study, the vibration characteristic can be investigated and performance of diesel engine oil with hBN nanoparticle can also be determined. The results show that the addition of hBN nanoparticle in the lubricant functioning effectively in reducing vibrations of bearing in diesel engine oil.

2. INTRODUCTION

Studies have proved that the right lubricant needs to be used in order to reduce the friction, wear, operating temperature, corrosion of metal surfaces, and assists in keeping contaminants out of the system. Lubricants have many properties that can be mixed and matched the operating needs. Due to that reason, searching for new additives in the lubricant has becomes one of the most important technology from the researchers because the additives present in lubricant can reduce the friction and wear between the contacting surfaces [1]. The past research used the copper nanoparticles as additives to prevent severe anti-wear, load-carrying and friction reduction performances added in diesel engine oil. These findings were followed by other nanoparticles like zirconia/silica (ZrO_3/SiO_2) composite, copper oxide (CuO), titanium oxide (TiO_2) and also nano-diamond. All these nanoparticles were observed as efficient in improving tribological properties [2-3]. This nano-oil also actively reduced the wear rate of materials and this shows good quantitative agreement with coefficient of friction by dispersing the nanoparticles in conventional diesel engine oil. Hexagonal boron nitride was widely uses as lubricant additive for high temperature lubrication. Other than that, it can also uses as electrical insulators, standard parts materials, heat radiation material, aeronautics and

space application [4]. This shows that the crystal structure of this element make it can be used in widely range of field. There has been a few published papers shows that this type of nanoparticles has significant reduction in wear and friction. However, until now, none of this research has provides clarification of the reduction in vibration amplitude. Vibration method is one way of condition monitoring for the machine and also it is more versatile as it can reveal wider range of faults for the early deterioration or malfunction in machinery. Thus, in this paper, the vibration measurement technique is applied to obtain the amplitude of the ball bearing operated with hBN nanoparticles mixed with engine diesel oil.

3. METHODOLOGY

An experimental setup is designed and fabricated to determine the vibration measurement on ball bearing operated with hBN nanoparticles added with diesel engine oil. Fig. 1 depicts the schematic layout of the measurement system.

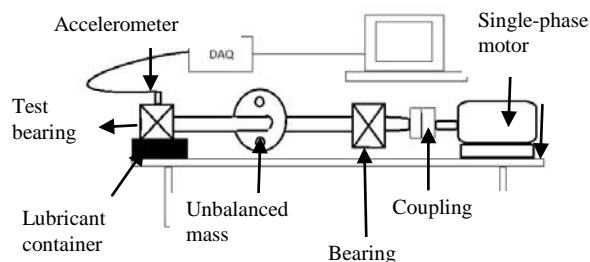


Fig. 1 The schematic layout of the measurement system

The main components of the experimental setup are motor, flexible coupling, ball bearing and container. The shaft is connected to the DC motor using flexible coupling and also supported by deep groove ball bearing. All the components are mounted on steel channel which is welded together to avoid the unwanted vibration. The steel channel has the heavy-duty caster for easy to mobilize around. A DC electric motor of 1 Horse Power (Volt-240V, Current-2.3 A) with operating speed of 1440 rpm is used in the experiment setup. An accelerometer was mounted on top of the bearing housing is connected with data by acquisition device DATA PHYSIC SignalCalc Analyser connected via USB port of the PC. The mixture of nanoparticles in the diesel engine oil was homogenized using an ultrasonic homogenizer for 30 minutes. Different concentrations (0%,

0.2%, 0.5%, 1.0%) of hBN nanoparticles was dispersed into SAE 15W40 diesel engine oil. This mixture was poured into lubricant container until the ball bearing was partially submerged by the lubricants and vibration signals were acquired. Then, the raw data was converted by Fast Fourier Transform (FFT) in MATLAB software to acquire the frequency waveform. The experiment were conducted with three different types of bearing which were new bearing, inner defect bearing and outer defect bearing with the different concentration of nanoparticles. Several loads were located at different places in order to introduce the unbalanced condition.

4. RESULT AND DISCUSSION

Table 1 shows the results obtained for a new bearing, outer defect bearing and inner defect bearing from the test.

Table 1 Acceleration values of the different types of bearing

Types of bearing	Acceleration (ms^{-2})			
	Vol.Concentration (%)			
	0.0	0.2	0.5	1.0
New bearing	0.1630	0.1410	0.2760	0.2790
Outer defect	0.0661	0.0360	0.0839	0.1920
Inner defect	0.0154	0.0150	0.0574	0.0701

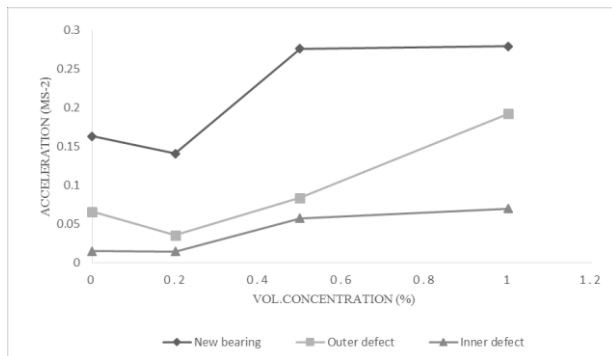


Fig. 2 Amplitude of vibration as a function of nanoparticles concentration

As shown in Fig. 2, the 0.2% vol. concentration of nanoparticles is the best concentration in reducing vibration for all type of different bearings compared to other concentration. The significant reduction in amplitude for 0.2% of concentration was obtained compared to base lubricant in which reduction of 13.5% for new bearing, 45.5% for outer defect bearing and 2.6% for inner defect bearing. The amplitude of the mixed nano-lubricants was decreased compared to the base lubricant because of the formation of full film lubrication regime formed around the ball bearing. Also, vibration performances of this mixed lubricants are slightly better than the base lubricant due to the different in particles sizes formed. The significant peaks for outer and inner defect of bearings can be observed at 4.5X and 5.4X as shown in Fig. 3 and 4.

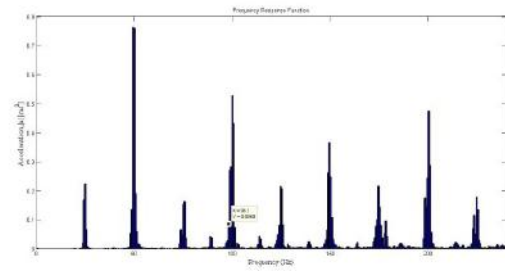


Fig. 3 The outer defect significant peaks

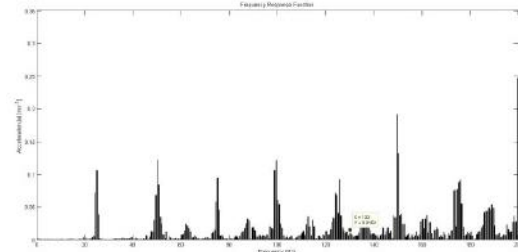


Fig. 4 The inner defect significant peaks

5. CONCLUSION

The hBN nanoparticles mixed lubricants can function effectively in reducing the vibration measurement in the ball bearing in order to decrease the emission and better fuel efficiency.

6. ACKNOWLEDGEMENT

The authors gratefully acknowledged the Green Tribology and Engine Performances (G-TriboE) research group of Centre for Advanced Research on Energy (CARE), the financial support from Universiti Teknikal Malaysia Melaka and The ministry of Education, Malaysia under Short Term Research Grant, Grant no. RAGS/1/2014/TK01/FKM/B00066.

REFERENCES

- [1] M.I.H.C. Abdullah, M.F.B. Abdollah, H. Amiruddin, N.Tamaldin, N.R. Mat Nuri, Effect of Hbn/Al₂O₃ Nanoparticle Additive on the Tribological Performance of Engine Oil, Jurnal Teknologi (Sciences and Engineering), 66:3 (2014), pp. 1-6.
- [2] Prakash, E., Siva Kumar, K., and Muthu Kumar, K. (2013). Experimental studies on vibration characteristics on ball bearing operated with cooper oxide nano particle mixed lubricant. International Journal of Engineering and Technology, 5(5), 4127-4130, 2013.
- [3] S.M. Muzakkir, "Design and Development of Experimental setup for Direct Acting Overhead Camshaft (DOHC) Valve System", vol.5, no.3, 2013.
- [4] C.V. Vazhappilly, V.K. Manoj Kumar, C.R. Praveen Raj, P. Kamalesan, Experimental Analysis of Vibration of Ball Bearing Considering Solid Contaminants in Lubricants, International Journal of Engineering Research and Applications, 3(5), pp.1576-1580, 2013.

THE EFFECT OF PURE ALUMINIUM PIN ON STEEL DISC WITH VARIES SPEED AND CONSTANT LOAD

A. M. S. Zuan¹, S. Syahrullail¹, and S. M. Azhar¹

¹*Faculty of Mechanical Engineering, Universiti Teknologi Malaysia, 81310 UTM Skudai, Johor, Malaysia.*

1. INTRODUCTION

Friction are found generally in an internal combustion engine of vehicles, grinding operation, strip movement in metal rolling, control of chatter in a machine tool slide way, etc. In lubrication, it is more important to maintain steady friction than to obtain the lowest possible friction. Lubricant also acts to reduce wear, to prevent overheating and corrosion, and forms a film thickness that cover the parts of object that under friction. Mineral Oil performance has been seen through its viscosity, thermal properties, oxidation stability, ability to dissolve additives and contaminants. With the rapid development globally, the high demand to this petroleum based oil keep increasing and leading to a depletion and price hike. Therefore, an initiative to use vegetable oil as lubricant has been study where vegetable oil is known for low pollution to the environment, high biodegradability, compatibility with additives, low production cost, low toxicity and wide production possibilities [1]. The performance of two types of lubricants of vegetable oil Palm Stearin (PS) and commercial mineral engine oil (CMEO) are being tested by using pin on disc tribotester machine following ASTM G99 standard. The materials used for this experiment are pure aluminium pin (A110) with spherical head and stainless steel disc (SKD11) with four grooves. In this study, the coefficient of friction (COF) obtained by palm stearin is higher than CMEO oil. The COF for both oils are inversely proportional with sliding speed. Besides, the wear rate of palm stearin is bigger than CMEO. This shows that CMEO is better than palm stearin.

2. METHODOLOGY

This study was using a pin on disc tribotester machine that connected to controller and display the data in the computer and according to the ASTM G99 standards. The speed are varied from 1.5m/s to 3.5m/s with an increment of 1m/s. The load and time remain constant at 1kg and 1 hour. The oil volume that applied on the disc is 2.5ml. The specimens used are pure aluminium pin (A110) and stainless steel disc (SKD11). The lubricants used palm stearin (PS) and a direct comparison with commercialized mineral engine oil (CMEO). In this study, the data obtained from the controller of pin-on disc machine are wear and frictional force. The pin-on-disc machine is attached with LVDT sensor that able to detect the wear rate of the pin and disc. Then the coefficient of friction is calculated by using this formula:

$$\text{coefficient of friction} = \frac{\text{frictional force}}{\text{normal load}} \quad (1)$$

Wear scar diameter (WSD) of the pin was measured by using charge-coupled device (CCD) microscope. Surface roughness of the pin is measured by using surface roughness tester (Mitutoyo SJ210). The wear scar diameter and surface roughness of the pin is reflected to the wear mechanism that highlighted in the objective.

3. RESULT AND DISCUSSION

3.1. Coefficient of Friction

From Figure 1, the value of COF of both oils are decreasing when the sliding speed increases. This happen due to wear debris that produced and will interact with the metal surface and will act as protective layer to overcome high frictional force and metal to metal direct contact. This result supported by Riyadh et al. [2]. COF of PS is recorded higher than CMEO. This is due to PS has low resistance to oxidative degradation and poor low temperature properties and CMEO has the existence of the additive [3].

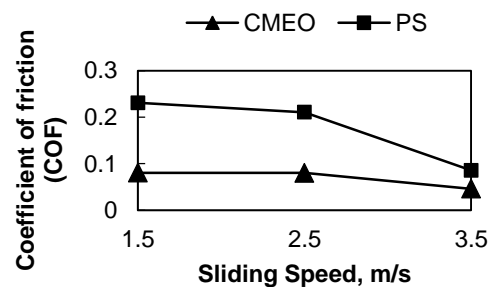


Fig. 1 Coefficient of friction versus Sliding Speed

Researcher indicate that petroleum-based mineral oils which is without any additives have lower lubricity and viscosity temperature properties compared to vegetable oils [4]. Vegetable oils comprised of triglycerides consist of a glycerol molecule with three different long-chain fatty acids attached with an ester linkage. As the increase in fatty acid content occurs, a decrease in the coefficient of friction is observed [5].

3.2. Wear

Figure 2 shows graph of wear against sliding speed for PS and CMEO. In this graph, wear of PS is increasing when sliding speed increase and wear of CMEO decreasing when

sliding speed increase. CME0 recorded higher wear at early stage of sliding speed because the static friction is high and when the speed increases its already enter dynamic friction and in a stable sliding condition. However PS recorded increase in wear because the temperature at surface contact increases when speed is increases. Therefore the bulk temperature will decrease the yield strength of the material and lead to changes in the wear mechanism and the real contact configuration [6].

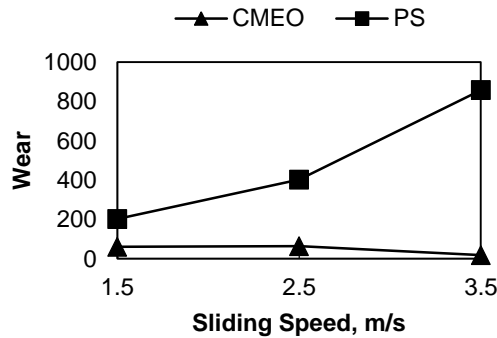


Fig. 2 Wear versus Sliding Speed

Fatty acid content has a significance effect to reduce wear rate [7] where the presence of long-chain fatty acid produces hydrocarbon layer that protects wearing surface. However, higher level of unsaturation fatty acid will give a negative influence on the performance of fatty acids as boundary wear reducers [8,9]. In other word, when the level of unsaturated fatty acids increases, the wear rate will also increase.

3.3. Surface Roughness

Figure 3.3 shows that the graph of surface roughness of pin against the sliding speed for both lubricants palm stearin and CME0. It was observed that the trend for CME0 is surface roughness of pin is inversely proportional to the sliding speed while palm stearin surface roughness of pin is directly proportional to the sliding speed. The CME0 surface roughness of pin has value 0.3875micron at speed of 1.5m/s and decrease to 0.2680micron at speed 2.5m/s and lastly decrease only a little difference to 0.2585micron at speed 3.5m/s. For palm stearin surface roughness value of pin has highest value 0.600micron at speed 3.5m/s. At the starting it has value of 0.2285micron at speed 1.5m/s and then increase to 0.3450micron.

4. CONCLUSION

As a conclusion as sliding speed increase, the coefficient of friction values are decrease for both oils and Palm stearin has higher coefficient of friction compared to CME0 at all speed. The value of wear rates is directly proportional to the sliding speed for palm stearin and has higher wear rates compared to commercial mineral engine oil. Whereas commercial mineral oil has wear rates inversely proportional to the sliding speed. CME0 recorded stable

surface roughness while PS is increases when speed increases.

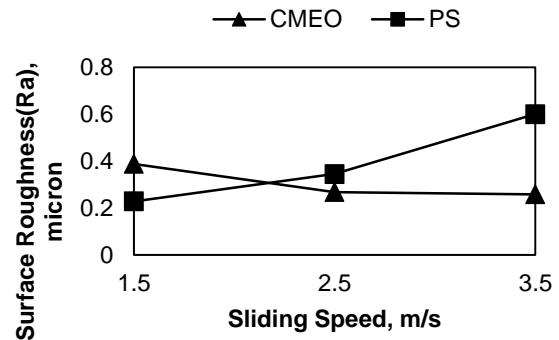


Fig. 3 Surface roughness of pin versus sliding speed

5. ACKNOWLEDGEMENT

The authors would like to express their thanks to the Research Management Centre (RMC) of Universiti Teknologi Malaysia for the Research University Grant, GUP (12H98, 09H64), Fundamental Research Grant Scheme, FRGS (4F610), and Ministry of Education of Malaysia and Ministry of Higher Education for their support; they also thank the Faculty of Mechanical Engineering, Universiti Teknologi Malaysia for the laboratory facilities.

REFERENCES

- [1] Shashidhara, Y. M. Ā., & Jayaram, S. R., *Tribology International Vegetable oils as a potential cutting fluid — An evolution*. Tribology International, 43(5-6), 1073–1081, 2010.
- [2] Riyadh A. Al-Samarai, Haftirman, Khairrel Rafezi Ahmad, & Y. Al-Douri, *Effect of Load and Sliding Speed on Wear and Friction of Aluminium- Silicon Casting Alloy*. International Journal of Scientific and Research Publications, 2012.
- [3] Erhan, S. Z., & Asadauskas, S., *Lubricant basestocks from vegetable oils*. Industrial Crops and Products, 11(2-3), 277–282, 2000.
- [4] Duzcukoglu, H., & Şahin, Ö. S., *Investigation of Wear Performance of Canola Oil Containing Boric Acid under Boundary Friction Condition*. Tribology Transactions, 54(1), 57–61, 2010.
- [5] Baumgart, P., Canzi, G., Hanashiro, T., Doezenia, L. A., & Siniawski, M. T., *Influence of fatty acid additives on the tribological performance of sunflower oil*, (August), 2010.
- [6] So, H., *Characteristics of wear results tested by pin-on-disc at moderate to high speeds*. Tribology International, 29(5), 415–423, 1996.
- [7] Fox, N. J., Tyrer, B., & Stachowiak, G. W., *Boundary Lubrication Performance of Free Fatty Acids in Sunflower Oil*. Tribology Letters, 16(4), 275–281, 2004.
- [8] Adhvaryu, A., Erhan, S. ., & Perez, J., *Tribological studies of thermally and chemically modified vegetable oils for use as environmentally friendly lubricants*. Wear, 257(3-4), 359–367, 2004.
- [9] Arumugam, S., & Sriram, G., *Effect of Bio-Lubricant and Biodiesel-Contaminated Lubricant on Tribological Behavior of Cylinder Liner-Piston Ring Combination*. Tribology Transactions, 55(4), 438–445, 2012.

TRIBOLOGICAL BEHAVIOUR OF SURFACE TEXTURED HYDROGENATED AMORPHOUS CARBON COATING IN THE PRESENCE OF PAO AT VARIOUS TEMPERATURES

A. A. Arslan¹, B. H. H. Masjuki¹, C. M. A. Kalam¹, D. M. Varman¹, E. R. A. Mufti², F. M. H. Mosarof¹, and G. L. S. Khoun¹

¹Center of Energy Sciences, University of Malaya, Kuala Lumpur, Malaysia.

²SMME, NUST, Islamabad, Pakistan.

1. INTRODUCTION

In the last few years, effects of surface texturing have been investigated on diamond-like carbon (DLC) coated surfaces in oil-lubricated sliding conditions. DLC coatings are increasingly being used to improve the tribological performance of engineering components like bearings, gears, seals, metal cutting, and forming tools, magnetic hard disks and biomedical, due to their hardness and excellent mechanical and tribological properties [1]. Because of the higher tribological performance, the use of DLC in automotive components is also increasing. As automotive components are subject to higher temperatures, loads, and oxidative environments, to maintain the performance of DLC at these harsh conditions, DLC is doped with hydrogen, various metals, nitrides, and carbides [2]. Surface texturing has recently been considered as one of the methods to maintain and enhance the tribological performance of DLC coating [3]. Most of the work done in this regard is at room temperature. It is well known that DLC coatings possess lower thermal stability at higher temperatures. Therefore, in the present study, the authors have investigated the effect of textures on hydrogenated amorphous carbon (a-C:H) DLC coating at various temperatures.

2. METHADODOLOGY

Micro textures with approximate dimensions of dimple depth, diameter, and density of 8 μm , 100 μm , and 20% were created on the substrate using a pico second laser with a power of 10 W and a wave length of 1.06 μm . After surface texturing, the DLC coating was deposited by hybrid magnetron sputtering. To evaluate the a-C:H DLC coating performance under various temperatures, a reciprocating sliding tribological testing apparatus with a ball on a flat configuration was used. The diameter of ball was 6.35-mm. Poly alpha olefin was used as a lubricant. Experimental conditions used are as follows: load 100 N; temperature 30, 80, and 125 $^{\circ}\text{C}$; frequency 5 Hz; test duration was 2 h and stroke length was 2.5 mm.

3. RESULTS

PAO-T30 showed lower COF compared to PAO-C30 (Fig. 1). Textures helped in lowering the COF by acting as

lubricant reservoirs and wear particle traps [4]. PAO-T30 showed the lowest wear coefficient compared to un-textured samples (Fig. 2). Textured samples (PAO-T80) showed lower wear coefficient compared to un-textured samples (PAO-C80) (Fig. 2). Higher COF was observed in textured case compared to un-textured DLC at 80 $^{\circ}\text{C}$ (Fig. 1). The reason for the decrease in COF of un-textured DLC at 80 and 125 $^{\circ}\text{C}$ may be due to graphitization transformation. The reduction in COF due to graphitization has been noticed previously [5]. Due to graphitization, the coating layer becomes soft and the load bearing capacity reduces and wear increases [6]. This could be the reason for the higher wear rate in the case of un-textured DLC at 30 $^{\circ}\text{C}$, 80 $^{\circ}\text{C}$ and 125 $^{\circ}\text{C}$, as can be seen in Fig. 2. This has been confirmed with Raman spectroscopy. Table 1 shows I_D/I_G ratios before and after tests. The increase in the I_D/I_G ratio indicate an increase in the sp^2 fraction in the DLC film [7, 8]. It can be observed that in textured cases the increase in ratio is less compared to un-textured samples. Which confirms higher graphitic transformation. In the case of textured DLC, COF increases with the increase in temperature (Fig. 1), which is different from un-textured DLC. This may be due to the suppression of graphitization by the textures. The reduction in graphitization transformation can explain the lower increase in the wear rate of textured DLC compared to un-textured DLC at various temperatures tested (Fig. 2). SEM of wear track shows that at 30 $^{\circ}\text{C}$ the PAO-T30 showed only polishing wear whereas un-textured PAO-C125 samples showed delamination with abrasive wearing (Fig. 3).

Fig. 1 CoF of DLC coated samples under PAO lubrication

whereas, at higher temperatures, this was due to the suppression of coating graphitization and textures behavior as fluid/wear debris reservoirs.

(2) At a lower temperature, 30 °C, textured DLC showed lower friction and wear compared to un-textured DLC.

(3) As the temperature increased to 80 and 125 °C, the textured DLC showed higher COF compared to un-textured DLC. This finding can be explained by the higher graphitization transformation in case of un-textured samples.

REFERENCES

- [1] Kalin, M., et al., *Review of boundary lubrication mechanisms of DLC coatings used in mechanical applications*. Meccanica, 2008. **43**(6): p. 623-637.
- [2] Neville, A., et al., *Compatibility between tribological surfaces and lubricant additives—How friction and wear reduction can be controlled by surface/lube synergies*. Tribology International, 2007. **40**(10-12): p. 1680-1695.
- [3] Arslan, A., et al., *Effects of texture diameter and depth on the tribological performance of DLC coating under lubricated sliding condition*. Applied Surface Science, 2015. **356**: p. 1135-1149.
- [4] Ahmed, A., et al., *An overview of geometrical parameters of surface texturing for piston/cylinder assembly and mechanical seals*. Meccanica, 2015. **51**(1): p. 9-23.
- [5] He, D., et al., *Improving tribological properties of titanium alloys by combining laser surface texturing and diamond-like carbon film*. Tribology International, 2015. **82**: p. 20-27.
- [6] Kalin, M., et al., *Metal-doped (Ti, WC) diamond-like-carbon coatings: Reactions with extreme-pressure oil additives under tribological and static conditions*. Thin Solid Films, 2010. **518**(15): p. 4336-4344.
- [7] Casiraghi, C., A.C. Ferrari, and J. Robertson, *Raman spectroscopy of hydrogenated amorphous carbons*. Physical Review B, 2005. **72**(8): p. 085401.
- [8] Ferrari, A.C. and J. Robertson, *Interpretation of Raman spectra of disordered and amorphous carbon*. Physical Review B, 2000. **61**(20): p. 14095-14107.

Fig. 2 Wear Coefficient of DLC coated samples under PAO lubrication

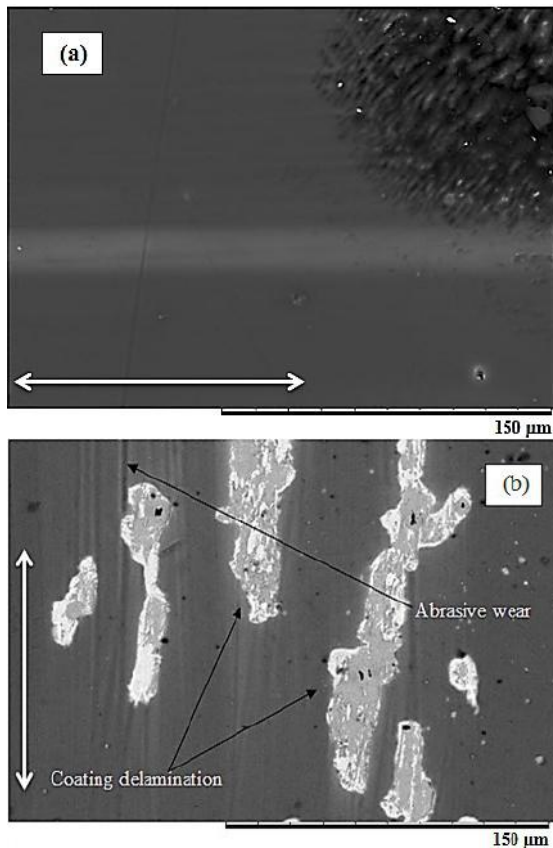


Fig. 3 SEM images (a) PAO-T30 (b) PAO-C125

Table 1: I_D/I_G ratio of textured and Un-textured DLC samples

Sample	I_D/I_G Ratio Before	I_D/I_G Ratio After
PAO-C30	1.17	1.41
PAO-T30	1.04	1.03
PAO-C125	1.17	2.01
PAO-T125	1.14	1.18

4. CONCLUSION

(1) The results show that micro textures improved the wear resistance of a-C:H DLC coating compared to untextured DLC at 30, 80, and 125 °C temperatures under PAO. This was due to textures behaving as fluid/wear debris reservoirs,

FRICITION BEHAVIOR OF POLYMER OVERLAYS CONTAINING SOLID LUBRICANTS COATED ON THE MICRO-TEXTUED ALMINUM SUBSTRATE

T. Doi¹, K. Enomoto², and H. Usami²

¹ *Division of materials science and engineering, Graduate school of Meijo University
 1-501, Shiogamaguchi, Tempaku-ku, Nagoya, Aichi, Japan.*

² *Department of materials science and engineering, Meijo University
 1-501, Shiogamaguchi, Tempaku-ku, Nagoya, Aichi, Japan.*

1. INTRODUCTION

In order to reduce fuel consumption, downsizing of the internal combustion engines is progressing. In particular, in sliding equipment, there is also demand for the reduction of friction loss under poor lubrication conditions, for higher contact pressure and for longer lifetime. For example, in actual journal bearings, texturing technology such as micro-grooving [1] and overlay technology such as foamed soft thin films [2] have been applied to the sliding surface in order to improve initial running-in and seizure resistance.

In previous studies, it has been reported that the creation of a micro-scale texture on a sliding metal surface and the squeezing of a solid lubricant such as molybdenum disulfide (MoS₂) into the fabricated texture are effective means for reducing the friction coefficient and improving seizure resistance [3].

On the other hand, in the overlay technology, a polymer overlay containing solid lubricants is an effective method for moderate initial running-in. In our recent research, the application of a subsurface micro texture fabricated through micro shot peening and a multi-layered structure for the overlay were effective for improving the durability of the overlay [4]. However, the effects of detailed structure, such as film thickness, volume fraction of MoS₂ and the alignment of MoS₂, have yet to be explained.

The present study describes the fundamental friction behavior under mixed/boundary lubrication condition of a polyamide-imide (PAI) overlay containing molybdenum disulfide (MoS₂) powder. Specimens with different layer structures for the overlay were prepared, and the effects of the layer structure of overlays were investigated experimentally.

2. METHODOLOGY

An aluminum cast alloy (AC8A) disc was employed as the metal substrate. The surface texture of the substrate was mainly fabricated using micro shot peening, to improve the adhesion strength between the overlay and the substrate. PAI was employed as the overlay material. PAI overlay and a composite overlay dispersed solid lubricant such as MoS₂ were coated onto the micro-textured surface using a spin coating technique. First the intermediate layer of PAI was coated onto the textured substrate then the surface layer of PAI or PAI+MoS₂ was coated onto the intermediate layer.

It was possible to control the thickness of the overlay layers through the revolution speed of the spin coating. The specimens were baked in an electric furnace after vaporizing the solvent on a hot plate. The film thickness and surface profile of the surface layer were controlled by polishing using diamond slurry. The total film thickness was 10 μm. Fig. 1 shows the surface morphology of the non-treated surfaces (NT, Fig.1(a)), textured surfaces (SP, Fig.1(b)), overlay surfaces (OL, Fig.1(c)), and polished surfaces (P, Fig.1(d)). Four types of specimens with different layer structures were prepared, as shown in Fig. 2. The alignment of MoS₂ in the overlay layers was evaluated using wide-angle X-ray diffraction.

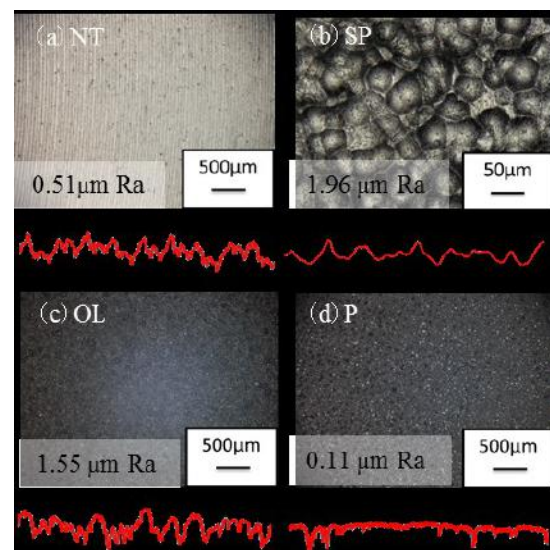


Fig. 1 Optical microscope images and profiles of the surfaces of the specimens before friction test.

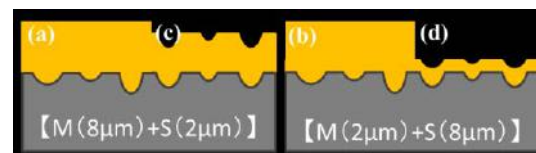


Fig. 2 Schematics of the prepared overlay structures that were coated onto the micro-textured substrates.

(M: Middle layer, S: Surface layer)

- (a) 2 μm PAI surface layer on 8 μm PAI middle layer
- (b) 2 μm PAI+MoS₂ surface layer on 8 μm PAI middle layer
- (c) 8 μm PAI surface layer on 2 μm PAI middle layer
- (d) 8 μm PAI+MoS₂ surface layer on 2 μm PAI middle layer

Friction behaviors were evaluated using a three-ball-on-disc type testing apparatus under lubricated conditions. The mating specimens were chromium alloy steel (SUS304) balls. The testing surfaces were flat, 1.5 mm in diameter and with a mirror finish, and the balls were placed at equal intervals (=120 degrees) on the same circumference. The testing conditions were a sliding speed of 0.25 m/s, an applied load of 200 N (an apparent contact pressure of 40 MPa), the sliding time of 3600 sec. 40 μ l of PAO (5 cSt at 313 K) were employed as a lubricant.

3. RESULTS AND DISCUSSION

3.1. MoS₂ alignment

In the case of MoS₂ powder, the strongest diffraction peak that was observed derived from the (002) of MoS₂ at 14.3°. Diffraction peaks deriving from the (004) and (006) were also observed. On the other hand, in the case of the overlay containing MoS₂, the strongest peak that was observed derived from the (002) of MoS₂, and another peak was observed at 39°. This peak was derived from the (103) of MoS₂, perpendicular to the (002) of MoS₂. In order to compare the alignments of MoS₂, an intensity ratio ($I_{(002)}/I_{(103)}$) was calculated. In the case of the thin top PAI+MoS₂ layer, the value of $I_{(002)}/I_{(103)}$ was 57.1, which was higher than the value for the thick top PAI+MoS₂ layer (39.1). This result indicates that the MoS₂ in the surface overlay layer became highly aligned through the high-speed spin coating process.

3.2. Friction behavior

Fig. 3 shows the initial friction behavior of the various overlays. In the case of the overlays without MoS₂, the coefficient of friction increased in the early stages, then became almost constant with a gradual decrease. However, in the case of the overlays containing MoS₂, the coefficient of friction became almost constant with a gradual increase. These results indicate that aligned MoS₂ in the surface layers was effective for moderate running-in.

Fig. 4 shows optical micrographs of the overlay surfaces without/with MoS₂ after the friction test. In the case of the overlay surface without MoS₂, some grooves were observed at the center on the friction track in Fig. 4(a) and (c). Almost no differences by the resulting from thickness of the surface layers were observed. On the other hand, in the case of the overlay surface with MoS₂, Friction tracks were observed on the right side. In Fig. 4(b) and (d), the red dots indicate MoS₂ particles on the surface. Before the friction test, many agglomerates of MoS₂ were observed on the surface. After the friction test however, few agglomerates were observed on the wear track.

4. CONCLUSION

The present study describes the tribological behavior of PAI overlays containing MoS₂ powder. The MoS₂ in the surface overlay layers became highly aligned through a

high-speed spin coating process. In the case of the overlays containing MoS₂, the coefficient of friction became almost constant with a gradual increase, and this was in contrast to the case of the overlays without MoS₂.

REFERENCES

- [1] Y. Kumada, K. Hashizume and Y. Kimura, "Performance of Plain Bearings with Circumferential Microgrooves", *J. of Japanese Soc. of Tribologists*, Vol. 43, No. 6, pp.456-461, 1998. (in Japanese)
- [2] H. Sonobe, "Trend of Plain Bearing Overlays for Diesel Engines", *J. of the Japan Institution of Marine Engineering*, Vol. 46, No. 5, pp.674-677, 2011. (in Japanese)
- [3] Y. Horiba, S. Kobayashi, H. Akita and H. Usami, "Friction properties of MoS₂ penetrated aluminum alloy", *Proc. of JAST Tribology Conference 2013 Autumn*, L0146, 2013. (in Japanese)
- [4] J. Ishihara, Y. Horiba, K. Enomoto and H. Usami, "Tribological properties of polymer overlay coated on the micro-textured metal substrate", *Proc. of Malaysian International Tribology Conference 2015*, pp.294-295, 2015.

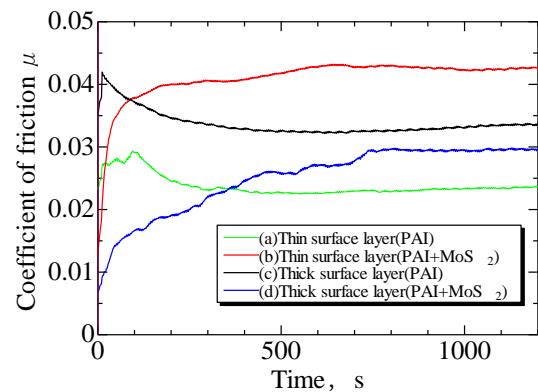


Fig. 3 Initial friction behavior of the various overlays.

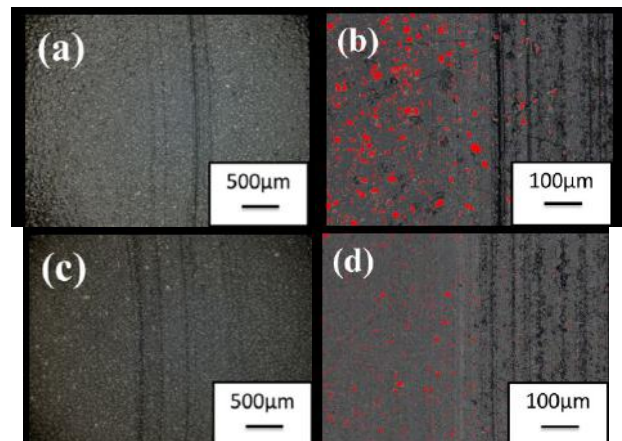


Fig. 4 Overlay surfaces without MoS₂ and with MoS₂ after friction test.

- (a) Thin surface layer without MoS₂
- (b) Thin surface layer with MoS₂
- (c) Thick surface layer without MoS₂
- (d) Thick surface layer with MoS₂

Red dots indicate MoS₂ particles on the surface

DRY SLIDING WEAR PERFORMANCE OF TIG EMBEDDED COMPOSITE COATINGS USING TAGUCHI BASED GREY RELATIONAL ANALYSIS APPROACH

K. A. Bello ^{1,2}, M. A. Maleque ¹, and A. A. Adebisi ¹

¹*Department of Manufacturing and Materials Engineering, International Islamic University Malaysia, Darul Salam, 53100 Gombak, Selangor, Malaysia.*

²*Department of Metallurgical and Materials Engineering, Ahmadu Bello University Zaria, Nigeria.
 E-mail: bello.kamilu@live.iium.edu.my or bellkamm@gmail.com*

1. ABSTRACT

Many tribological coatings working under high temperature environment require combination of low wear rates and friction coefficients, which presents a significant challenge to the tribology community. This study presents an approach based on the Taguchi design with grey relational analysis (GRA) for optimizing the tungsten inert gas (TIG) torch process parameters with consideration of multiple performance characteristics in order to minimize the wear and friction characteristics of TIG embedded composite coatings simultaneously. Taguchi based grey relational analysis with L-16 orthogonal array is employed to analyze the effects of the welding current, welding speed, welding voltage and argon gas flow rate (AFR) on the multiple response characteristics. A grey relational grade from the GRA is used as the performance index to determine the optimal process parameters for the coating system. The experimental results indicate that welding current parameter has the most significant contribution in controlling the wear and friction characteristics. Finally, confirmatory experiment was conducted to ensure the validity of the predicted GRA optimal parameter model.

2. INTRODUCTION

Wear and friction failures account for the major phenomena reducing the effectiveness and life of most mechanical components in sliding contacts. Among carbide ceramic materials, titanium carbides (TiC) particles have attracted much interest because of certain properties that make them desirable for tribological application. Chief among these properties are high hardness, high melting point, good thermal and chemical stability [1]. Ceramic composite coatings containing TiC particles have been employed to enhance the surface wear performance of low alloy steel (LAS) materials. Attempts have been made to fabricate TiC composite coatings using TIG torch melting technique. The coating process is conducted by melting the powder with the energy provided by the TIG arc welding process [2]. The property and quality of TIG modified surfaces depend on the operating parameters of the process. In order to achieve the best functional coating layer exhibiting combination of lower wear rate and friction coefficient (CoF) characteristics, statistical approach with multi-objective consideration can be employed for identification of optimal process parameters. In recent years, Taguchi

based grey analysis has become a widely accepted approach for investigating multiple performance characteristics of overlay welding process in surface coating [3]. Hence, in this work, Taguchi based GRA method was adopted to investigate the effects of the welding current, welding speed, welding voltage and AFR on the wear rate and coefficient of friction of TIG embedded composite coatings.

3. MATERIAL AND METHOD

3.1 MATERIALS AND METHODS

The rectangular blocks of AISI 4340 low alloy steel with size of 100 mm x 40 mm x 15 mm were used as substrates. Prior to powder preplacement, the surface of the substrates was ground to a surface roughness of about $R_a = 0.4 \mu\text{m}$ and then cleaned with acetone under ultrasonic waves for 30 minutes. Titanium carbide particle (40 μm and 99.9 wt. % purity) supplied by Sigma Aldrich USA was used as the coating material in this study. The powder mixed with organic powder (PVA), distilled water and alcohol was preplaced onto the substrate and then dried in the oven at 80 °C. After one hour, the preplaced samples were allowed to melt and resolidify with an overlapping track ratio of 50 % using TIG torch technique. The selection and design of parameter for the TIG torch melting experimental process were conducted according to Taguchi L-16 orthogonal array. Sixteen experimental trials were performed as per the Taguchi design. The parameters used in this study and their levels (L1-L4) for depositing TiC composite coating on LAS are given in Table 1. After TIG surface coating experiments, a TR-20-PHM-CHM-600 (DUCOM) ball-on-disc tribometer was used to evaluate the high-temperature dry sliding wear and friction coefficients behavior of the coatings at 600 °C.

Table 1 Process parameters and their levels

Symbol	Parameter	Unit	L1	L2	L3	L4
A	current	A	70	80	90	100
B	Speed	mm/s	1.0	1.5	2.0	2.5
C	voltage	V	20	25	30	35
D	AFR	L/min	10	15	20	25

The sliding wear test was performed using a normal load of 10 N, rotating speed of 0.2 m/s, a sliding distance of 500 m, an alumina ball of 6 mm diameter and track diameter of 7 mm. Finally, the wear worn surfaces of the coatings were investigated using SEM.

4. RESULT AND ANALYSIS

Table 2 shows the experimental studies conducted based on the L-16 OA. The wear and coefficient of friction from the sliding wear test experiment are given in Table 2. Based on these experimental values, the grey relational grades (GRG) calculated through grey analysis procedures are also given in the table.

Table 2 L-16 OA experimental results, grey relational grade and its order for TiC Composite coatings

Exp. No.	Wear rate mm ³ /Nm	Coefficient of friction	Grey relational grade	Order
1	9.8072E-06	0.5600	0.9112	2
2	1.0825E-05	0.5800	0.7636	4
3	8.3717E-06	0.6300	0.7267	5
4	2.5134E-05	0.6000	0.4848	16
5	8.5910E-06	0.5800	0.8543	3
6	1.2182E-05	0.6500	0.5538	12
7	1.1809E-05	0.6300	0.5951	10
8	1.2262E-05	0.7000	0.4996	15
9	9.7859E-06	0.6600	0.6179	7
10	1.1206E-05	0.6300	0.6127	8
11	1.2645E-05	0.6300	0.5734	11
12	7.9527E-06	0.5700	0.9375	1
13	1.2795E-05	0.4700	0.6379	6
14	1.7089E-05	0.4500	0.5115	14
15	1.4426E-05	0.4700	0.5351	13
16	1.9787E-05	0.4400	0.5992	9

According to the result shown in Table 2, experiment number-12 had highest grey relational grade of 0.9375 among the sixteen experiments. This indicates that experiment 12 has the best multiple characteristic for minimum wear rate and CoF.

Table 3 Mean GRG for TiC composite coating

Level	A	B	C	D
1	0.6453	0.6104	0.6133	0.6189
2	0.5449	0.6660	0.6107	0.6174
3	0.7651	0.6334	0.6461	0.7756
4	0.6483	0.6939	0.7335	0.5917
Delta	0.2202	0.0835	0.1228	0.1840
Rank	1	4	3	2

Table 3 shows the mean grey relational grade for each level of the process parameter. The delta value is used for evaluating the relative importance of each process parameter on the multi-performance of wear rate and CoF. From Table 3, the maximum delta value is 0.2202. This therefore reveals that welding current has the strongest effect on the multi-performance characteristics among various TIG process parameter investigated. The process parameter influencing the GRG is shown in Figure 1. Basically, the level of the parameter with the highest GRG gives the optimal level.

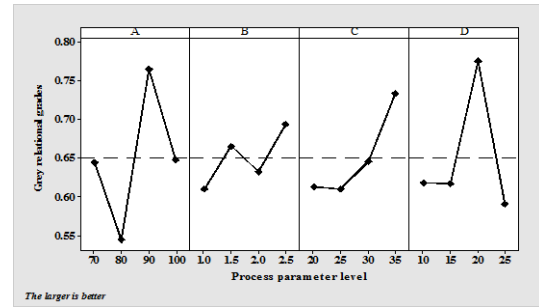


Fig 1 Influence of process parameter on GRG

From Fig. 1, the optimal parameter condition for minimizing multi-response characteristics of wear rate and CoF were welding current of 90A, welding speed of 2.5 mm/s speed, welding voltage of 35 V and argon flow rate of 20 L/min (A3-B4-C4-D3). In order to validate the result of the optimized condition, further experiment was conducted using the optimal level of the process parameter. The result shows an improvement of 5% and prediction error of 2.4 %, indicating the accuracy of the analysis. Figure 2 compares the SEM micrographs of worn out surfaces produced under optimized parameter condition and the best condition suggested by GRG ranking (experiment 12, Table 2). As shown in Figure 2, the sample produced with the optimized condition shows clearly finer grooves, less delamination and few craters (Fig. 2a) due to mild abrasive wear as compared to that of the best GRG's parameter condition (Fig. 2b).

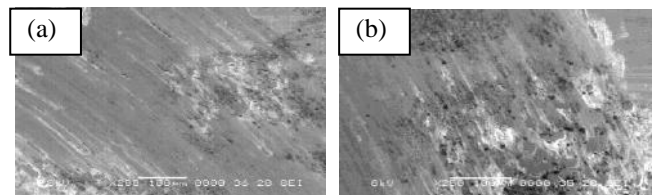


Fig 2 Wear worn surfaces of coating produced using (a) Optimized condition (b) Best condition predicted by GRG.

5. CONCLUSION

From grey relational analysis, it was found that the best combination of TIG process parameters for minimizing wear rate and CoF in TiC composite coating are welding current of 90A, welding speed of 2.5 mm/s speed, welding voltage of 35 V and argon flow rate of 20 L/min. Under this condition, the surface of the worn out sample show minimal wear damage characterized by mild abrasive wear.

REFERENCES

- [1] D.X. Peng, "The Effects of Welding Parameters on Wear Performance of Clad Layer with TiC Ceramic," *Industrial Lubrication Tribology*, Vol. 64, No. 5, pp. 303-311, 2012.
- [2] K.A. Bello, M. A. Maleque, A. A. Adebisi, and A. Dube, "Preparation and Characterization of TIG-Alloyed Hybrid Composite Coatings for High-Temperature Tribological Applications," *Transactions of the IMF*, Vol. 94, No. 4, pp. 211-221, 2016.
- [3] Y.S. Tarn, S.C. Juang and C.H. Chang, "The Use of Grey-Based Taguchi Methods to Determine Submerged Arc Welding Process Parameters in Hardfacing," *Journal of materials processing technology*, Vol.128, pp. 1-6, 2002.

TRIBOLOGICAL PROPERTIES OF PLASTIC MATERIALS RUBBED AGAINST 6061-T6 ALUMINUM ALLOY UNDER HIGH-TEMPERATURE HYDROGEN ATMOSPHERE

T. Yasugi¹, T. Iwai¹, T. Ueda¹, and Y. Shoukaku¹

¹Graduate School of Natural Science and Technology, Kanazawa University, Japan.

1. INTRODUCTION

Environmental problems such as global warming and air pollution caused by fossil fuel consumption are currently reaching serious levels. Hydrogen is thus receiving attention as a potential clean energy. Hydrogen-related equipment such as fuel-cell vehicles (FCV) and hydrogen stations are being developed. Compressor and pressure reducers for these have sliding parts under hydrogen atmosphere because compressed hydrogen is used. Polytetrafluoroethylene (PTFE) is often used as the sliding material in such equipment because of its low friction coefficient. On the other hand, metallic materials often show hydrogen embrittlement, so it is necessary to employ materials resistant to hydrogen embrittlement. SUS316L stainless steel and 6061-T6 aluminum alloy are reportedly appropriate materials [1]. The use of 6061-T6 aluminum alloy is expected to reduce weight and cost. However, there have been a few reports about the tribological properties of plastic materials, including PTFE composites, when rubbed against aluminum alloy in a hydrogen environment.

The purpose of this study was to clarify the influence of the hydrogen environment on the tribological properties of unfilled PTFE, graphite-filled PTFE, and polyamide 610 (PA 610) rubbed against 6061-T6 aluminum alloy.

2. EXPERIMENTAL METHOD

A pin-on-disk type tribometer was used in this study. Unfilled PTFE, graphite-filled PTFE, and PA 610 were used as the pin specimen with 3-mm diameters. The disk specimen was 6061-T6 aluminum alloy. The surface roughness of the disk was adjusted to $Ra=0.02\text{ }\mu\text{m}$, the contact pressure was 0.7 MPa, and sliding speed was 0.05 m/s. The experiments were conducted at 23 °C and 150 °C in an atmosphere of hydrogen, nitrogen, and air. Friction force was measured by strain gauge, and wear depth was measured by differential transformer. For the high-temperature experiment, heated hydrogen and nitrogen gas were kept flowing into the chamber.

3. RESULTS AND DISCUSSION

3.1. Friction coefficient and specific wear rate

Figure 1 shows the friction coefficient and specific wear rate of pin specimens rubbed against 6061-T6 aluminum alloy. Friction coefficients of unfilled PTFE and graphite-filled PTFE were around 0.2, irrespective of the environment and temperature. Friction coefficients of PA 610 were around 0.5, also independent of the environment

and temperature. The differences in specific wear rates of pin specimens between the atmospheres were not large. It was found that specific wear rates of unfilled PTFE at 150 °C were around 1/100 compared to those at 23 °C. Specific wear rates of graphite-filled PTFE at 150 °C were smaller than those at 23 °C. Specific wear rates of PA 610 at 150 °C were around 10 times as large as those at 23 °C.

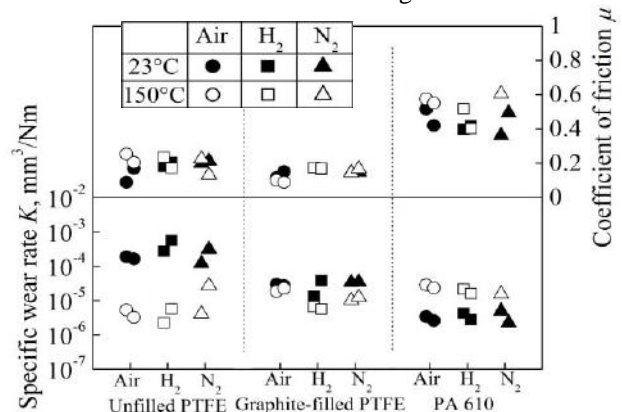


Fig. 1 Friction coefficient and specific wear rate

3.2. Profile curve and surface roughness of disk

Figure 2 shows the profile curves and surface roughness of the sliding surface of disks rubbed against unfilled PTFE. Profile curves and surface roughness were measured by stylus profilometer. Surface roughness in air was almost unchanged. In hydrogen and nitrogen, it was found that the aluminum disk was damaged. In addition, the amount of damage at 150 °C was smaller than at 23 °C. This decrease may have been because the smaller amount of oxygen remaining in chamber prompted the disk surface to oxidize at 150 °C, and the oxide film prevented disk damage.

Figure 3 shows the profile curves and surface roughness of the sliding surface of disks rubbed against graphite-filled PTFE. Surface roughness under air at 23 °C was almost unchanged. Under other environments, surface roughness was increased.

Figure 4 shows the profile curves and surface roughness of the sliding surface of disks rubbed against PA 610. The aluminum disk was damaged under each environment. It was found that the amount of damage at 150 °C was larger than at 23 °C.

5.3. EDX analysis of pin specimen

Eneegy dispersive x-ray spectrometry (EDX) analysis was applied to the sliding surface of each pin specimen. Figure 5 shows EDX maps of the sliding surface of each

pin specimen under hydrogen at 23 °C. Fluorine (F) concluded unfilled PTFE and graphite-filled PTFE, were

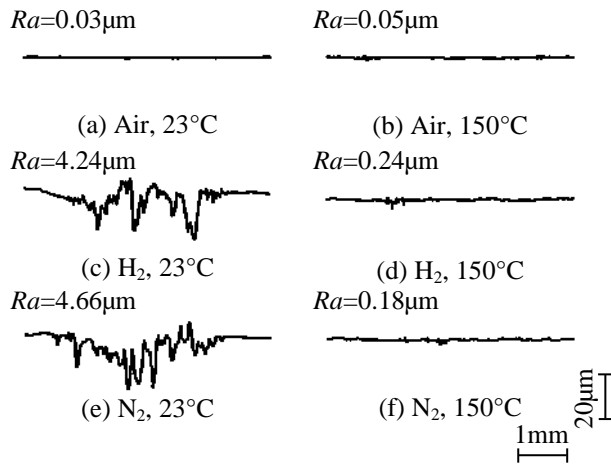


Fig. 2 Profile curves and surface roughness of sliding surface of disks rubbed against unfilled PTFE

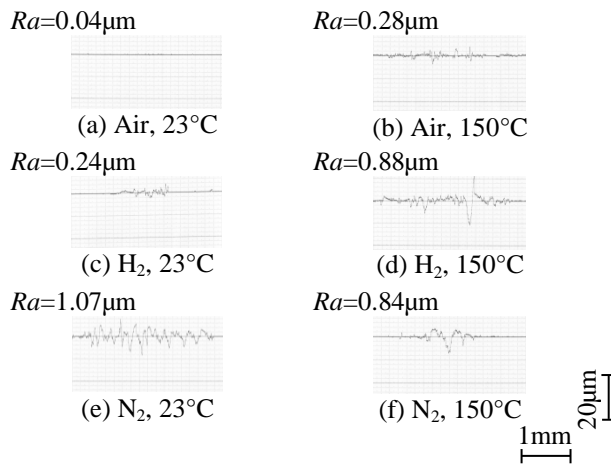


Fig. 3 Profile curves and surface roughness of sliding surface of disks rubbed against graphite-filled PTFE

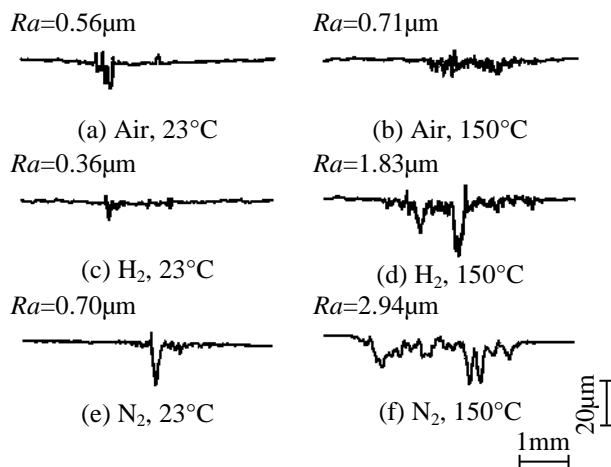


Fig. 4 Profile curves and surface roughness of sliding surface of disks rubbed against PA 610

observed on the sliding surface of unfilled PTFE and graphite-filled PTFE. Aluminum (Al) was also observed on

these sliding surfaces. Some Al and F were observed in the same area. It has been reported that aluminum fluoride was generated [2]. So it is considered that aluminum fluoride may have been produced in this experiment. On the sliding surfaces of PA 610, Al was also observed. Abundant oxygen (O) was observed in the Al area, so it is thought that this substance was probably aluminum oxide.

4. CONCLUSIONS

Unfilled PTFE, graphite-filled PTFE and PA 610 were rubbed against 6061-T6 aluminum alloy under hydrogen atmosphere at 23 °C and 150 °C.

- 1) 6061-T6 aluminum alloy rubbed against each specimen was damaged at both temperatures.
- 2) Disk damage from rubbing against unfilled PTFE was larger at 150 °C than at 23 °C. Specific wear rate of unfilled PTFE and graphite-filled PTFE at 150 °C were decreased.
- 3) Disk damage from rubbing against PA 610 was smaller at 150 °C than at 23 °C. Specific wear rate of PA 610 at 150 °C was increased.
- 4) Al was observed on the sliding surface at each temperature.

REFERENCES

- [1] *Progress report*, "New Energy and Industrial Technology Development Organization," 2005.
- [2] Y. Takeichi, K. Onyu, T. Okada, "Effect of the Generation of Aluminum Fluoride on the Wear of Aluminum Alloy Rubbed with PTFE," *Proceedings of JAST Tribology Conference*, pp. 337-338, 2009.

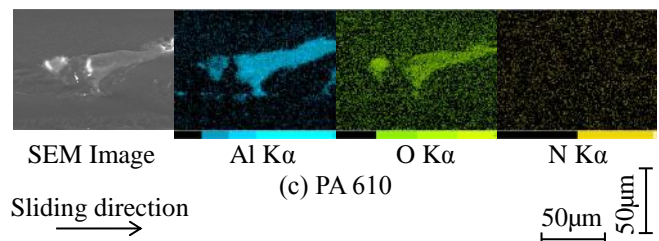
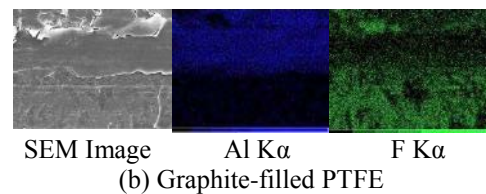
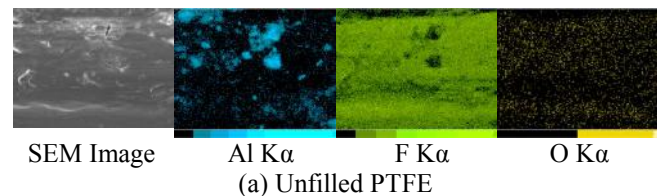


Fig. 5 EDX maps of sliding surface of pin specimens under hydrogen atmosphere at 23 °C

ANALYSIS ON THE EARLY STAGE OF CONTACT ADHESION IN DIFFERENT RELATIVE HUMIDITY

Z. A. Subhi ¹, and K. Fukuda ¹

¹*Malaysia-Japan International Institute of Technology, Universiti Teknologi Malaysia, Malaysia.*
aszaid3@live.utm.my

1. INTRODUCTION

When two surfaces are placed in contact and subjected to applied load, surface roughness causes contacts to occur at discrete contact spots (asperities). The closeness of the asperities results in adhesive contacts caused by either interatomic attractions between solid-solid or can be due liquid assisted adhesion if water presented on the surfaces. In the tribology of micro contacts, frictional and adhesive properties are sensitive to the adsorbed water because surface phenomena become more dominant than volumetric phenomena. The atmospheric humidity causes the water vapor to adsorb on the surfaces. Researchers found that friction force and wear in sliding can be influenced even by extremely low level as the several parts per billion (ppb) concentration of the water on the surfaces [1, 2]. However, in most of published papers about unlubricated friction and wear experiments, the relative humidity of the environment is rarely controlled and often is not stated [3]. The adsorbed water layer can be unfavorable for lubrication and facilitate tribological failures [4]. When a thin liquid film with a small contact angle presents at the interface will result in so-called liquid-mediated adhesion [5]. Nevertheless, there is still a lack of a clear-cut elucidation on the mechanisms of humidity changes to influence the adhesion at the interface. This paper aimed to explore the mechanism of humidity to influence the adhesion by the observation of the tribological behavior during the very early stage of sliding.

2. METHODOLOGY

In order to observe the tribological performance of very local area of contact for the period of the very early stage of sliding, a unidirectional ball-on-ball configuration tribo-contact simulator (T-CS) was developed and used in the current study. The schematic drawing of T-CS and the configuration of the specimens are shown in Fig. 1. T-CS was developed together with a data acquisition system which acquires the data from the sensors of friction force, normal force, specimen displacement, RH rate, and electrical conductivity. Each datum acquired is synchronized to the measurement position on the specimens while sliding. The spatial resolution of data collection for each measured item is 5 μm . In the current study, the friction force, specimen displacement, and electrical conductivity were evaluated as a function of distance with different RH rates. The T-CS was equipped with an air-humidity controller and the RH range can be regulated at

the value between 4% and 95%. The flow rate of humidity controlled air delivered to the testing chamber can be regulated from 1 to 10 square cubic feet per hour (SCFH). The experiments were performed at 8, 55, and 95 % RH, respectively. The materials of the ball specimens used in the experiments were JIS SUS316 with 4 mm diameter. In order to maintain the spherical shape, the surface of the ball specimens was not polished and used with original surface finishing as purchased. The measured average surface roughness of SUS316 ball specimens was approximately 0.85 μm Ra. All of the ball specimens were ultrasonically cleaned in a 50:50 mixture of acetone and hexane for 10 minutes and subsequently the samples were fixed up in the chamber of the tribotester after drying. The T-CS was operated at 2,000 $\mu\text{m/s}$ sliding speed. The distance of measurement was 3,200 μm . An overlap distance between the ball specimens was necessary to generate the area of contact while sliding. The overlap distance was adjusted to 90 μm before the test is conducted. The applied load while sliding was 10 N. A D.C. voltage source of 150 mV was applied between the samples to check the electrical conductivity while sliding. The test was conducted for three measurement cycles at each RH rate, because the purpose of this study is to investigate the very early stage of sliding.

3. RESULTS AND DISCUSSION

In general, the results of friction force showed in Fig. 2 (a) displayed its lowest trend during the first cycle at all RH rate. This is perhaps because the protective layer of the oxides and surface contaminations were capable to fully or partially prevent direct metal-metal contact. As for the second and third cycles, the results showed higher friction forces especially and the case of RH 8 and 55%. At RH 55% the interface maybe experienced both solid-solid adhesion as well as liquid-mediated adhesion by the meniscus forces around the opposing asperities. In medium rate of RH, the adsorbed water layer could form a meniscus bridge around the contacting asperities which worked to increase the pull-off forces. This pull of forces results from the negative Laplace pressure that generated an attractive force to proximate the opposing asperities into each other's. This situation can result in excessive damage on the surfaces as can be seen in the results of the specimen displacement in Fig. 2 (b). Our suggestion fairly agrees with Ando's study when he found that increment of friction force with RH was caused by the increase of both pull-off force and viscous resistance of water film at the rate of at

the rate RH 67% for multi asperity arrays [6]. The presence of thick water layer [6] can be confirmed from the results of electrical conductivity in Fig 2 (c) at RH 95%. The ball specimens were fully conductive throughout the 3 cycles and this is due to the presence of thick adsorbed water layer on the surface.

3. CONCLUSIONS

The results have manifested the mechanism of the humidity changes to influence the adhesion during the very early stage of sliding. The results suggest that at medium RH rate can be a critical condition for the tribological phenomenon due to the effect of liquid assisted adhesion. However, in order to accomplish the understanding of the current results, the surface characteristics and properties from the physical and chemical viewpoints need to be further studied.

ACKNOWLEDGEMENTS

This work was supported by matching grant scheme Vote No. 00M82 by Universiti Teknologi Malaysia and Ministry of Higher Education, Malaysia.

REFERENCES

- [1] K. Fukuda, M. Hashimoto, and J. Sugimura, "Friction and Wear of Ferrous Materials in a Hydrogen Gas Environment," *Tribology online*, Vol. 6, No. 2, pp. 142-127, 2011.
- [2] K. Fukuda and J. Sugimura, "Influences of Trace Water in a Hydrogen Environment on the Tribological Properties of Pure Iron," *Tribology online*, Vol. 8, No. 1, pp. 22-27, 2013.
- [3] J.K. Lancaster, "A review of the influence of environmental humidity and water friction, lubrication and wear," *Tribology International*, Vol. 23, No. 6, pp. 371-389, 1990.
- [4] S.J. Park, J.K. Kim, K.R. Lee and D.H. Ko, "Humidity dependence of the tribological behavior of diamond-like carbon films against steel ball," *Diamond and Related Materials*, Vol. 12, pp.1517-1523, 2003.
- [5] B. Bhushan, "Adhesion and stiction: Mechanisms, measurement techniques, and methods for reduction," *Journal of Vacuum Science & Technology B*, Vol. 21, 2262-2296, 2003.
- [6] Y. Ando, "The Effect of Relative Humidity on Friction and Pull-Off Forces Measured on Submicron-Size Asperity Arrays," *Wear*, Vol. 238, pp. 12-19, 2000.
- [7] Z. A. Subhi, K. Fukuda, and T. Morita, "Quantitative Estimation of Adsorbed Water Layer on Austenitic Stainless Steel," Vol. 10, No. 5, 314-319, 2015.

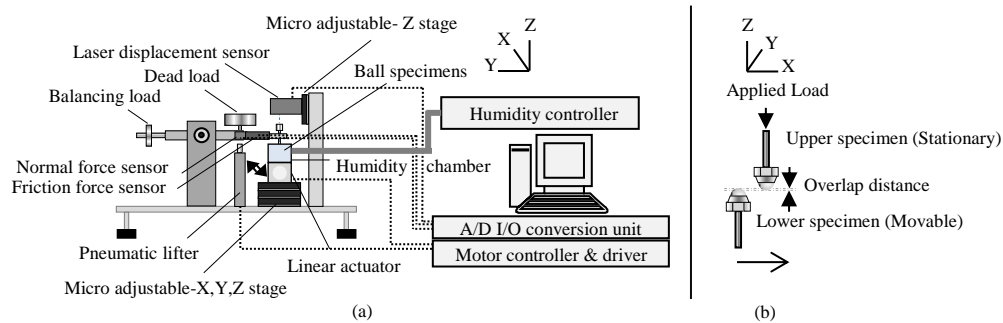


Fig 1 (a) Schematic drawing of T-CS and (b) The configuration of ball specimens in T-CS.

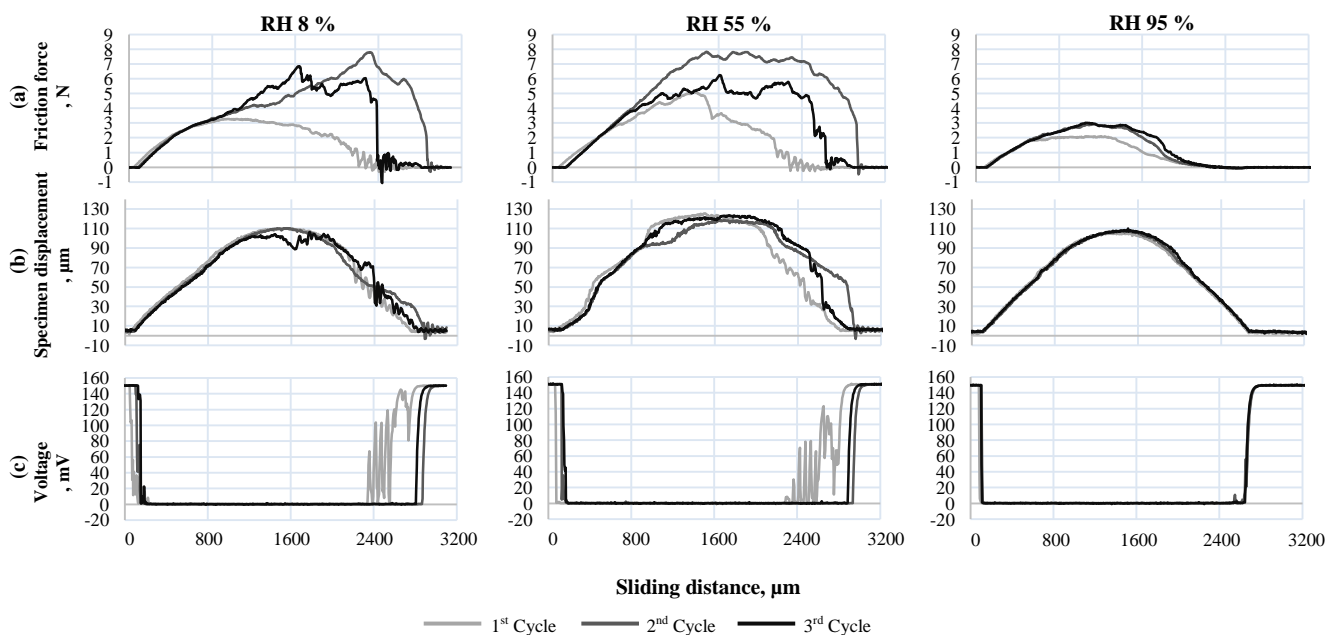


Fig. 2 (a) Friction force, (b) Specimen's displacement, and (c) Voltage, at different RH rate.

EFFECTS OF SLIDING SPEED ON FRICTION AND WEAR OF CARBON FIBER FILLED PTFE IN HYDROGEN

T. Morita^{1,2}, Y. Abe³, Y. Sawae^{1,2}, J. Sugimura^{1,2,4}

¹Faculty of Engineering, Kyushu University, Japan.

²International Institute for Carbon-Neutral Energy Research, Kyushu University, Japan.

³Graduate School of Engineering, Kyushu University, Japan.

⁴Research Center for Hydrogen Industrial Use and Storage, Kyushu University, Japan.

1. INTRODUCTION

In recent years, environmental problems such as global warming, air pollution, cut down the amount of carbon dioxide and exhaustion of fossil fuel have become international issue. Hydrogen is a promising energy carrier in energy and transportation systems in the future because it's low environmental load. Recently, Fuel cell vehicle (FCV) just came out in Japan. For further expansion of the use of FCV, it is necessary to solve a lot of tribological problems associated with hydrogen production, storage and use. In these systems, polymers are used as gas seals in many valves and compressors and sliding against metal counterface in hydrogen gas environment.

Polytetrafluoroethylene (PTFE) based composites are widely used in a reciprocating gas compressor as dynamic seals, such as piston rings rider rings and rod packings. Our results indicated that carbon fiber filled PTFE was compatible with hydrogen gas environment and showed relatively better friction and wear behavior compared with glass fiber filled PTFE and PPS filled PTFE[1]. In this study, tribological characteristics of the carbon fiber filled PTFE composite

was examined in different sliding speed and sliding distance in the hydrogen gas environment and the effects were discussed.

2. MATERIAL AND METHODS

Sliding test were carried out with a pion-on-disk type testing machine that have a vacuum chamber. Pins were prepared from 20% Polyacrylonitrile (PAN) –based CF fiber filled PTFE. Tungsten carbide (WC) disks were used as sliding conterface. Surface roughness (Ra) of disc specimens were 0.04 μm .

All experiments were conducted under dry condition with

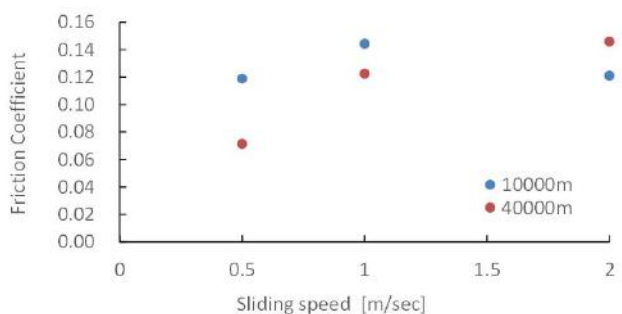


Fig. 1 Friction coefficient with sliding speed

ambient temperature 373 K in hydrogen gas. Sliding speed were 0.5, 1 and 2 m/s. Contact pressure was 1 MPa. Sliding distance were 10000m and 40000m.

After the sliding test, detailed observation and chemical analyses with Raman microscopy and spectroscopic ellipsometry were conducted for the polymer worn surface to understand the obtained friction and wear mechanisms in the hydrogen environment.

3. RESULT AND DISCUSSIONS

Figure 1 showed the final average friction coefficient (the last 1000m) with different sliding distance plotted against sliding speed. In the short sliding distance, the influence of the sliding speed on the friction coefficient was not recognized. In contrast, the tendency that the coefficient of friction became smaller when speed became small at the long sliding distance was recognized.

Figure 2 showed the volumetric wear rate of pin plotted against sliding speed. The wear rate decreased with increasing the sliding speed. The wear reduction by the extended sliding distance became the most significant under the lowest sliding speed.

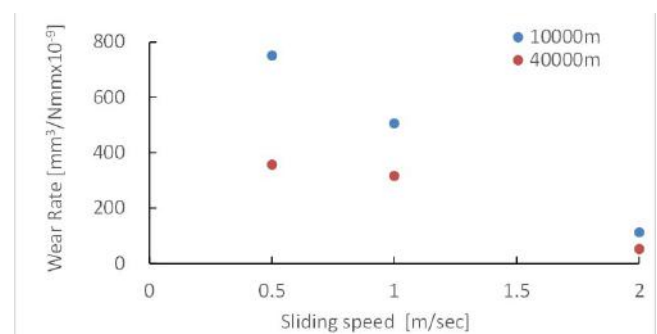


Fig. 2 Wear rate with sliding speed



(a) 0.5m/s (b) 1m/s (c) 2m/s

Fig.3 Pictures of the surface of pins after test at 40000m

These results indicated that the effects of sliding speed on friction coefficient and wear rate were not negligible.

Microscopic images of polymer worn surfaces taken after sliding tests were shown in Fig. 3. Comparing these pictures, it indicated that the pin surface slid under 2m/s was covered with thin white film. The area of this thin white film was decreased with the reduction of sliding speed. Furthermore, to investigate the thickness of the white film on the pin surfaces, the worn surfaces were analyzed with spectroscopic ellipsometry. Figure 4 showed the film thickness formed on the pin surfaces with different sliding distance plotted against the sliding speed. The film thickness of the pin surface were depended on the sliding speed, but it was not proportion to the sliding speed.

To analyze the chemical structure of white thin film, the Raman spectroscopy was conducted. Figure 5, 6 and 7 showed the Raman spectra of the white film area on the pin surfaces with different sliding speed at 40000m sliding distance. The peaks of the graphite structure-derived G-band and the defect-derived D-band appeared at around 1580 cm^{-1} and 1360 cm^{-1} of the all sliding speed experiments. These results clearly indicating that the white film formed during sliding test consist of carbon molecules with some graphite structure. The carbon based peak area intensity of the spectra (peak area from $900\text{ to }1800\text{ cm}^{-1}$) became larger with increasing the sliding speed. It means that the amount of carbon contained in the white film was larger under higher sliding speed. The ratio of G-band/D-band were about 1.2 at sliding speed 1m and 2m, but the ratio was about 1 at sliding speed 0.5m/s. It means that the structure of the white carbon film was different with the sliding speed. Therefore, the difference in the amount and structure of carbon film formed on the composite surface had some influence on friction and wear characteristics.

4. CONCLUSIONS

In this study, we conducted sliding test between PAN-based CF filled PTFE and tungsten carbide to investigate how sliding speed and sliding distance in hydrogen gas influences the friction and wear characteristics. From the experiments, it was revealed that the increase of sliding speed resulted in the decrease of the wear rate, but increase of the friction coefficient. On the other hand, chemical analysis indicated that white carbon films were formed on the pin surfaces and amount and structure of the carbon film were affected by the sliding speed. Consequently, the thick carbon film formed on the composite surface during sliding would be responsible for the reduced wear rate under the high sliding speed. To explore more detailed mechanisms, further experiments wider range of PV value and detailed analysis might be necessary.

REFERENCES

- [1] Y. Sawae et al. " Friction and Wear Mechanism of Carbon Fiber Filled PTFE in High purity Hydrogen ", Proc. JAST Tribology Conference, 2016.

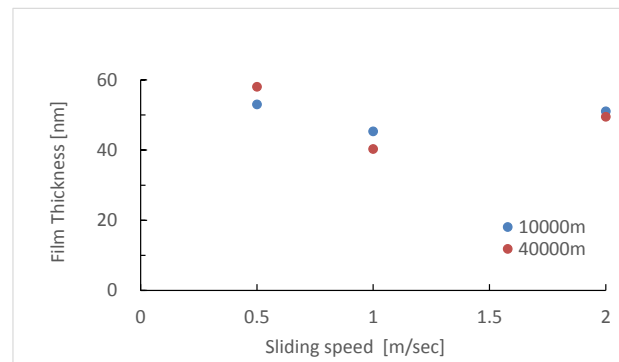


Fig. 4 Film thickness by spectroscopic ellipsometry with sliding speed

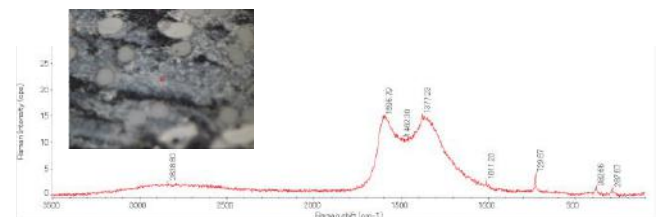


Fig. 5 Raman spectra of 0.5m/s sliding speed at 4000m

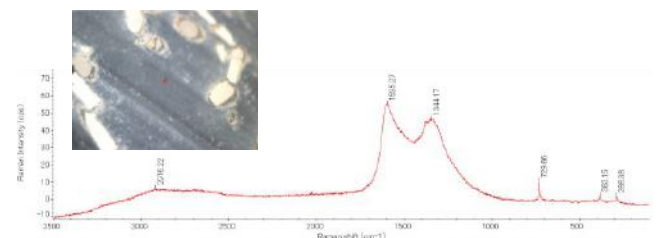


Fig. 6 Raman spectra of 1m/s sliding speed at 4000m

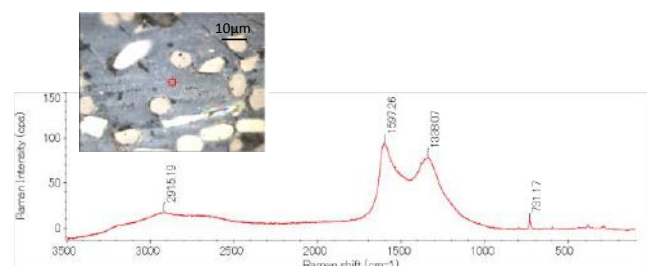


Fig. 7 Raman spectra of 2m/s sliding speed at 4000m

TIME DEPENDENT CHANGE OF WATER ADSORPTION ON AUSTENITIC STAINLESS STEEL

N. D. A. Manaf¹, K. Fukuda¹, Z. A. Subhi¹, M. F. M. Radzi¹

¹Department of Mechanical Precision Engineering, Malaysia-Japan International Institute of Technology, Universiti Teknologi Malaysia, Malaysia.

1. INTRODUCTION

The adsorption of water on surfaces plays an important role in tribology, and the influences of the adsorbed water have been investigated for many years since it has attracted much attention from many researchers in tribology fields. Henderson [1] showed that the adsorption of water onto surfaces has been studied in great detail and reviewed several times over the past decades. Quantitative study on adsorbed water on austenitic stainless steel was done by Subhi et. al [2] and reported as 1,800 s was long enough for reaching the saturation level of water adsorption. However, the experimental study was done for the surface as machined finish by a manufacturer and necessary time for the adsorbed water to be stabilized on the surfaces with different roughness is left unknown. In this study, the time dependent changes of water adsorption on the surface of austenitic stainless steel (JIS SUS 304) with 2 different surface roughness level were determined in different relative humidity conditions. The obtained results will be discussed in terms of both adsorption of water and time scale.

2. EXPERIMENTAL METHOD

In this study, the experiments were carried out using a weighing method [2]. Specimens were made of austenitic stainless steel (JIS SUS 304) with dimensions of 100 x 100 x 0.2 mm thickness. One of the specimens was used as purchased (machine finished by a manufacturer) and two were used after finishing surface using sand paper with grain sizes of #1000 and #120, respectively. Average

surface roughness was measured by a stylus type profilometer (Mitutoyo SJ-410). The stylus was calibrated before the test and the measurement was conducted at room temperature. Average roughness (Ra) value for each specimen is shown on Table 1. Firstly, specimens were ultrasonically cleaned in the mixed solution made of 50:50 hexane and acetone for one cycle of 600 s. After that, the specimens were dried in air naturally and the weight of the specimens was measured using an electrical balance and then recorded. The specimen was hanged (unloaded) in a chamber in which humidity controlled air was inlet and then the specimen was loaded on the electrical balance to evaluate its weight as shown in Fig. 1. RH rate of air was changed suddenly from RH of laboratory room to around 12% and kept until the weight of the specimen got stabilized. After confirming the stabilization, the RH of air was change suddenly to around 90% and kept until the weight of the specimen got stabilized. The measurement of the weight of the specimen and RH of air in the chamber was done every 300s interval. Before each measurement of weight, the specimen was unloaded and the electrical balance was calibrated. Three times measurement was taken for each RH rate to ensure the repeatability of the data.

Table 1 Average surface roughness (Ra) values of the SUS 304 specimens

Specimen	Surface finishing	Ra (μm)
1	As purchased	0.055
2	#1000	0.057
3	#120	0.184

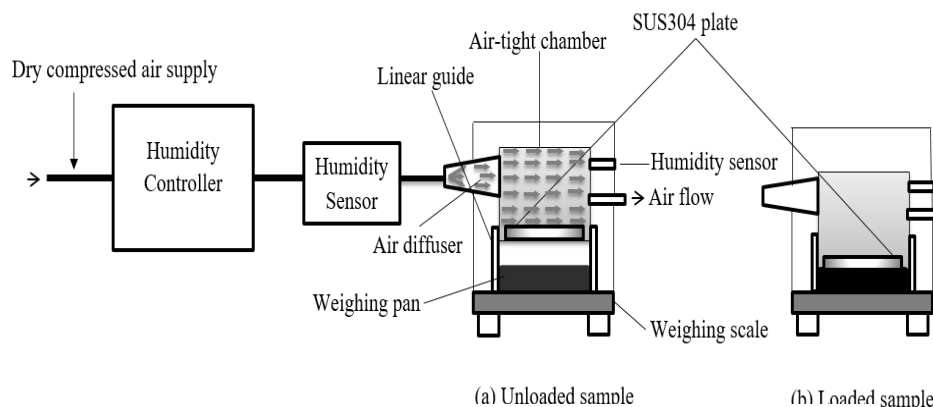


Fig. 1: Schematic illustration of the measurement device

3. RESULTS AND DISCUSSION

Figure 2 shows the changes of the specimen weight and RH as a function of time for the case of specimen as purchased. RH of inlet air was changed suddenly but reading of humidity meter got some delay. The delay should be attributed to the time constants due to the volume of the chamber and sensor response of the setup which is employed in the current study. The differential weight of the specimen in dry (around RH 10%) air and wet (around RH 90%) which can be regarded as adsorbed water was 0.46 mg. Fig. 3 shows the relationship between the surface roughness of the specimen and the weight of adsorbed water. According to these results we can expect the tendency that rougher surface will get more water adsorption. Another fact which can be noticed from Fig.2 is that time t' necessary to dry the specimen is significantly longer than time t to wet the specimen. Fig. 4 shows t and t' for different surface finishing of specimens. Rougher surface finished with #120 sandpaper spent longer time for both wetting (10,200 s) and drying (12,000 s) than other finishing surface did. It should be noted that specimens as purchased and finished with #1,200 sand paper showed very different t and t' while they showed similar values for surface roughness and the weight of adsorbed water. This means t and t' are not simply determined by surface roughness but influenced by other factors. In this study, it was clarified that stabilization in the weight of a specimen in each RH condition should be confirmed while determining the relationship between the weight of adsorbed water and RH rates.

4. CONCLUSIONS

In this study, time scale has a significant effect on adsorption, both in terms of the total amount adsorbed as well as the material surface. It could be clarified that the difference in the surface roughness can influence the time scale and the weight of water adsorption significantly. In addition, the rougher surface takes longer time to wetting and drying than the smoother surface and other factors than surface roughness gives influences on the time. It was suggested that the confirmation on the stabilization in the weight of a specimen is important for determining the amount of adsorbed water. To further investigate these phenomena, it is necessary to make the additional experimental works that will determine how water exist on the metallic surfaces to reveal unknown factors which control the wetting and drying time.

5. REFERENCES

- [1] Henderson, M. A. The Interaction of Water with Solid Surfaces: Fundamental Aspects Revisited. *Surf. Sci. Rep.* 2002, 46, 1-308.
- [2] Subhi, Z. A., Fukuda, K., Morita, T., & Sugimura, J. (2015). Quantitative Estimation of Adsorbed Water Layer on Austenitic Stainless Steel. *Tribology Online*, 10 (5), 314-319.

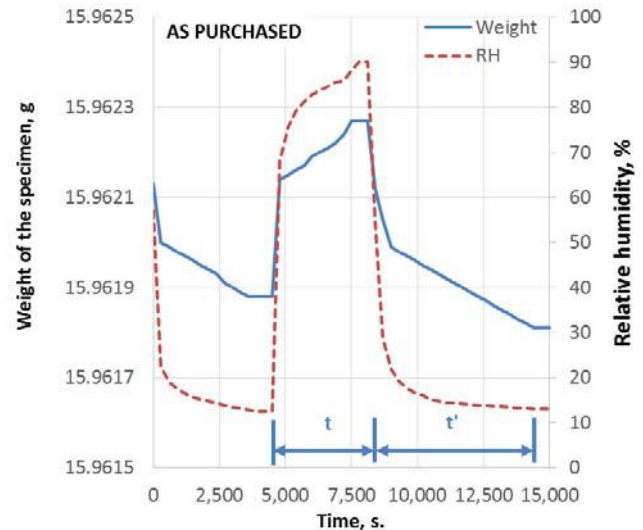


Fig. 2 Changes in weight as purchased SUS 304 plate in different RH as a function of time.

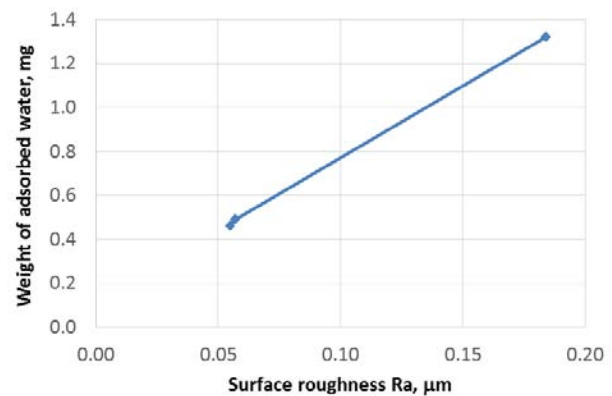


Fig. 3 Weight of adsorption water compared to the result from the average surface roughness.

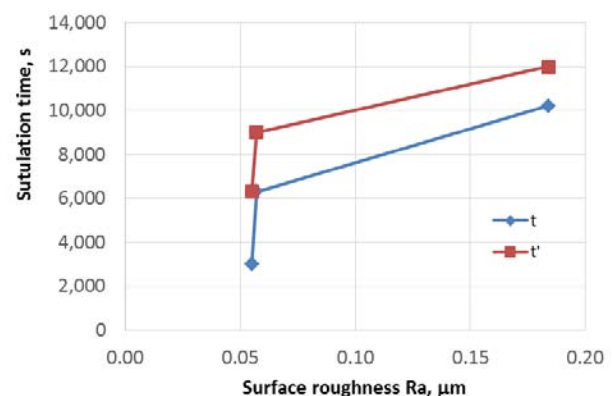


Fig. 4 Time to be taken for wetting and drying compared to the result from the average surface roughness.



TAAT BESTARI SDN BHD

(CO. NO. 438402-D)
(SYARIKAT BUMIPUTRA)

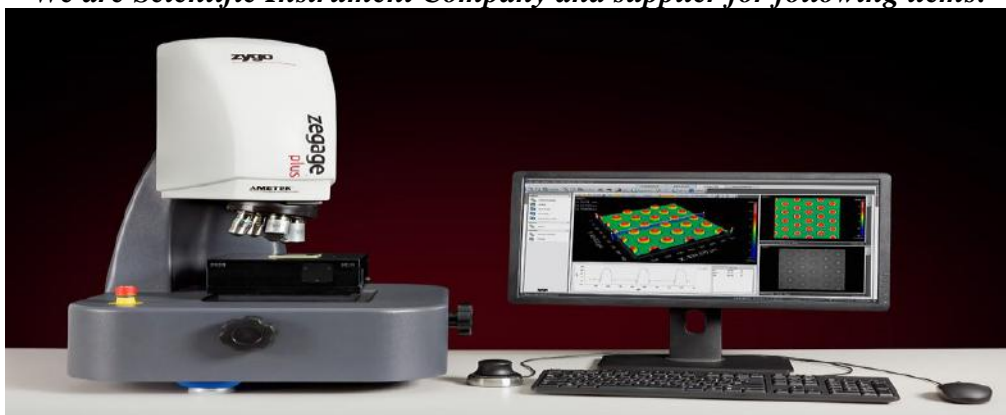
No. 12 & 12-1, Jalan Avenue 1, Ampang Avenue, 68000 Ampang,
Selangor Darul Ehsan, Malaysia.

Tel: 603-4297 0041

Fax: 603-4297 0042

E-mail: sales@taatbestari.com

We are Scientific Instrument Company and supplier for following items:



SOLE AGENT : ZYGO 3D OPTICAL SURFACE PROFILER (USA), ISOLAB GLASSWARE (GERMANY)



AUTHORISED DEALER : ANTON PAAR PIN ON DISC TRIBOMETER, SCRATCH TESTER, INDENTATION TESTER



**EXCLUSIVE DEALER :
METTLER TOLEDO, THERMO SCIENTIFIC AND OTHERS.
CUSTOM MADE FOR FURNACE, HYDRALIC PRESS AND GLASSWARE.**

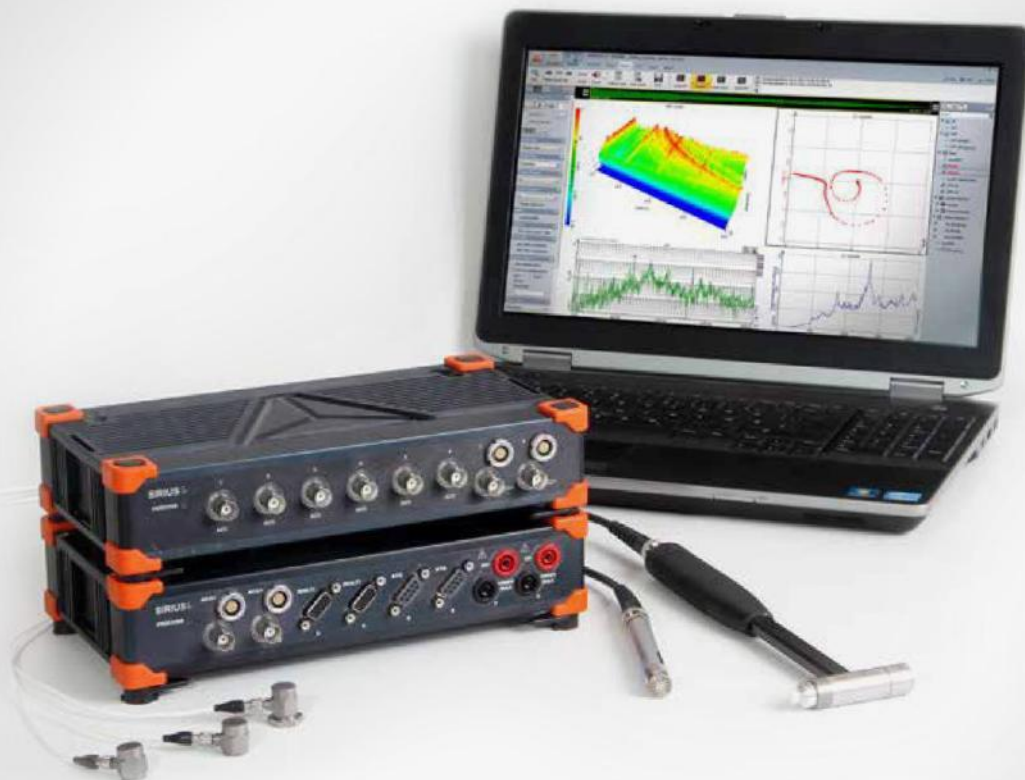
For more info, please contact:

Shah Rizal Saupi. Phone: 0132626955 .Email: shahrizal@taatbestari

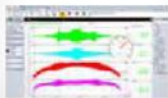
DEWE SOLUTIONS SDN. BHD.

Experts in Test & Measurement Equipment

Dynamic Signal Analysis



**NOISE &
VIBRATION**



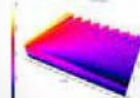
**ROTATING
MACHINERY**



**STRUCTURAL
ANALYSIS**



**ACOUSTIC
ANALYSIS**



PCB PIEZOTRONICS



Write or Call us For Discussion:
Muhammad Redzuan: 012 482 6709
redzuan@dewesolutions.sg

DEWESoft®
measurement innovation

Rolling Bearings





MSITECH GROUP OF COMPANIES

MSITECH (ASIA-PACIFIC) PTE LTD
MSITECH (SINGAPORE) PTE LTD
MSI TECHNOLOGIES (MALAYSIA) SDN BHD
MSI TECHNOLOGIES (PENANG) SDN BHD
MSI TECHNOLOGIES (THAILAND) CO. LTD
PT MSITECH TEKNOLOGY

SINGAPORE

- Corporate Head Quarter

MSITECH (Asia-Pacific) PTE LTD

No. 33, Ubi Avenue 3,
#06-41 Vertex,
Singapore 408868
Tel: 00 65 6509 6938
Fax: 00 65 6509 6939
Web-Site: www.msitech.net

MALAYSIA

- Kuala Lumpur Office

MSI Technologies (Malaysia) Sdn. Bhd.

No. 13, Jalan 16/155C
Bandar Bukit Jalil, 57000 Kuala Lumpur,
Wilayah persekutuan, Malaysia.
Tel: 00 603 8993 9711 / 722
Fax: 00 603 8993 9755

Customer Satisfaction through Quality Products and Services